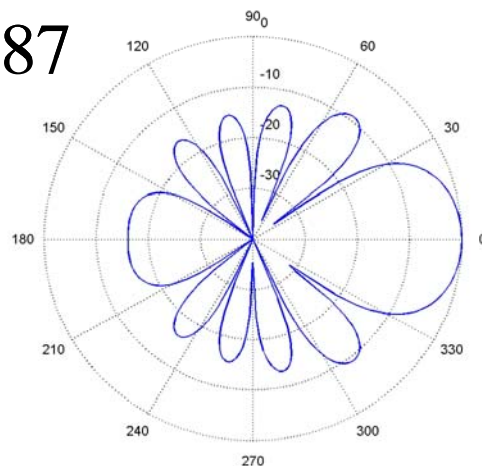
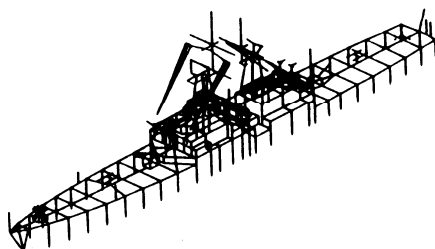
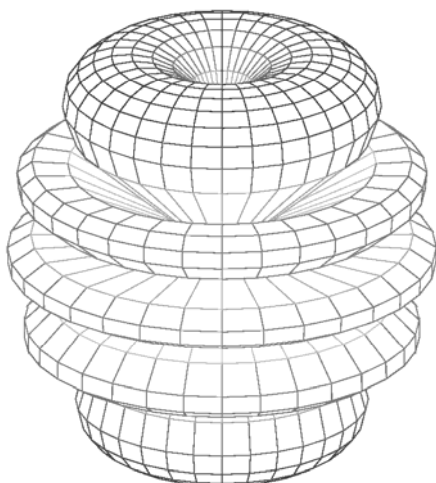
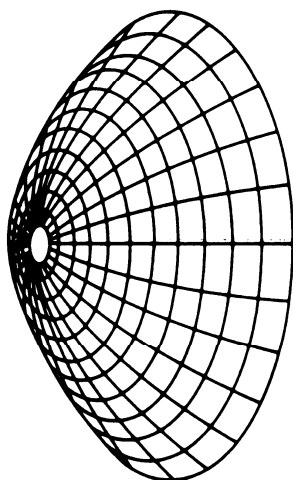
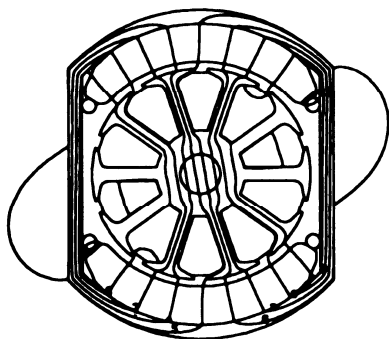
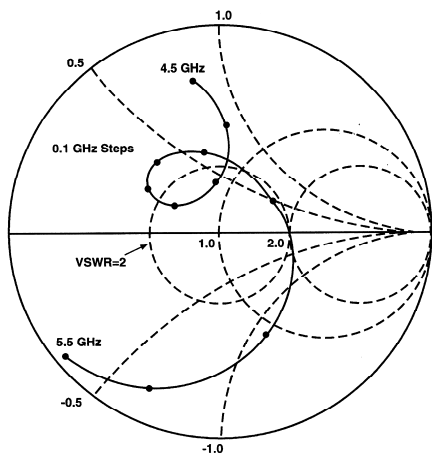


Applied Computational Electromagnetics Society Journal

Special Issue on
**Computational and Experimental
Techniques for RFID Systems and
Applications, Part II**

Guest Editors
**Lauri Sydänheimo, Fan Yang,
and Leena Ukkonen**

June 2010
Vol. 25 No. 6
ISSN 1054-4887



GENERAL PURPOSE AND SCOPE: The Applied Computational Electromagnetics Society (*ACES*) Journal hereinafter known as the *ACES Journal* is devoted to the exchange of information in computational electromagnetics, to the advancement of the state-of-the art, and the promotion of related technical activities. A primary objective of the information exchange is the elimination of the need to “re-invent the wheel” to solve a previously-solved computational problem in electrical engineering, physics, or related fields of study. The technical activities promoted by this publication include code validation, performance analysis, and input/output standardization; code or technique optimization and error minimization; innovations in solution technique or in data input/output; identification of new applications for electromagnetics modeling codes and techniques; integration of computational electromagnetics techniques with new computer architectures; and correlation of computational parameters with physical mechanisms.

SUBMISSIONS: The *ACES Journal* welcomes original papers relating to applied computational electromagnetics. Typical papers will represent the computational electromagnetics aspects of research in electrical engineering, physics, or related disciplines. However, papers which represent research in applied computational electromagnetics itself are equally acceptable.

Manuscripts are to be submitted through the upload system of *ACES* web site <http://aces.ee.olemiss.edu> See “Information for Authors” on inside of back cover and at *ACES* web site. For additional information contact the Editor-in-Chief:

Dr. Atef Elsherbeni

Department of Electrical Engineering
The University of Mississippi
University, MS 386377 USA
Phone: 662-915-5382 Fax: 662-915-7231
Email: atef@olemiss.edu

SUBSCRIPTIONS: Members of the Applied Computational Electromagnetics Society who have paid their subscription fees are entitled to download any published journal article available at <http://aces.ee.olemiss.edu>, and have the option to receive the *ACES Journal* with a minimum of three issues per calendar year.

Back issues, when available, are \$15 each. Subscriptions to *ACES* is available through the web site. Orders for back issues of the *ACES Journal* and changes of addresses should be sent directly to *ACES*:

Dr. Allen W. Glisson

302 Anderson Hall
Dept. of Electrical Engineering
Fax: 662-915-7231
Email: aglisson@olemiss.edu

Allow four week’s advance notice for change of address. Claims for missing issues will not be honored because of insufficient notice or address change or loss in mail unless the *ACES* Treasurer is notified within 60 days for USA and Canadian subscribers or 90 days for subscribers in other countries, from the last day of the month of publication. For information regarding reprints of individual papers or other materials, see “Information for Authors”.

LIABILITY. Neither *ACES*, nor the *ACES Journal* editors, are responsible for any consequence of misinformation or claims, express or implied, in any published material in an *ACES Journal* issue. This also applies to advertising, for which only camera-ready copies are accepted. Authors are responsible for information contained in their papers. If any material submitted for publication includes material which has already been published elsewhere, it is the author’s responsibility to obtain written permission to reproduce such material.

APPLIED COMPUTATIONAL ELECTROMAGNETICS SOCIETY JOURNAL

Guest Editors

**Lauri Sydänheimo, Fan Yang,
and Leena Ukkonen**

June 2010

Vol. 25 No. 6

ISSN 1054-4887

The ACES Journal is abstracted in INSPEC, in Engineering Index, DTIC, Science Citation Index Expanded, the Research Alert, and to Current Contents/Engineering, Computing & Technology.

The first, fourth, and sixth illustrations on the front cover have been obtained from the Department of Electrical Engineering at the University of Mississippi.

The third and fifth illustrations on the front cover have been obtained from Lawrence Livermore National Laboratory.

The second illustration on the front cover has been obtained from FLUX2D software, CEDRAT S.S. France, MAGSOFT Corporation, New York.

THE APPLIED COMPUTATIONAL ELECTROMAGNETICS SOCIETY

<http://aces.ee.olemiss.edu>

ACES JOURNAL EDITOR-IN-CHIEF

Atef Elsherbeni

University of Mississippi, EE Dept.
University, MS 38677, USA

ACES JOURNAL ASSOCIATE EDITORS-IN-CHIEF

Sami Barmada

University of Pisa, EE Dept.
Pisa, Italy, 56126

Fan Yang

University of Mississippi, EE Dept.
University, MS 38677, USA

Mohamed Bakr

McMaster University, ECE Dept.
Hamilton, ON, L8S 4K1, Canada

ACES JOURNAL EDITORIAL ASSISTANTS

Matthew J. Inman

University of Mississippi, EE Dept.
University, MS 38677, USA

Mohamed Al Sharkawy

Arab Academy for Science and
Technology, ECE Dept.
Alexandria, Egypt

Christina Bonnington

University of Mississippi, EE Dept.
University, MS 38677, USA

Khaled ElMaghoub

University of Mississippi, EE Dept.
University, MS 38677, USA

ACES JOURNAL EMERITUS EDITORS-IN-CHIEF

Duncan C. Baker

EE Dept. U. of Pretoria
0002 Pretoria, South Africa

Allen Glisson

University of Mississippi, EE Dept.
University, MS 38677, USA

David E. Stein

USAF Scientific Advisory Board
Washington, DC 20330, USA

Robert M. Bevensee

Box 812
Alamo, CA 94507-0516, USA

Ahmed Kishk

University of Mississippi, EE Dept.
University, MS 38677, USA

ACES JOURNAL EMERITUS ASSOCIATE EDITORS-IN-CHIEF

Alexander Yakovlev

University of Mississippi, EE Dept.
University, MS 38677, USA

Erdem Topsakal

Mississippi State University, EE Dept.
Mississippi State, MS 39762, USA

JUNE 2010 REVIEWERS

Mohamed Al-Sharkaway

Sami Barmada

J. Berenger

Malgorzata Celuch

Deb Chatterjee

Veysel Demir

AbdelKader Hamid

Matthew Inman

Ozlem Kilic

Jeremy Knopp

Michiko Kuroda

Qinjiang Rao

C. J. Reddy

Levent Sevgi

Lauri Sydanheimo

Alan Taflove

Leena Ukkonen

John Volakis

Fan Yang

THE APPLIED COMPUTATIONAL ELECTROMAGNETICS SOCIETY
JOURNAL

Vol. 25 No. 6

June 2010

TABLE OF CONTENTS

“Platform Tolerant and Conformal RFID Tag Antenna: Design, Construction and Measurements” H. Rajagopalan and Y. Rahmat-Samii.....	486
“A Reliable Approach for Evaluating the Platform Tolerance of RFID Tag Antennas” L. Li and R. Mittra.....	498
“Importance of Computational Electromagnetic Modeling in the Development of RFID Tags for Paper Reel Identification” L. Ukkonen, T. Björninen, L. Sydänheimo, A. Elsherbeni, and F. Yang.....	505
“Space-Filling Curve Radio Frequency Identification Tags” J. A. McVay, A. Hoorfar, and N. Engheta.....	517
“Compact Metamaterial-Based UHF RFID Antennas: Deformed Omega and Split-Ring Resonator Structures” B. D. Braaten, R. P. Scheeler, M. Reich, R. M. Nelson, C. Bauer-Reich, J. Glower, and G. J. Owen.....	530
“UHF-HF RFID Integrated Transponder for Moving Vehicle Identification” A. Toccafondi, C. D. Giovampaola, P. Braconi, A. Cucini.....	543
“Feasibility of Passive Wireless Sensors Based on Reflected Electro-Material Signatures” A. Hasan, A. F. Peterson, and G. D. Durgin.....	552
“Survey of Laboratory Scale Fabrication Techniques for Passive UHF RFID Tags” T. Elsherbeni, K. ElMahgoub, L. Sydänheimo, L. Ukkonen, A. Elsherbeni, F. Yang.....	561

Platform Tolerant and Conformal RFID Tag Antenna: Design, Construction and Measurements

Harish Rajagopalan and Yahya Rahmat-Samii

Electrical Engineering Department
University of California at Los Angeles
Los Angeles, CA, 90095-1594, USA
harish@ee.ucla.edu, rahmat@ee.ucla.edu

Abstract— This paper presents the design of a novel platform tolerant and conformal RFID (Radio Frequency Identification) tag antenna, which operates at the 902–928 MHz UHF band. The antenna has a simple, low-profile (1.8 mm thick) structure. It consists of two microstrip patches, which are separated by a narrow gap and driven by a microchip in the gap. The tag is designed to complex conjugate match an Alien-Higgs2 microchip. The performance of the tag is investigated on different surfaces (free space, human and metal) through simulations using parameters like power reflection coefficient, input impedance and radiation patterns. The effects of bending are investigated on the tag design. Experimental read-range, radiation pattern and impedance measurements are performed for the tag. High Frequency Structure Simulator (HFSS) simulation validation has been achieved due to excellent agreement with measurements for this particular application. The experimental measurements show that the maximum boresight average read range of the designed RFID tag on different platforms is about 3.5m (4 W EIRP).

Index Terms— Conformal, metal, RFID, tag.

I. INTRODUCTION

Radio frequency identification (RFID) systems have attracted considerable attention in recent years. These systems have become very popular in applications like asset identification, inventory management and human monitoring [1, 2]. In processes like supply chain management, the RFID tags can keep a track of the products throughout the supply course assembly chain [3]. RFID tags in the form of an implantable chip [4] or wrist-bands [5] can be used to track the movement of people in different environments

(like hospitals). Due to the non line-of sight operation, larger read range and ability to store more information, RFID tags serve as a possible replacement to bar codes [6]. A typical RFID system consists of a reader and a tag where the tag is a passive device consisting of an antenna and a microchip. Near-field (13.56 MHz) RFID systems work on the principle of inductive coupling between the reader and the tag [7]. Far-field (915 MHz, 2.4GHz) RFID tags work on the principle of traveling waves between the reader and the tag [8, 9]. The UHF (860–960 MHz) band is of particular interest due to the long read range possibility and low manufacturing costs. These RFID systems operate at various frequency bands around the world (902–928 MHz in North and South America).

Passive UHF RFID tags are attached to the required object for tagging purposes. At the UHF frequency, high-dielectric (human) or high-conductivity (metal) objects degrade the performance of the tag affecting the tag impedance, ability to couple power to the microchip and the read range of the tag. These RFID tag problems are well documented in [10, 11]. Various metal-mountable tag designs have been proposed in literature [12–14]. Slim tag with vias designed on high-impedance surface [15], tag on a lossy substrate with a stacked structure [16] and small loop tag [17] are some other examples of metal mountable tags where the tag antennas are designed such that the tag antenna parameters like frequency, efficiency, bandwidth, radiation pattern and input impedance do not undergo severe degradation on metal. Platform-tolerant tag designs have also been proposed where the tag demonstrates stable performance on different surfaces [18].

Technological progress in RFID readers and tags enables new and interesting applications and more efficient ways of using current systems. The design of the antenna is a critical part of the RFID tag design [19]. A number of challenges have to be addressed while developing RFID antennas which include simple design for low cost mass production (as bar code are much cheaper than tags at present), reliable performance in free space and on different surfaces, low profile structure and structural conformality (for nonplanar objects). Most of the tag designs in literature answer some of these challenges [20–22]. Therefore, there is a need to develop new RFID tag antenna designs which successfully deal with all the challenges presented. Large demand still exists in the market for UHF band disposal, multipurpose RFID tags. Good, practical solutions are still missing.

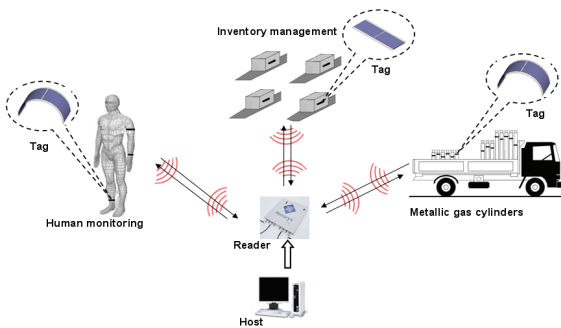


Fig. 1. Potential security and safety applications of the proposed RFID tag.

In this paper, we propose the design of a novel UHF RFID tag which operates in the US (902–928 MHz) band. The low profile unique design makes the tag ideal for low cost mass production (no via structure). The tag operates on different surfaces making it platform tolerant. The tag also operates on non planar surfaces. This RFID tag antenna is designed to match the Alien Higgs-2 microchip. Firstly, the planar version of the tag is discussed in detail, both in free space and on metal plate. Impedance and pattern measurements are performed for the planar tag. After the successful investigation of the planar tag, the tag is conformed to study effects of structural bending on the tag performance. This conformal tag is then placed on different surfaces (human, metal) and

through simulations the power reflection coefficient, input impedance and radiation patterns are investigated to study the effects of these surfaces on the tag performance. Finally, read-range measurements are performed using both planar and conformal tags in different environments. Initial investigations show that this tag can be used for both security and safety applications such as inventory control and reporting of high risk materials, gas cylinder movement and tracking, and human monitoring as shown in Fig. 1.

II. TAG ANTENNA DESIGN

The goal of tag antenna is to maximize the detection range of the RFID tag. The antenna input impedance has to be conjugate matched to the microchip impedance to ensure maximum power transmission to the microchip. The power reflection coefficient between the antenna and the microchip is given by

$$\rho = 1 - \tau = 1 - \frac{4R_a R_{mc}}{|Z_a + Z_{mc}|^2}, \quad (1)$$

where ρ is the power reflection coefficient, τ is the power transmission coefficient and $Z_a = R_a + jX_a$ and $Z_{mc} = R_{mc} + jX_{mc}$ are the complex antenna and microchip input impedances, respectively [1]. The antenna is designed to conjugate match to a microchip, Alien Higgs-2, which has an input parallel resistance of 1500 Ω and a capacitance of 1.2 pF (at 915 MHz, the microchip impedance is $14 - j145 \Omega$) as shown in Fig. 2.

Figure 2 shows the design of the planar RFID tag antenna. The tag antenna consists of two quarter-wave microstrip patches shorted to the ground plane by the shorting plates. These patches are placed next to each other separated by a gap and connected by a microchip in the feed location. The patches are placed on a thin FR-4 substrate ($\epsilon_r = 4.4$ and $\tan\delta = 0.02$) and foam layer backed by a ground plane (116mm x 40mm). The reason for choosing a thin FR-4 layer is that the FR-4 can be potentially replaced by paper substrate to form a green tag. The structure is simulated with High Frequency Structure Simulator (HFSS). The tag

dimensions are chosen such that it can operate both in free space and on metal and satisfy the condition: minimum -3dB half power bandwidth. To study the effect of metal plate, the tag is placed on a 250mm x 250mm x 2mm (approximately $0.9\lambda \times 0.9\lambda \times 0.006\lambda$ at 915 MHz) copper metal plate. The power reflection coefficient, input impedance, and radiation patterns are compared for the planar tag in free space and on metal ground plane to better understand the working of the tag.

The matching frequency (corresponds to the minimum value of power reflection coefficient in dB) is tuned by adjusting the patch length and gap width. The matching frequency decreases when the patch length is increased and it increases when the gap width is increased. The foam layer is used to improve bandwidth and radiation efficiency. The input resistance of the tag is controlled by changing the patch width (resistance increases when the patch width is reduced). The tag ground plane width is chosen such that the tag can satisfy the -3dB criteria for both free space and on metal.

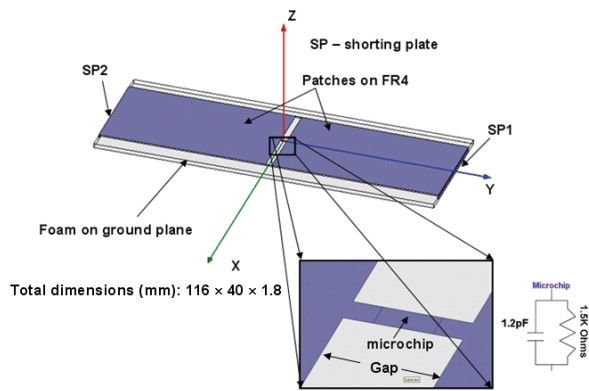


Fig. 2. Design of the RFID tag antenna.

The microchip has variable impedance over the frequency band and tag parameters are optimized taking this fact into consideration. Once the input impedance of the tag and the microchip are obtained, these values are inserted into eq. (1) to obtain power reflection coefficient. Figure 3 shows the power reflection coefficient calculated from the input impedance and the Alien Higgs-2 chip impedance for both free space and on metal. The optimized total dimensions of the tag are 40mm x 116mm x 1.8mm. Individual dimensions

are as follows: patch-30mm x 57mm, Fr-4 substrate-30mm x 116mm x 0.4mm, foam substrate-30mm x 116mm x 0.4mm, shorting plate-30mm x 1.8mm, ground plane-40mm x 116mm and gap width-2mm.

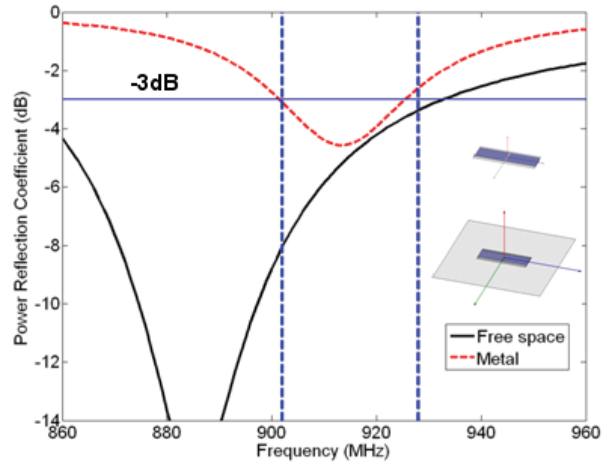
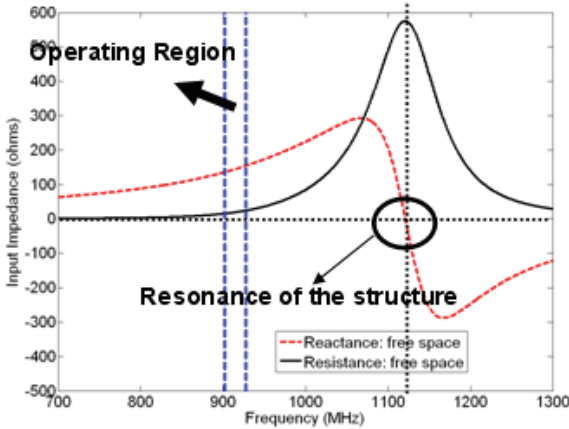


Fig. 3. Power reflection coefficient calculated from the antenna and the microchip impedance. The 902–928 MHz band is marked by two vertical lines.

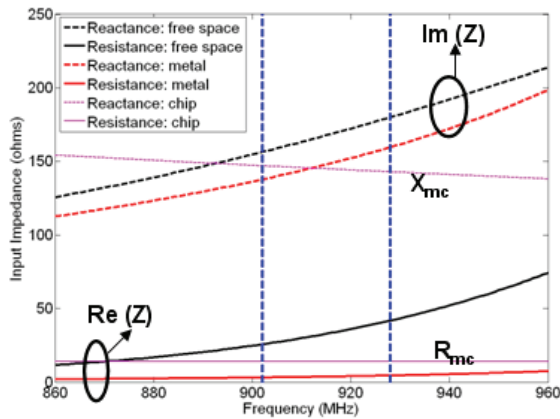
Figure 4(a) shows the simulated input impedance when the optimized tag antenna is in free space. It can be clearly seen that the antenna resonance occurs close to 1100MHz (length of the antenna 116mm $\sim \lambda_g/2$). The operating region of the tag is marked with dotted lines. Figure 4(b) shows the input impedance (both real and imaginary part) of the tag in free space and on a 250mm x 250mm x 2mm copper plate. It can be seen that there is a change in the input impedance when the tag is placed on metal. Therefore, the tag is optimized to work well in free space and on metal plate. The input impedance of the tag at 915 MHz in free space and on metal is $32.9 + j167.8$ and $3.7 + j147.9$, respectively.

Figure 5(a) shows the change in power reflection coefficient for gap width variation. It can be seen that when all other design parameters are fixed to optimum values and the gap width is varied, the matching frequency increases significantly as the gap width increases for both free space and metal plate case. Figure 5(b) shows the effect of different size ground planes on the

tag performance. It can be seen that when all other design parameters are fixed to optimum values and the ground plane size is varied (thickness of ground plane fixed at 2mm), the matching frequency satisfies the -3dB condition over the entire band showing the robustness of the tag to metal attachment.



(a)

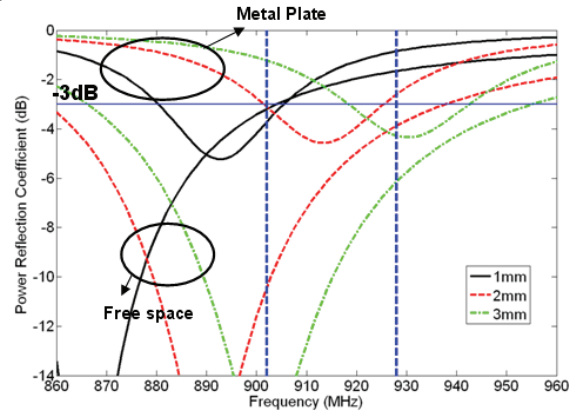


(b)

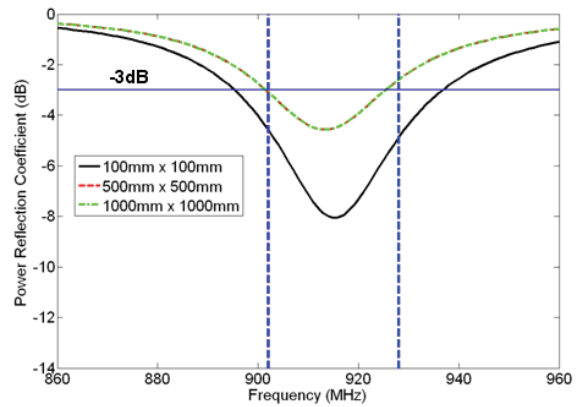
Fig. 4. Simulated input impedance of the antenna. (a) In free space. (b) In free space and on a 250mm x 250mm x 2mm copper plate. The 902–928 MHz band is marked by two vertical lines.

Complex interactions of currents and fields due to the antenna structure cause the tag to operate in a large loop-patch hybrid mode. From the current distribution view point, the tag appears to act in patch mode and from radiation pattern view point, the tag appears to operate in large loop mode (circumference of the loop is approximately 1λ at 915MHz). Figure 6(a) shows the current distribution on the top surface of the patches and ground plane for the planar tag in free space at

915 MHz. It is clear that the currents are maximum at the edges and minimum at the center of the tag (emulating a quarter-wave patch). The direction of current flow on the ground plane is in the opposite direction to the current on the top patch surface.



(a)



(b)

Fig. 5. Power reflection coefficient (a) Gap width variation. (b) Ground plane size variation.

Figure 6(b) shows the electric field distribution in the 0.4mm thick FR-4 substrate and the 1.4mm thick foam layer for the planar tag in free space at 915 MHz. The fields are maximum at the center. The fields are in the $+z$ direction on one patch and in the $-z$ direction on the other patch. Across the gap, the fields point in the $+y$ direction (horizontal electric field across the gap radiates).

III. IMPEDANCE AND RADIATION PATTERN MEASUREMENTS

Extensive measurements were performed on the planar tag both in free space and on metal

plate. A prototype planar tag antenna was built and its input impedance and radiation patterns were measured.

A. Impedance Measurements

Input impedance measurement of the tag is crucial as it helps to optimize the tag performance and improve its modelling in simulations. Due to a balanced structure, the impedance of the dual-patch microstrip antenna cannot be measured directly with a network analyzer. This is because the feed points of the balanced antenna should be driven by equal and opposite currents, which is not true if the antenna is connected to an unbalanced coax port of the network analyzer. In order to measure the input impedance of this antenna, a quarter-wave balun was designed with the center frequency at 915MHz. Fig. 7 shows the prototype antenna and the balun used for impedance measurements.

Suitable scheme is applied to calibrate the balun out of the measurement. The impedance measurement was done in free space, i.e., when the tag was placed on a low-permittivity polystyrene support, and also when the tag was placed on a 250mm × 250 mm x 2mm copper plate. The measurements were carried out in an anechoic chamber to ensure stable distortion-free conditions. Figure 8 shows the measured input impedance of the planar tag both in free space and on metal. Figure 8(a) shows the comparison of the input impedance between simulation and measurement in free space. Both the real and the imaginary part of the input impedance measured data follow the simulation curves very closely (in the band of operation). Figure 8(b) shows the comparison of the input impedance between simulation and measurement when the tag is placed on a metal plate. The measurements show the decrease in the real part as predicted from the simulation. There is very good agreement between the measured and simulated data. The difference at higher frequencies for the resistive part may be caused due to the balun-tag coupling and the balun bandwidth limitation.

B. Radiation Pattern Measurements

Radiation pattern measurements were performed in the UCLA far-field anechoic chamber placing the tag on a polystyrene support

and rotating it by an antenna positioner. Mercury4 reader with M/A-COM Dual antenna (5.9dBi gain) was used for reading the tag with single frequency operation at 915MHz (shown in Fig. 14(a)). The reader was controlled by a host computer. The maximum transmitted power was 4 W EIRP (for the US band). The minimum transmitted power required for reading the tag was determined at each measurement angle and the normalized radiation pattern was computed. Figure 9 shows the measurement setup and the normalized measured radiation pattern in the two principal planes when the tag is in free space and when the tag is plate on a metal plate. The peak

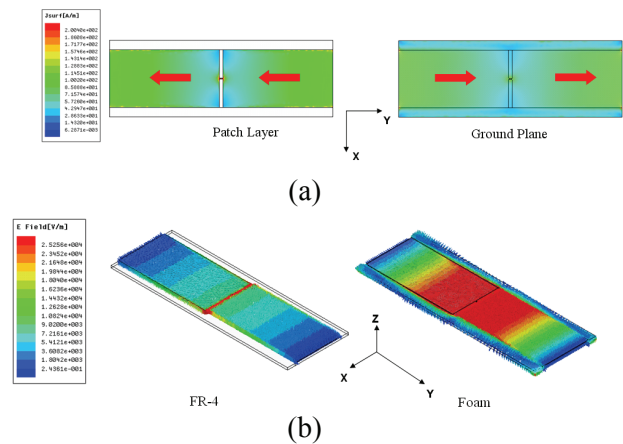


Fig. 6. (a) Surface currents on the planar tag in free space at 915 MHz. (b) Electric field distribution for the planar tag in free space at 915 MHz.

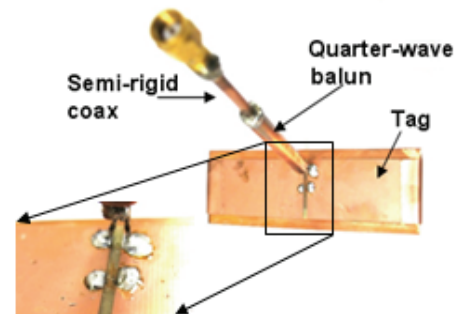


Fig. 7. Quarter-wave balun soldered to the prototype tag.

simulated directivity for the tag in free space and on metal plate are 3.53dB and 6.86dB at 915 MHz. All the patterns are normalized to their respective maximum values. The tag and the

reader were placed in the anechoic at a distance of 2m (far-field region of the reader antenna). The reader power was incremented in steps of 0.1dBm to find the minimum transmitted RF signal required to activate the tag. This activation was based on the criterion that the back-scattered modulated signal from the tag should be read continuously for 90 seconds. The positioner was rotated in steps of 5°.

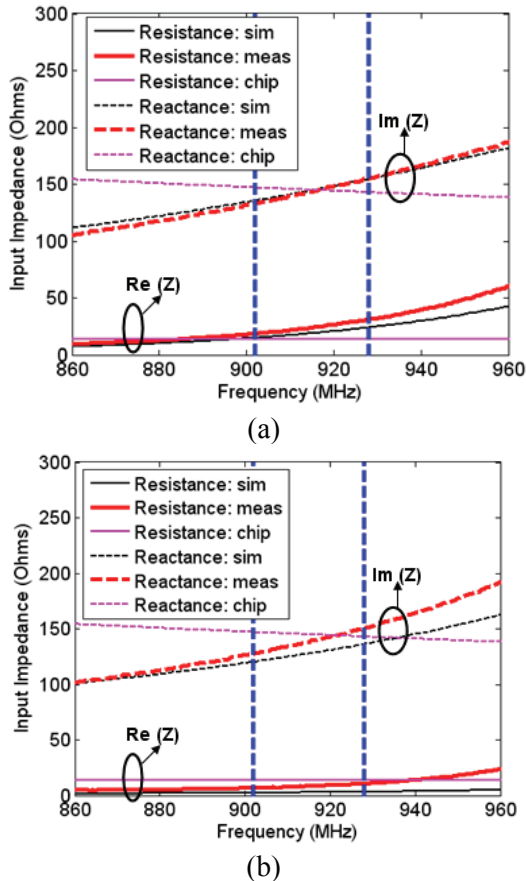


Fig. 8. Input impedance measurement (a) Free space. (b) Metal plate. The 902–928 MHz band is marked by two vertical lines.

Figure 9(b) shows the simulated and measured patterns for the tag in the xz -plane in both free space and on metal at 915 MHz. It can be seen that in free space the tag has omnidirectional pattern and on metal the tag is more directive with a small back lobe (present due to diffraction from the metallic plate edges). Due to the nature of the operating mechanism which involves both folded-dipole and patch characteristics, the pattern is omnidirectional in the xz -plane and Fig. 8 in the yz -plane (loop like pattern in both planes). Figure

9(c) shows the simulated and measured patterns for the tag in the yz -plane in both free space and on metal at 915 MHz. It can be seen that in free space the tag has a figure-8 pattern and on metal the tag has a broader pattern than in the xz -plane. The measured patterns follow the simulated patterns very closely in free space in both planes.

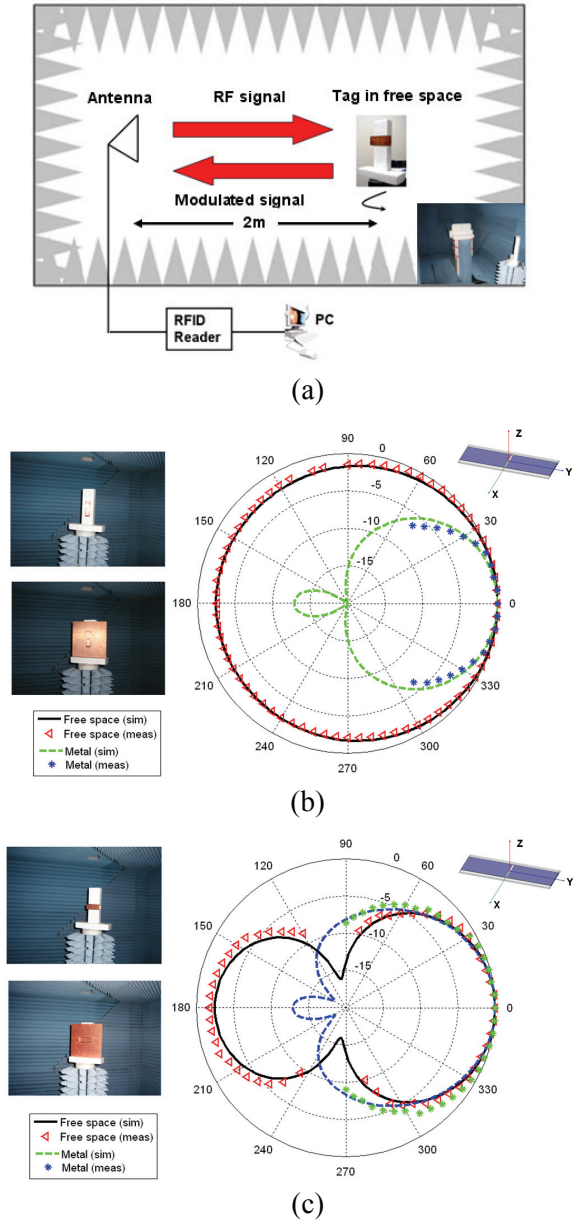


Fig. 9. (a) Radiation pattern measurement setup. (b) Normalized measured and simulated radiation pattern in the XZ -plane ($\Phi = 0^\circ$). (c) Normalized measured and simulated radiation pattern in the YZ -plane ($\Phi = 90^\circ$). The antenna is in free space and on a 250 mm \times 250mm \times 2mm copper plate. The scale is in dB.

On metal, the measured patterns follow the simulated patterns closely in both planes up to certain angles. At large angles, due to reader power limitations, the received power was too low to activate the tag. All the patterns are normalized to their maximum value. The read range measurements for the planar tag will be discussed later. The excellent agreement between the measured and simulated results for both the tag input impedance and radiation pattern shows that commercial radio frequency (RF) computer aided-design (CAD) software can be successfully used for RFID-type applications.

IV. BENDING EFFECTS ON THE TAG

Once the planar design was investigated in detail, the tag was conformed in order to understand the effects of bending on the tag antenna performance.

Figure 10(a) shows the conformal tag in free space. The tag antenna is bent about a cylinder with radius of about 45mm. All the dimensions of the planar tag are kept constant. The input impedance of the tag at 915 MHz in planar and conformal form is $32.9 + j167.8$ and $21.4 + j170.7$, respectively. It can be seen that the input impedance for both planar and conformal forms of the tag are similar and the design is robust to conformality.

After understanding that bending does not appreciably affect the performance of the tag in free space, the conformal tag was mounted on different surfaces to study the effect of these surfaces on the antenna performance. The antenna was conformed around a metal cylinder (copper) as shown in Fig. 10(b). As shown in Fig. 10(c), the tag was also conformed around human model. The model is a typical representation of upper human arm (radius about 45mm). For simplicity, the human model was considered homogeneous (with dielectric constant of 58.8 and conductivity of 0.84S/m). Figure 11 shows that the input impedance of the tag does not change when placed on metal and human arm. The input impedance of the conformal tag at 915 MHz on metal cylinder and human arm is $4.1 + j150.7$ and $6.7 + j151.47$, respectively. Figure 12 shows the comparison of

the power reflection coefficient between the planar and conformal tag and it can be seen that the bending does not change the performance significantly. Figure 12 also shows that the resonant frequency of the conformal tag does not change on different surfaces. It is also observed that the power reflection coefficient satisfies the half-power bandwidth for all the cases. Similar half-power bandwidth and input impedance characteristics were obtained when the tag was placed on multilayer human models as discussed in [2].

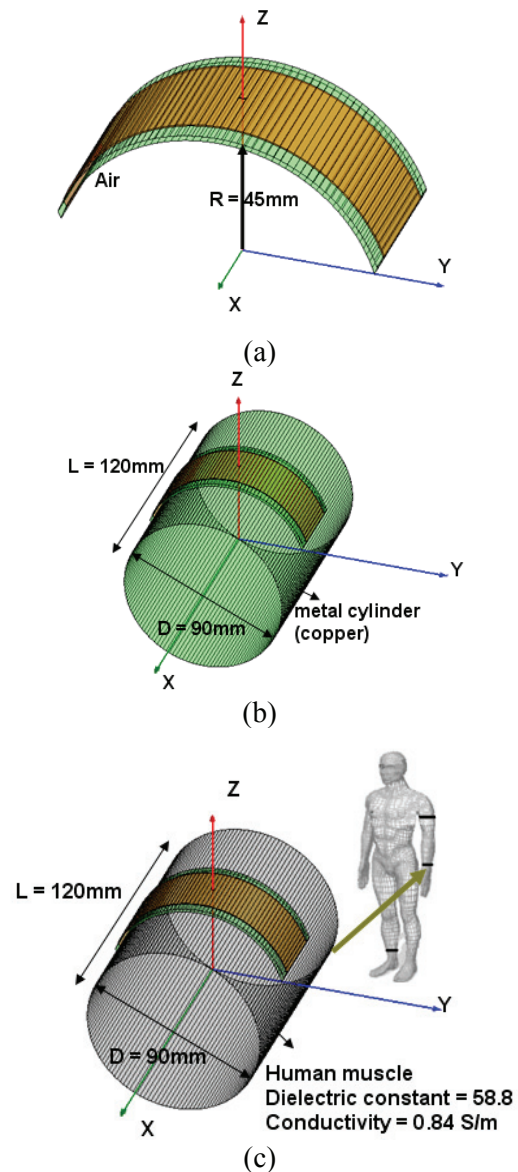


Fig. 10. (a) Conformal RFID tag design. (b) RFID conformal tag on metal cylinder. (c) RFID conformal tag on upper part of human arm.

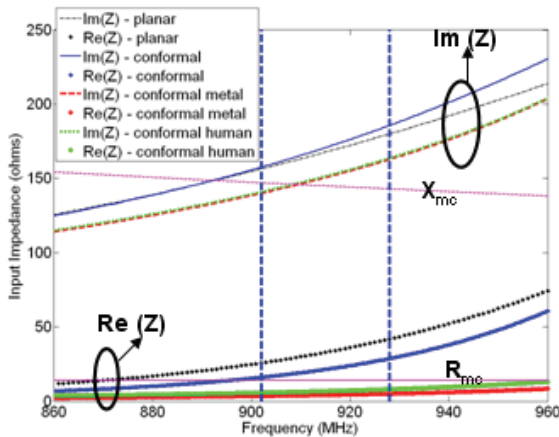


Fig. 11. Simulated input impedance of the antenna for the three cases described in Fig. 10. The 902–928 MHz band is marked by two vertical lines.

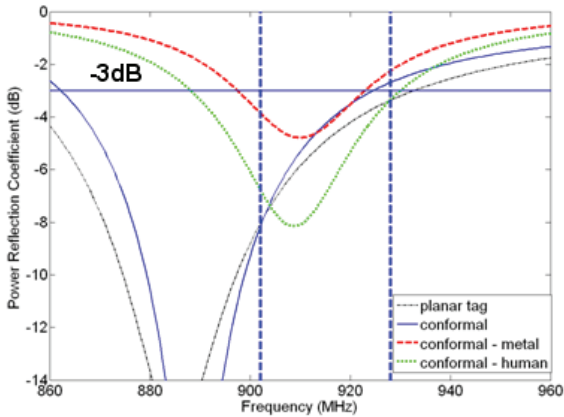
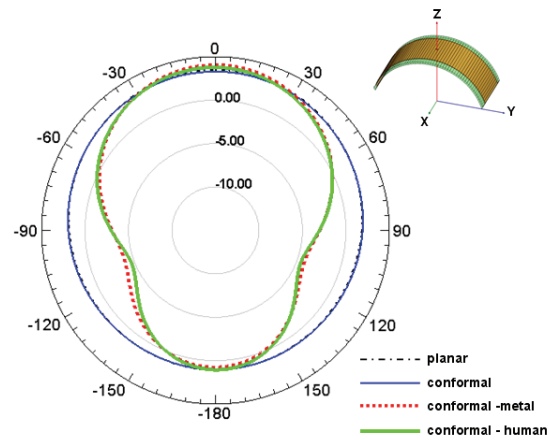
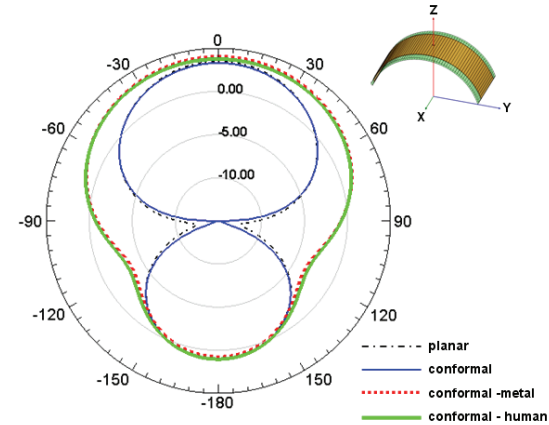


Fig. 12. Power reflection coefficient calculated for the simulated antenna input impedance and the Alien Higgs-2 microchip for the three cases described in Fig. 10. The 902–928 MHz band is marked by vertical lines.

Figure 13 shows the comparison of the radiation patterns (directivity in dB) between planar tag, conformal tag, conformal tag on metal and conformal tag on human arm in the xz -plane and yz -plane at 915 MHz. It is observed that the directivity slightly decreases for the bending case (conformal) with respect to planar tag but the patterns are similar. Figure 13 also shows that the radiation patterns are only slightly different in the xz -plane and yz -plane for metal cylinder and human arm case. It is also clear that when placed on metal cylinder, the directivity of the tag increases which is expected.



(a)



(b)

Fig. 13. Comparison between planar tag, conformal tag, conformal tag on metal and conformal tag on human arm. (a) Radiation pattern in the xz -plane ($\phi = 0^\circ$). (b) Radiation pattern in the yz -plane ($\phi = 90^\circ$).

V. READ RANGE MEASUREMENTS

Typically, 2–5m read range is desired with passive UHF RFID systems. Read range measurements were conducted in an open environment to avoid reflections from surroundings at the single operating frequency of the reader (915MHz). The measurement setup is shown in Fig. 14(a). Microwave absorbers were placed on the floor to avoid ground reflections.

Figure 14(a) shows the reader antenna and central unit on a trolley (reader antenna dimensions were 230mm × 480mm). The maximum read range was defined as the maximum

line-of-sight distance from the reader antenna where the reader detects the tag continuously without interruption for 90 seconds. Once the tag is moved further from the maximum read range, it did not satisfy the criteria of continuous detection. The output power of the reader is fixed at 30.1dBm. The reader antenna gain is 5.9 dBi. The read range formula is given by

$$r_{\max} = d \sqrt{\frac{EIRP}{P_{\min} G_t L_c}}, \quad (2)$$

where P_{\min} is the minimum power required to communicate with the tag is recorded, L_c is the loss of the connecting cable (1dB), G_t is the gain of the transmitting antenna (5.9dBi), d is the distance of the reader to the tag and EIRP is effective isotropic radiated power (36dBm) [1].

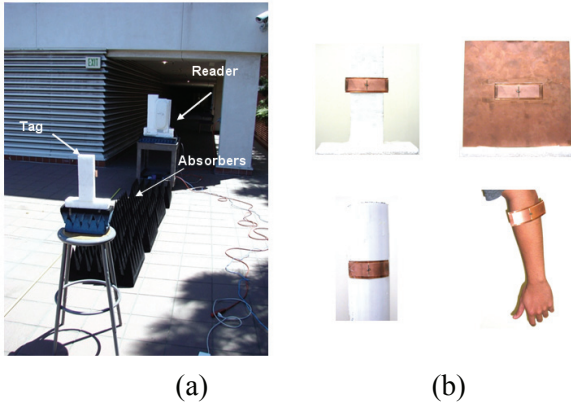


Fig. 14. (a) Read range measurement setup. (b) The prototype tag on the polystyrene support in free space, on metal plate, on PVC cylinder and on human arm.

Figure 15 shows the plot of maximum measured boresight read range and the corresponding minimum power to activate the tag for both free space and on metal operation at 915MHz. The regression lines are drawn using equation (2) and fit well with measurements. Table I shows the maximum read range for the tag in free space and on different surfaces like flat metal plate, metal cylinder, human arm and lower part of human leg some of which are shown in Fig. 14(b) at the boresight direction. The reading distance remains fairly constant with an average boresight read range of about 3.5m on different

platforms with the current reader configuration. The radiation efficiency of the tag is approximately 95% in free space, 60% on metal and about 50% on human arm model. The read range values differ for different platforms due to different matching (with chip impedance), directivity and radiation efficiencies. The structure is inherently less lossy (thin FR4 substrate) and it has a higher radiation resistance compared to small loop tags. Therefore, the tag has significantly better read range than the small loop tag [17].

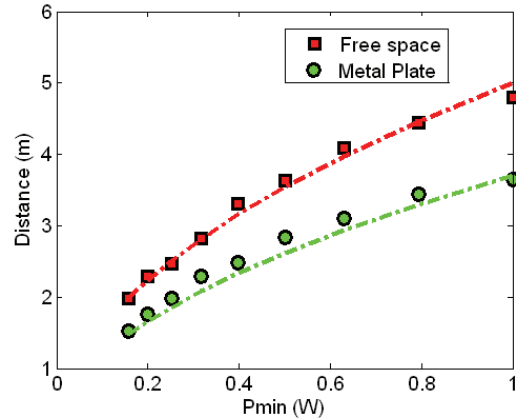


Fig. 15. Maximum measured boresight read range versus minimum power for tag in free space and on metal plate with best-fit curves.

Table 1: Maximum measured boresight read distance of the tag on different surfaces at 915MHz at 4W EIRP.

On polystyrene support (free space)	4.8m
On 250mm × 250mm x 2mm copper plate	3.8 m
On PVC pipe (free space) – radius (50mm)	4.5m
On metal cylinder – radius (50mm)	3.9 m
On human arm	3.5 m
On lower part of human leg	3.4 m
On lower part of human leg (with clothing)	3.4 m

VI. CONCLUSION

A simple, conformal, low-profile (1.8 mm) microstrip antenna suitable for RFID tags has been proposed. The tag is designed to conjugate match Alien-Higgs2 microchip impedance ($14 - j145\Omega$ at 915MHz) and the tag operates at the 902–928 MHz UHF band. A prototype of the tag was built

and tested by measuring its input impedance and radiation pattern. The input impedance measurements were performed using balun approach due to the balanced geometry of the tag. Excellent agreement was achieved between the measured and HFSS simulated data for both input impedance and radiation pattern for the planar tag. The bending effects were studied for the tag and it was observed that the tag was robust to conformality. The conformal tag was then placed on different surfaces and through simulations it was observed that the tag performed well on all different surfaces. Read range measurements were performed for the tag in planar and conformal form on different surfaces and an average successful read range of about 3.5m was achieved (4W EIRP).

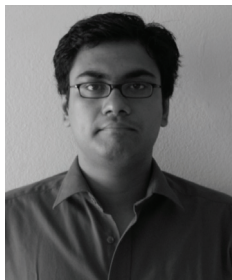
ACKNOWLEDGMENT

The authors would like to thank Tomi Koskinen (post-doc visiting scholar from Finland) for the fruitful discussions. The authors would also like to thank Dr. Keisuke Noguchi (visiting professor from Japan) for his suggestions with the impedance measurements and Jeffrey Akamine (undergraduate student from UCLA) for helping with outdoor read range measurements.

REFERENCES

- [1] K. V. S. Rao, P. V. Nikitin, and S. F. Lam, "Antenna design for UHF RFID tags: A review and a practical application," *IEEE Transactions on Antennas and Propagation*, vol. 53, no. 12, pp. 3870–3876, Dec. 2005.
- [2] G. Marrocco, "The art of UHF RFID antenna design: impedance-matching and size-reduction techniques," *IEEE Antennas and Propagation Magazine*, vol. 50, no. 1, pp. 66–79, Feb. 2008.
- [3] R. Glidden et al. "Design of ultra-low-cost UHF RFID tags for supply chain applications," *IEEE Communications Magazine*, vol. 42, no. 8, pp. 140–151, Aug. 2004.
- [4] K. R. Foster and J. Jaeger, "RFID inside: The murky ethics of implanted chips," *IEEE Spectrum*, pp. 24–29, March 2007.
- [5] L. Yang, L. J. Martin, D. Staiculescu, C. P. Wong, and M. M. Tentzeris, "Conformal Magnetic Composite RFID for Wearable RF and Bio-Monitoring Applications," *IEEE Transactions on Microwave Theory and Techniques*, vol. 56, no. 12, pp. 3223–3230, Dec. 2008.
- [6] R. Weinstein, "RFID: a technical overview and its application to the enterprise," *IT Professional*, vol. 7, no. 3, pp. 27–33, May–June 2005.
- [7] K. Myny, S. Van Winckel, S. Steudel, P. Vicca, S. De Jonge, M. J. Beenhakkers, C. W. Sele, N. A. J. van Aerle, G. H. Gelinck, J. Genoe, and P. Heremans, "An Inductively-Coupled 64b Organic RFID Tag operating at 13.56MHz with a Data Rate of 787b/s," *IEEE International Solid-State Circuits Conference*, pp. 290–614, Feb. 2008.
- [8] G. Marrocco, "Gain-optimized self-resonant meander line antennas for RFID applications," *Antennas Wireless Propag. Lett.*, vol. 2, no. 21, pp. 302–305, 2003.
- [9] Q. Xianming and Y. Ning, "A folded dipole antenna for RFID," *Proc. IEEE Antennas and Propagation Soc. Int. Symp.*, vol. 1, Jun. 2004, pp. 97–100.
- [10] P. R. Foster and R. A. Burberry, "Antenna problems in RFID systems," *Proc. Inst. Elect. Eng. Colloquium RFID Technology*, pp. 3/1–3/5, Oct. 1999.
- [11] D. M. Dobkin and S. M. Weigand, "Environmental effects on RFID tag antennas," *IEEE MTT-S International Microwave Symposium*, pp. 135–138, June 2005.
- [12] B. Yu, S. -J. Kim, B. Jung, F. J. Harackiewicz, and B. Lee, "RFID tag antenna using two-shortened microstrip patches mountable on metallic objects," *Microwave and optical technology letters*, vol. 49, no. 2, pp. 414–416, Feb. 2007.
- [13] M. Hirvonen, P. Pursula, K. Jaakkola, and K. Laukkanen, "Planar inverted-F antenna for radio frequency identification," *Electronics Letters*, vol. 40, no. 14, pp. 848–850, July 2004.
- [14] K. H. Kim, J. G. Song, D. H. Kim, H. S. Hu, and J. H. Park, "Fork-shaped RFID tag antenna mountable on metallic surfaces," *Electronics Letters*, vol. 43, no. 25, pp. 1400–1402, Dec. 2007.

- [15] S. -L. Chen and K. -H. Lin, "A Slim RFID Tag Antenna Design for Metallic Object Applications," *Antennas Wireless Propag. Lett.*, vol. 7, pp. 729–732, 2008.
- [16] H. W. Son, "Design of RFID tag antenna for metallic surfaces using lossy substrate," *Electronics Letters*, vol. 44, no. 12, pp. 711–713, June 2005.
- [17] M. L. Ng, K. S. Leong, and P. H. Cole, "A small passive UHF RFID tag for metallic item identification," *International Technical Conference on Circuits/Systems, Computers and Communications*, Jul. 2006.
- [18] L. S. Chan, K. W. Leung, R. Mittra, K. V. S. Rao, "Platform-tolerant Design for an RFID Tag Antenna," *IEEE International Workshop on Anti-counterfeiting, Security, Identification*, pp. 57–60, April 2007.
- [19] J. T. Prothro, "Improved performance of a Radio frequency identification tag antenna on a metal ground plane," *M.S. Thesis*, Georgia Institute of Technology, 2007.
- [20] H. W. Son and C. S. Tyo, "Design of RFID Tag Antennas Using an Inductively Coupled Feed," *Electronics Letters*, vol. 41, no. 18, pp. 994–996, Sept. 2005.
- [21] C. Cho, H. Choo and I. Park, "Design of Novel RFID Tag Antennas for Metallic Objects," *IEEE International Symposium on Antennas and Propagation Digest*, pp. 3245–3248, July 2006.
- [22] N. Michishita and Y. Yamada, "A Novel Impedance Matching Structure for a Dielectric Loaded 0.05 Wavelength Small Meander Line Antenna," *IEEE International Symposium on Antennas and Propagation*, pp. 1347–1350, July 2006.



Harish Rajagopalan (S'03) received the B.E. degree from Government College of Engineering, Pune, India in Electronics and Telecommunications in August 2002, and M.S. degree from Auburn University, AL, USA in Electrical Engineering in June 2005. He is currently working toward the

Ph.D. degree at University of California, Los Angeles (UCLA). He has worked in the Antenna Research, Analysis, and Measurement Laboratory at UCLA under the direction of Prof. Y. Rahmat-Samii since July of 2005. His research interests include characterization of reflectarray elements, microstrip and reconfigurable antenna designs, bio-medical applications of electromagnetics and RFID systems.



Yahya Rahmat-Samii

(S'73-M'75-SM'79-F'85) received the M.S. and Ph.D. degrees in electrical engineering from the University of Illinois, Urbana-Champaign.

He is a Distinguished Professor, holder of the Northrop Grumman Chair in Electromagnetics, and past Chairman of the Electrical Engineering Department, University of California, Los Angeles (UCLA). He was a Senior Research Scientist with the National Aeronautics and Space Administration (NASA) Jet Propulsion Laboratory (JPL), California Institute of Technology prior to joining UCLA in 1989. In summer 1986, he was a Guest Professor with the Technical University of Denmark (TUD). He has also been a consultant to numerous aerospace and wireless companies.

He has been Editor and Guest editor of numerous technical journals and books. He has authored and coauthored over 750 technical journal and conference papers and has written 25 book chapters. He is a coauthor of *Electromagnetic Band Gap Structures in Antenna Engineering* (New York: Cambridge, 2009), *Implanted Antennas in Medical Wireless Communications* (Morgan & Claypool Publishers, 2006), *Electromagnetic Optimization by Genetic Algorithms* (New York: Wiley, 1999), and *Impedance Boundary Conditions in Electromagnetics* (New York: Taylor & Francis, 1995). He has received several patents. He has had pioneering research contributions in diverse areas of electromagnetics, antennas, measurement and diagnostics techniques, numerical and asymptotic methods, satellite and personal communications, human/antenna interactions, frequency selective

surfaces, electromagnetic band-gap structures, applications of the genetic algorithms and particle swarm optimization, etc., (visit <http://www.antlab.ee.ucla.edu/>).

Dr. Rahmat-Samii is a Fellow of the Institute of Advances in Engineering (IAE) and a member of Commissions A, B, J and K of USNC/URSI, the Antenna Measurement Techniques Association (AMTA), Sigma Xi, Eta Kappa Nu and the Electromagnetics Academy. He was Vice-President and President of the IEEE Antennas and Propagation Society in 1994 and 1995, respectively. He was appointed an IEEE AP-S Distinguished Lecturer and presented lectures internationally. He was a member of the Strategic Planning and Review Committee (SPARC) of the IEEE. He was the IEEE AP-S Los Angeles Chapter Chairman (1987-1989); his chapter won the best chapter awards in two consecutive years. He is listed in Who's Who in America, Who's Who in Frontiers of Science and Technology and Who's Who in Engineering. Professor Rahmat-Samii is the designer of the IEEE Antennas and Propagation Society (IEEE AP-S) logo displayed on all IEEE-AP-S publications. He has been the plenary and millennium session speaker at numerous national and international symposia. He has been the organizer and presenter of many successful short courses worldwide. He was a Directors and Vice President of AMTA for three years. He has been Chairman and Co-chairman of several national and international symposia. He was a member of the University of California at Los Angeles (UCLA) Graduate council for three years.

For his contributions, Dr. Rahmat-Samii has received numerous NASA and JPL Certificates of Recognition. In 1984, he received the Henry Booker Award from URSI, which is given triennially to the most outstanding young radio scientist in North America. Since 1987, he has been designated every three years as one of the Academy of Science's Research Council Representatives to the URSI General Assemblies held in various parts of the world. He was also invited speaker to address the URSI 75th anniversary in Belgium. In 1992 and 1995, he received the Best Application Paper Prize Award (Wheeler Award) for papers published in 1991 and 1993 IEEE Transactions on Antennas and

Propagation. In 1999, he received the University of Illinois ECE Distinguished Alumni Award. In 2000, Prof. Rahmat-Samii received the IEEE Third Millennium Medal and the AMTA Distinguished Achievement Award. In 2001, Rahmat-Samii received an Honorary Doctorate in physics from the University of Santiago de Compostela, Spain. In 2001, he became a Foreign Member of the Royal Flemish Academy of Belgium for Science and the Arts. In 2002, he received the Technical Excellence Award from JPL. He received the 2005 URSI Booker Gold Medal presented at the URSI General Assembly. He is the recipient of the 2007 Chen-To Tai Distinguished Educator Award of the IEEE Antennas and Propagation Society. In 2008, he was elected to the membership of the National Academy of Engineering (NAE). In 2009, he was selected to receive the IEEE Antennas and Propagation Society highest award, Distinguished Achievement Award, for his outstanding career contributions. Prof. Rahmat-Samii is the designer of the IEEE AP-S logo which is displayed on all IEEE AP-S publications.

A Reliable Approach for Evaluating the Platform Tolerance of RFID Tag Antennas

Li Li^{1,2,3} and Raj Mittra³

¹ Electromagnetic Communication Laboratory, Communication University of China
1307 Yifu Bldg, Communication University of China, Beijing, 100024 China

² Information Engineering School, Communication University of China
1st Floor Main Bldg, Communication University of China, Beijing, 100024 China
racky@cuc.edu.cn

³ Electromagnetic Communication Laboratory, Pennsylvania State University
319 EE East, University Park, PA 16802 USA
rajmittra@ieee.org

Abstract—This paper describes a novel approach for evaluating the performance of an RFID tag on the basis of the simulation of its input impedance. A systematic and reliable approach to compute the impedance is presented and the platform tolerance characteristics of two tags are investigated on the basis of the variations of their input impedances.

Index Terms—Radio frequency identification (RFID), finite difference time domain (FDTD), planer inverse F antenna (PIFA) tag, meander tag, coax feed.

I. INTRODUCTION

Recent years have witnessed the use of Radio Frequency Identification (RFID) systems for a wide variety of applications, such as tracking and inventory control. The RFID reader uses the backscattered field from a tag, typically operating at or near the frequencies of 915MHz and 2.4GHz. Other frequencies, such as 125 kHz and 13.56 MHz, are also used in some systems, which rely on near-field communication technology [1-2]. The system is comprised of a reader, which includes an antenna, and the tag (also referred to as a transponder) that contains the tag antenna and a chip which stores the ID data. The antenna is

designed to have an impedance which is different from the usual 50 Ω , so that it can provide a conjugate match to the chip impedance, which usually has a small resistive part accompanied by a relatively large reactance, typically 140 Ω , or even higher.

An important attribute as well as performance metric of an RFID tag is its read range. Typically we use the modified Friis equation below to compute the read range,

$$r = \frac{\lambda |a_r \cdot a_t|}{4\pi} \sqrt{\frac{EIRP G_t G_r (1 - |\Gamma_t|^2) (1 - |\Gamma_r|^2)}{P_{th}}}, \quad (1)$$

where, a_r and a_t are the polarization vectors of the reader and tag antennas, respectively, and λ is the wavelength of the operating frequency. EIRP stands for equivalent isotropically radiated power, (usually 4 W). G_t and G_r are the gains of the reader and tag antennas, respectively. Γ_t and Γ_r are reflection coefficients of the reader and tag antennas, respectively. P_{th} is the threshold of tag antenna, which is usually a design parameter of the tag chip.

When the tag is placed on different types of platforms, e.g., cardboard, plastic, glass or metal, the read range of the tag is affected, because its

resonant frequency, input impedance, gain, etc. vary with the change in its environment. In [3], the authors also state that: “The differential RCS of an RFID tag is an important parameter which determines the power of the modulated backscattered signal.” The differential RCS, in turn, can be affected by a change in the input impedance; hence, it is important to study the input impedance behavior of an RFID tag, especially when it is mounted on different platforms.

In this paper, we present a systematic approach for estimating the tolerance of a tag when its environment is modified. We show that this information, which is very helpful at the design stage of a tag, can be obtained in a reliable way — even when the tag is placed on different platforms — by estimating the impedance of the antenna. Conventional models of the feed used by most CEM codes render the impedance estimate to be highly sensitive to the geometry of the feed region. This is evidenced by the fact that different computational codes using different feed models often yield widely varying results. This is partly due to the fact that the real part of the input impedance of the tag is relatively small, and the slope of the reactance is large at the operating frequency of the tag. Regardless of the CEM codes used, the results for the impedances can be inaccurate when the impedance is evaluated in the feed region where the higher-order modes are present. Specifically, measuring the voltage and current directly at the feed point in the presence of the higher-order modes can corrupt the results and yield non-physical values for the input impedance, e.g., one with a negative real part for a passive tag.

Consider, for instance, the case of a PIFA tag fed with a short coax as shown in Fig. 1(a). The red line in the coax indicates the excitation point, while the voltage and current measurement points are marked in blue. Figure 1(b) shows that the

input impedance is non-physical above 970MHz, because the real part of the impedance is negative, most likely because of the presence of the higher-order modes. In this work, we employ a longer

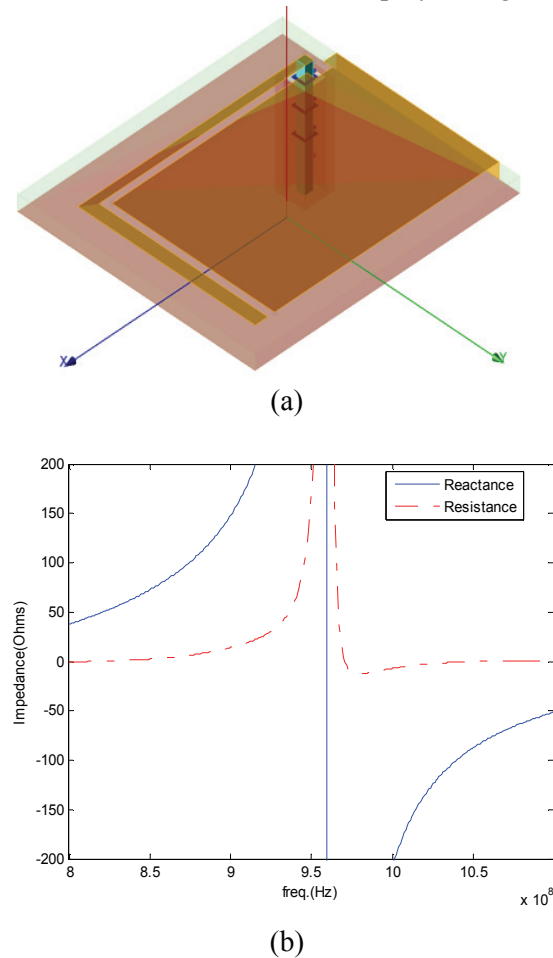


Fig. 1. Nonphysical results obtained when a short coax used to feed a PIFA tag: (a) Geometry of short coax feeding a PIFA tag; (b) Input impedance.

coax transmission line feed to obviate the above problem when computing the input impedance and evaluating the efficiency of power delivered to the chip embedded in the tag. Note that this alternate approach mimics the real-life measurement with a Vector Network Analyzer (VNA), and has been found to consistently yield realistic results.

We employ GEMS [4], a general-purpose EM solver, which has been parallelized for handling

complex EM problems in a time-efficient manner. As mentioned earlier, we use a coaxial line to feed the tag, as we would when measuring the return loss characteristic of a device using a VNA. We note that such a configuration is not handled easily by using the MoM-based commercial codes because of the nature of the Green's function used in the formulation of the numerical problem in such a code. Though the finite methods do not suffer from this drawback, they can, nonetheless, become burdensome in terms of CPU time and memory when modeling the tag-coax composite on a single PC. GEMS overcomes this problem by using a parallelized code, which scales with better than 90% efficiency, even on a large number of processors [4].

II. EVALUATION OF TAG IMPEDANCE USING A COAXIAL FEED

To evaluate the impedance of the tag we use the FDTD code to measure the voltage or current distributions along the feed line. Figure 2 shows a model of the structure simulated by using GEMS, where red indicates the outer part of the coax; the outputs of the voltage and current are plotted in blue; and black is the inner part of coax. The length of coax is chosen to be on the order of λ_{\max} of the frequency band of interest — typically, we choose this length to be at least $2/3\lambda_{\max}$ — so that we can capture at least one maximum and one minimum of the standing wave

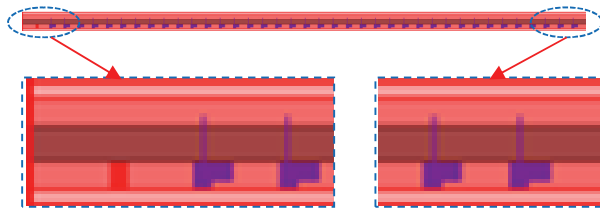


Fig. 2. Geometry of the longer coax simulated in GEMS with measurement points indicated in the figure. Coax' length is 200mm and the inner and outer diameters of the coax are 2mm and 5.08mm, respectively.

distribution in the coax. This enables us to evaluate the reflection coefficient of the TEM mode, without it being affected by the presence of the higher-order modes, which inevitably exist in the vicinity of the feed point.

The knowledge of Γ , the locations of the maxima and the minima of the standing waves, and the characteristic impedance Z_C of the coax enables us to compute the tag impedance by using the well known formulas, given below:

$$\Gamma = \frac{Z_L - Z_C}{Z_L + Z_C}, \quad (2)$$

where, Γ is reflection coefficient, and Z_L and Z_C are the load and characteristic impedances of the coax, respectively. Next, we obtain the SWR from:

$$SWR = \frac{V_{max}}{V_{min}} = \frac{I_{max}}{I_{min}} = \frac{1 + |\Gamma|}{1 - |\Gamma|}. \quad (3)$$

From (2) and (3), we can get

$$Z_L = Z_C \frac{1 + \Gamma}{1 - \Gamma} = Z_C \frac{1 + |\Gamma|e^{j\theta}}{1 - |\Gamma|e^{j\theta}}, \quad (4)$$

where, $\theta = \beta * d$ and d is the distance from load, and

$$|\Gamma| = \frac{SWR - 1}{SWR + 1}. \quad (5)$$

Note that from (4) we can obtain the Z_{Lmax} and Z_{Lmin} by setting $\theta=0$ and $\theta=\pi$, respectively. The relevant equations are:

$$Z_{Lmax} = Z_C \frac{1 + |\Gamma|}{1 - |\Gamma|} \quad (6)$$

$$Z_{Lmin} = Z_C \frac{1 - |\Gamma|}{1 + |\Gamma|}. \quad (7)$$

We can easily determine the locations of Z_{Lmax} and Z_{Lmin} , by determining the location of the voltage and current maxima along the coax, which yield d_{max} and d_{min} , respectively. Finally, we can drive Z_L by using

$$Z_L = Z_C \frac{Z_{Lmax} + j * Z_C \tan(-\beta d_{max})}{Z_C + j * Z_{Lmax} \tan(-\beta d_{max})} \quad (8)$$

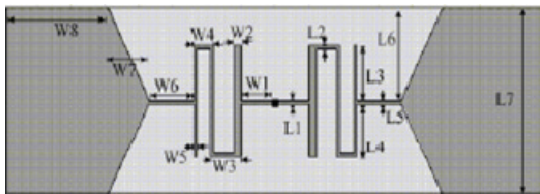
$$Z_L = Z_C \frac{Z_{Lmin} + j * Z_C \tan(-\beta d_{min})}{Z_C + j * Z_{Lmin} \tan(-\beta d_{min})}. \quad (9)$$

The sign of the phase is chosen to be negative because the origin of the coordinate system is

located at the load end. We can use (8) to compute the impedance if we utilize the voltage distribution, or (9) if we choose to employ the current distribution instead.

III. PLATFORM TOLERANCE STUDY OF TWO RFID TAGS

We will now present the results of the simulation of two different RFID tag antennas to illustrate the application of the approach for determining the tag impedance when we place the tags on different platforms. The two tags are: (i) PIFA [5], to which we add a loop near the feed point; and (ii) Meander Antenna [6], which is modified to render it to be more tolerant to the platforms by choosing its dielectric constant and thickness to be different from the one described in [6].



W1=4.5mm, W2=1mm, W3=4.5mm, W4=3mm, W5=0.5mm, W6=6.5mm, W7=6mm, W8=15mm, L1=0.5mm, L2=0.5mm, L3=7.25mm, L4=7.25mm, L5=0.5mm, L6=12.25mm, and L7=25mm.

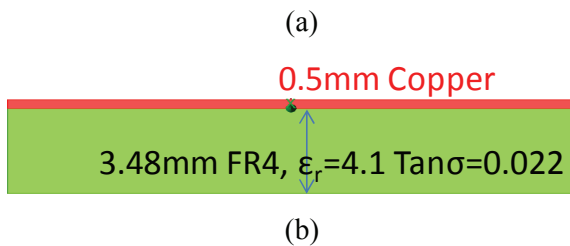
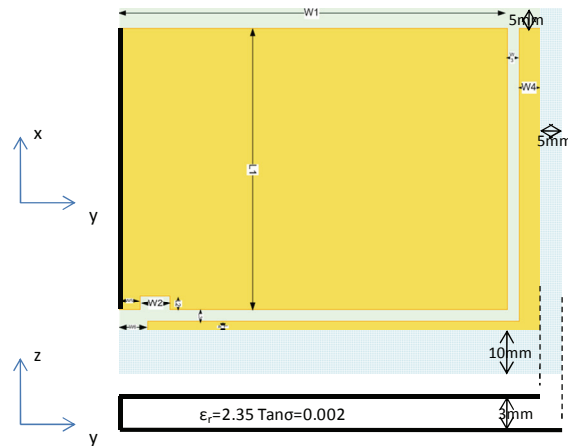


Fig. 3. Geometry of mender tag: (a) Top view; (b) Side view.

While placing the two tags on different types of materials, we introduce a 3 mm spacing between the tag and the material under test. Figure 5 shows the current distribution along the coax for the

PIFA. The vertical black and red lines indicate the locations of the ground plane and the dielectric substrate, respectively, along the coax for the PIFA case.



- L=56.3mm W1=53.2mm
- L1=38.5mm W2=4mm
- L2=2mm W3=1.6mm
- L3=1.5mm W4=3mm
- L4=1.3mm W5=3mm
- W=62.8mm W6=4mm

Fig. 4. Geometry of PIFA tag.

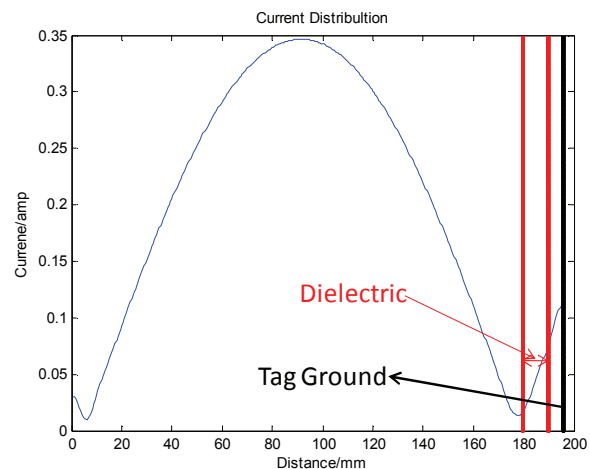
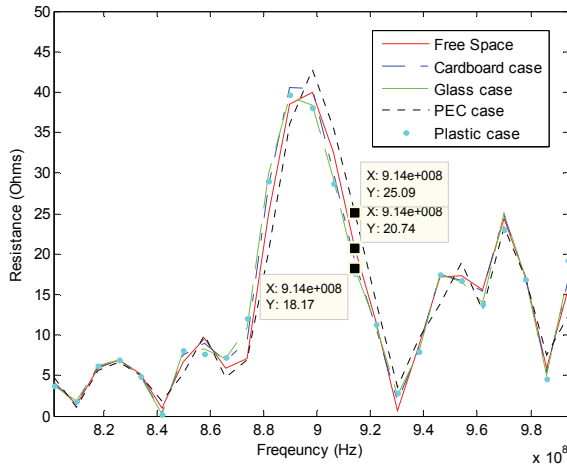
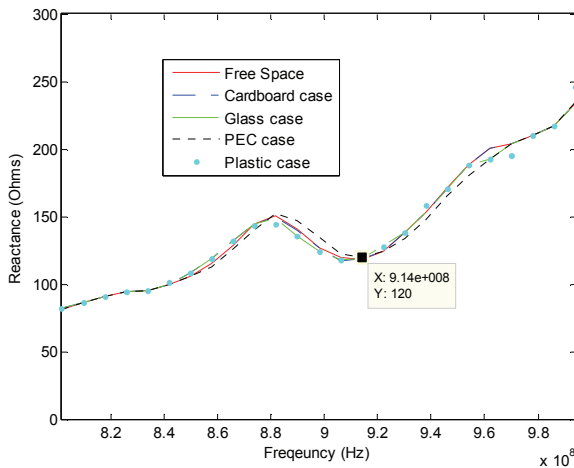


Fig. 5. Current distribution along longer coax fed for the PIFA tag.



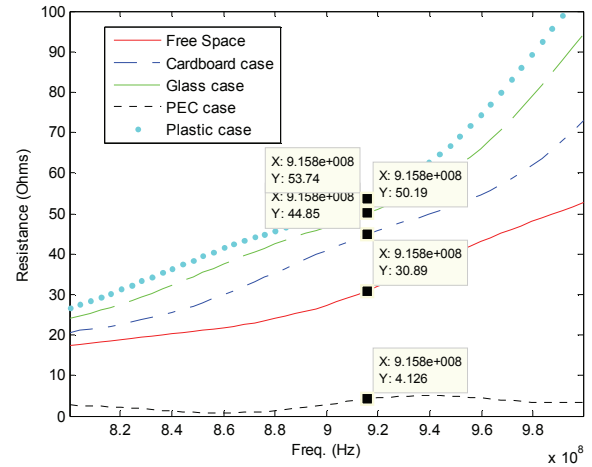
(a)



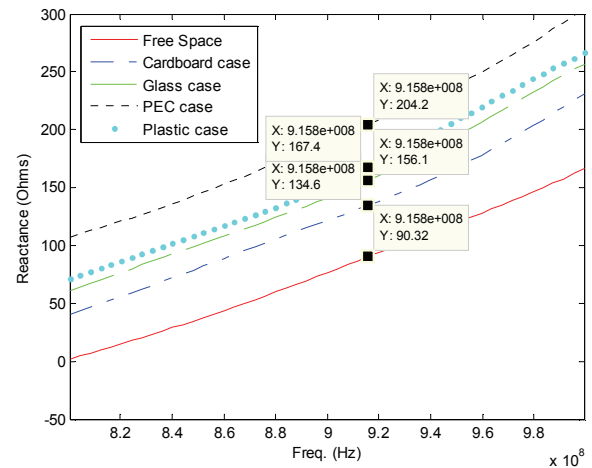
(b)

Fig. 6. Input impedance of PIFA: (a) Resistance; (b) Reactance.

The simulation results for the real and imaginary parts of the input impedance are presented in Figs. 6 and 7 for the PIFA and the Meander tag antennas, respectively. These figures show that the tag provide a good conjugate-match to the IC impedance when located in a free space environment, since the real and imaginary parts of their input impedance are approximately is 30ohms and 100ohms, respectively. we also note that both put on the PEC background, the FIPA tag performs much better than the meander tag antenna, when they are placed on different



(a)



(b)

Fig. 7. Input impedance of meander tag antenna: (a) Resistance; (b) Reactance.

platforms, including a metallic one (PEC case). Figure 8 presents the return loss (RL) characteristics of the tags, calculated as follows

$$Return Loss = 20 * \log_{10} \left(\frac{Z_A(f) - Z_C(f)^*}{Z_A(f) + Z_C(f)} \right), \quad (9)$$

where Z_A and Z_C are the impedances of the antenna and the chip, respectively, both of which are frequency dependent. The RL plots clearly show that the presence of the ground underneath plays a critical role in shielding the tag from the material

below, and that the two tags perform differently from this perspective.

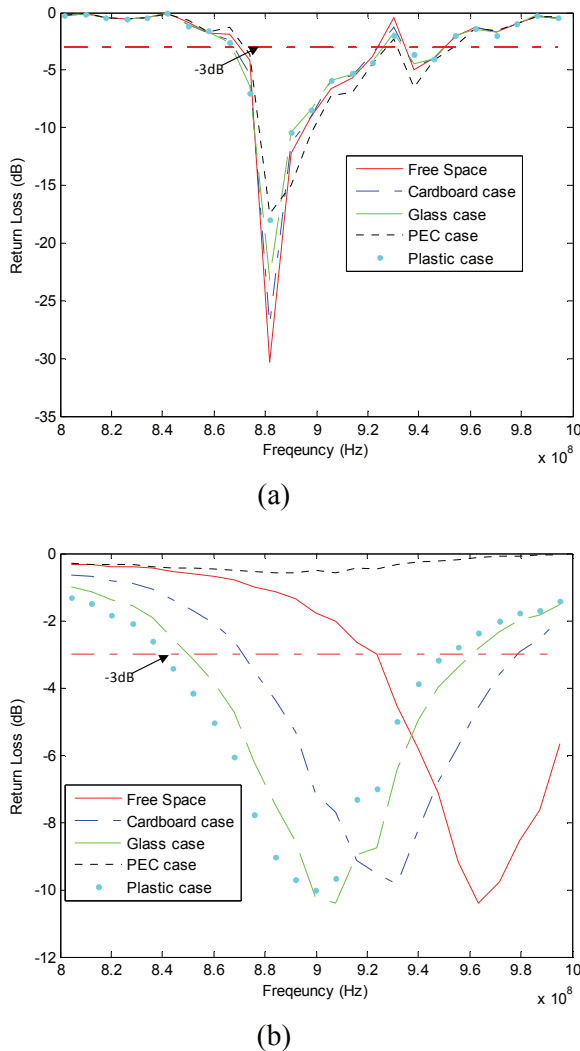


Fig. 8. Return Loss Characteristics of two tag antennas: (a) PIFA; (b) Meander tag.

IV. DISCUSSION OF RESULTS AND CONCLUSIONS

The platform tolerance of two types of tags have been investigated in this paper by using a novel simulation technique, described herein, which yields reliable and physically acceptable results for the input impedance, free of higher-order mode effects that are excited in the vicinity of the feed, and corrupt the impedance derived.

The simulation technique has been designed to mimic VNA measurements by using a coaxial line feed of sufficient length, rather than relying upon the conventional method of sampling the voltage and current at the feed point to compute the input impedance. Although the simulation could have been carried out by using either an FEM or MoM code, we have chosen to use a parallel version of the FDTD code, namely GEMS, because its superior ability to handle large, complex and multiscale problems over serial codes. We have found that when the meander tag, which has no ground plane, is placed on cardboard ($\epsilon_r=2.5$), glass ($\epsilon_r=3.8$), and plastic ($\epsilon_r=4.7$) [7], it performs reasonably well, its return loss remains below -3dB, and its impedance provides a good conjugate match the IC of chip of choice. However, this is no longer true when the same tag is placed on a metallic object. The tag performance is found to deteriorate significantly in this case, as may be clearly seen from Fig. 7a. In contrast to this, the PIFA tag continues to work well (see Fig.7b), not only when it is placed atop the three materials mentioned above, (cardboard, glass and plastic), but also when it is located above a metallic object, and its return loss remains better than -3dB for all of these scenarios. The PIFA exhibits a superior platform tolerance as compared to the Meander antenna because the former has its own built-in ground plane, which is larger than the footprint of the PIFA antenna itself by about $5*5*10$ mm (see Fig.4). However, despite its larger dimensions, the improved performance of the PIFA antenna, described herein, justifies its use in preference to the Meander tag, especially in situations where the platform tolerance feature is important.

ACKNOWLEDGMENT

This work was partly supported by the 111 Project (B 08042) and Beijing Municipal Natural Science Foundation (4092039). While this

research was conducted, Li Li was in the Electromagnetic Communication Laboratory, Pennsylvania State University, University Park, PA 16802, as a visiting scholar.

REFERENCES

- [1] P. V. Nikitin, K. V. S. Rao, and S. Lazar, "An Overview of Near Field UHF RFID," *IEEE International Conference on RFID*, March 2007.
- [2] V. Chawla and D. Sam Ha, "An overview of passive RFID," *IEEE Applications & Practice*, Sep. 2007.
- [3] P. V. Nikitin, K. V. S. Rao and R. D. Martinez, "Differential RCS of RFID tags," *Electronics letters* vol. 43, no. 8, April 2007.
- [4] GEMS website: www.2comu.com.
- [5] M. Hirvonen, K. Jaakkola, P. Pursula, and J. Saily, "Dual-Band Platform Tolerant Antennas for Radio-Frequency Identification," *IEEE Trans. Antennas Propagat.*, vol. AP-54, no. 9, pp. 2632-2637, Sept. 2006.
- [6] S. -J. Wu and T. -G. Ma, "A passive UHF RFID Meandered Tag Antenna with Tuning Stubs," *Asia-Pacific Microwave Conference (APMC)*, Dec. 2006.
- [7] A. S. Hoenshel, "A Parametric Study on the Platform Tolerance of RFID Tag Antennas and Their Performance Enhancement with Artificial Magnetic Conductors" *M.S. Thesis*, Pennsylvania State University, 2007.

Importance of Computational Electromagnetic Modeling in the Development of RFID Tags for Paper Reel Identification

Leena Ukkonen¹, Toni Björninen¹, Lauri Sydänheimo¹, Atef Elsherbeni², and Fan Yang²

¹ Tampere University of Technology, Department of Electronics, Rauma Research Unit, Kalliokatu 2, 26100 Rauma, FINLAND

leena.ukkonen@tut.fi, toni.bjorninen@tut.fi, lauri.sydanheimo@tut.fi

² Department of Electrical Engineering

University of Mississippi, University, MS 38677-1848, USA

atef@olemiss.edu, fyang@olemiss.edu

Abstract— Development of the RFID tag for paper reel identification in industrial environment is discussed. Paper reel supply chain and history of the development of the presented antenna design is explained. Modeling of the paper reel tag is discussed and a case study of tag antenna – paper reel co-design is presented.

Index Terms— UHF RFID, paper reel identification, tag antenna design.

I. INTRODUCTION

As the use of passive ultra-high frequency (UHF) radio frequency identification (RFID) systems emerges also the number of challenging applications increases. One of the most challenging applications for passive UHF RFID systems is identification of industrial paper reels. In paper industry there is a need for an automated identification system that would carry on the identification code of a specified reel throughout its life cycle. Nowadays when barcode identification systems are used in paper reel identification the identification code disappears when the wrapping paper and the barcode are removed. On the contrary, the RFID tag would be attached on the core of the reel and thereby the reel would be identifiable throughout its life cycle as long as the reel is in use. Since the tag will be attached on the core of the reel the tag has to be read through paper which attenuates the electromagnetic wave. As a dielectric material, paper also affects the electrical dimensions of the tag antenna design [1, 2]. Typically, the dielectric constant (ϵ_r) of paper varies from 2 to 4 [2] based on the paper quality and environmental conditions.

Thereby, the challenges in paper reel identification are due to the functioning principle of passive UHF RFID systems, the attenuating properties of paper and also the fact that the paper reel should be identified omnidirectionally [3].

Figure 1 presents the components of a passive UHF RFID system. Passive UHF RFID systems use electromagnetic waves in coupling and communication between reader unit and tag. The reader sends a continuous wave (CW) signal to the tag to activate its microchip, followed by commands that are modulated to the CW signal. The tag responds with its identification code using backscattering of the modulated electromagnetic wave. There is no internal source of energy in the tag's microchip, and it gets all the energy it needs to function from the electromagnetic wave transmitted by the reader.

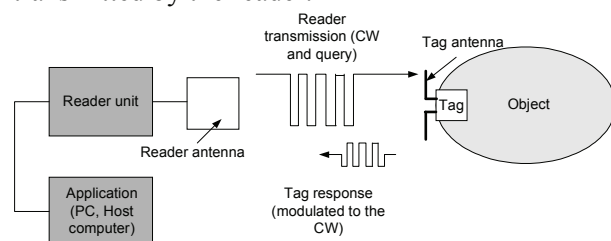


Fig. 1. Components of a passive UHF RFID system.

The communication between the reader and the tag is achieved by the tag switching its load impedance, which modulates the radar cross section (RCS) of the tag. The RCS of a scattering target is the equivalent area of the target based on the target reradiating or scattering the incident power. RCS can be described as a representation of how effectively a target can scatter the incident

power. Therefore, the RCS of a target is not necessarily equivalent to its physical size.

When the target is a loaded antenna, such as a tag antenna with an integrated circuit (IC) chip, the RCS can be altered by terminating the antenna with different load impedances. Typically, in RFID tags, the impedance of the IC chip is altered between matched and mismatched states. In the matched state the input impedance of the tag antenna and the IC chip are complex conjugate matched and therefore maximum power is transmitted through the antenna to the IC chip. In the mismatched state the impedance of the IC chip and the tag antenna are not complex conjugate matched and therefore the electromagnetic wave from the reader antenna will be reflected back. This way the tag's binary identification code is modulated and scattered back to the reader unit. The modulating depth of the RCS also affects the tag's read range: deeper RCS modulation results in longer read range [4, 5]. This may be essential in the most challenging applications, such as in paper reel identification, where significant backscattered signal attenuation is present.

In most cases the limiting factor for the read range achieved with passive UHF RFID systems is the amount of power delivered to the IC chip, i.e. the threshold power of the tag. In the case of paper reel identification, this requirement becomes crucial due to the attenuating properties of paper.

In terms of electromagnetic modeling and tag antenna design, paper reels are complex objects due to varying material properties and boundaries within the object. To verify the performance of the paper reel tags in industrial environment, the tags have to be tested and characterized at the paper mill. Before paper mill testing, the tags are tested in the laboratory environment with a suitably sized test paper reel. In this process electromagnetic modeling plays a paramount role. It is crucial in optimizing the paper reel tag parameters before moving on to laboratory and field testing. However, there are always some non-idealities when modeling results are applied in practice. Challenges also arise from the three-dimensional curved structure of the paper reel where the tag has to be embedded. In addition, the input impedance of the RFID IC is frequency dependent. Therefore, studying and developing the modeling methods for tag antennas is important.

In this paper we present the modeling based design process of a tag antenna for paper reel identification. The rest of the paper is organized as follows: Section II presents the paper reel supply chain. Section III concentrates on the requirements for the paper reel tag and Section IV presents the history of paper reel tag development. Modeling of the paper reel tag is discussed in Section V. Section VI presents the paper reel tag performance characterization results. Finally, conclusions are presented.

II. PAPER REEL SUPPLY CHAIN

The paper reel supply chain from the paper mill to the end user includes several stages. An example of a supply chain of paper reels is presented in Fig. 2 [3, 6]. The need for identification starts after the slitter machine where each reel is cut out from the parent reel and trimmed to have a specified width and web length. Nowadays, when barcode identification systems are used, the first barcode label is affixed on the other end of the reel core after the reel comes out from the slitter machine. This barcode includes the 14-character reel identification number. The identification numbers are given for each reel when the specific reel widths and other parameters of the reels are planned. The information about the reel – width, weight, paper quality etc. – are connected to the reel identification number and stored in the database. After the slitter machine, the reel is automatically carried forward to the packing plant using conveyor belts.

In the packing plant the reel is shielded using wear-resistant and waterproof wrapping paper. The wrapping paper is carefully folded around the reel and over the inner end disk which is a corrugated board disk that is shielding the ends of the reel. After that, the outer end disk is fixed. Nowadays when barcode systems are used in paper reel identification labels including such information as the weight of the reel, paper quality, length of the wound paper, manufacturer mill, reel width and diameter, reel identification number and the corresponding barcode are affixed on the outer surface of the reel. The label can also indicate the paper reel clamp pressure which can be used when the reel is lifted with a clamp truck. This information is also saved to a database with the barcode information and the identification number of the reel. Normally two labels are

attached on the reel: one on the other end of the reel and one on the belly of the reel. After this phase the reel is carried forward to the warehouse using conveyor belts.

Paper reels are normally stored at the mill and at their end destination. In some cases on the way from the mill to the end user, the reels are stored by middlemen: stockists, export merchants and wholesalers. Warehousing should be efficient and the reels should be stored in the warehouse or in the pressroom so that each reel is readily available in the first in – first out principle so that the stock turnover can be followed. Electronic warehouse management systems are used for optimizing the rotation of the stocks and the storage plan.

In many countries paper reels are transported on roadways using trucks or on railways. Road and railway transportation is also used for carrying reels from the mills to the sea ports. Occasionally the reels are delivered directly from the mill to the ship and from the ship to the end user. At the end user location, for example inside the printing house, automated guided vehicles (AGV) carry out the feeding of paper reels for continuous printing machines.

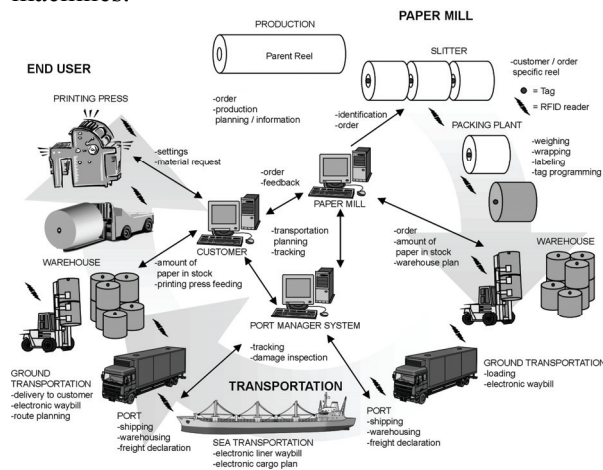


Fig. 2. Paper reel supply chain [6].

As the above explanation shows the environments in the paper reel supply chain are various and the physical properties of each of the identification points are also different. This sets a number of challenges for the use of passive UHF RFID systems in this application. For example, multipath propagation in the reflective paper mill environment may affect the identification of paper reels. In addition, to guarantee effective automatic

identification, the reels should be identified with paper reel clamp-integrated readers and reader antennas. This is challenging for both the performance requirements of the paper reel tag and the functioning of clamp-integrated reader antennas.

III. REQUIREMENTS FOR THE PAPER REEL TAG

To ensure identification of paper reels throughout the supply chain and also at the end user, the safest place for the paper reel tag would be on the outside surface of the reel core under the wrapped paper. This way the tag will remain non-tampered even if the reel would be lifted with a shaft that goes through the hollow reel core. With proper antenna design, the tag can be read efficiently through the thick paper layer. The effects of paper layer – attenuation of the electromagnetic wave [7], dielectric lens effect [8], effect on the wavelength and thereby the dimensions of the tag antenna [9] – have to be taken into account in the tag antenna design process.

The most crucial requirement for RFID systems to be used in paper reel identification is the omnidirectional reading of the tag on the reel core. The structure of the paper reel and the tag placement on the reel are presented in Fig. 3. The required omnidirectional reading means, that tag has to be readable 360 degrees around it in the xy-plane, when the coordinate system is fixed as shown in Fig. 3. This requirement is based on the automation systems within the supply chain of the paper reels. Paper reels are handled with paper reel clamp trucks and where the omnidirectional reading is essential: the truck driver has no way of knowing the direction of the tag on the reel core and the driver has no time to drive around the reel to find the tag's direction [3].

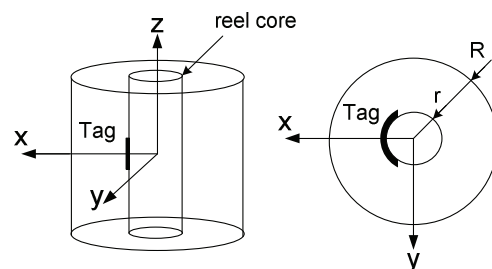


Fig. 3. Tag antenna placement on the reel core.

In addition to omnidirectional reading, there is a read range requirement for the paper reel tag. To be applicable within the supply chain, the read range of a paper reel has to be at least 1.5 m measured from the center point of the reel. Of this distance, usually 0.5-0.6 m is paper and the rest is air. Computational electromagnetic modeling plays an important role in optimization of the omnidirectional reading properties and maximizing the read range.

In addition, the paper reel tag has to be globally operable, and therefore its bandwidth should cover the frequency band used with passive UHF RFID systems (860 – 960 MHz). Also, to enhance global usage the tag's microchip should support general standardization. For this research we have used EPC Gen 2 –based microchips.

IV. HISTORY OF PAPER REEL TAG DEVELOPMENT

The lack of suitable paper reel tag has prevented RFID systems from being used in paper industry applications. Research work for developing a suitable tag has been going on since 1980s. A suitable paper reel tag should have an application specific antenna design and small and sensitive enough microchip. Therefore, the biggest challenge in this application has been the development of an omnidirectional tag antenna which provides long enough read range with a suitable microchip.

Measurements to characterize the attenuation properties of paper reels were carried out and the requirements of the UHF RFID system from the electromagnetic viewpoint were also studied.

Around the world several organizations have also worked on identification of paper reels with RFID systems. Technical Research Center of Finland (VTT) did research on passive bow-tie tag for paper reel identification in Palomar project. Also this tag antenna design was aimed for broadband operation. Ipico has published a paper reel identification system, which uses two different frequencies and coupling methods (125 kHz and 6.78 GHz). Challenges in using this system arise from using two different frequencies, which requires microchips and reader units which are specifically designed for this system. In 2006 PowerID brought into market a battery assisted ForReel tag (nowadays called a PowerR tag). Battery assisted tags are more expensive than

purely passive tags, and the durability of the battery in the environmental conditions of the paper reel supply chain has to be taken into account. Also active RFID systems have been tested in paper reel identification. The price of active tags has been the limiting factor for their widespread use in this application. In practice, active tags can be inserted to cores which are recycled to be used again in the supply chain. In this case the core material can be for example aluminum instead of paperboard materials that are normally used.

In the early stage of the research on paper reel identification different frequency bands and coupling methods were tested. In addition to passive UHF RFID systems, passive 13.56 MHz systems based on inductive coupling were studied. At lower frequencies the electromagnetic wave propagates through attenuating material with lower losses, but the large size of the reader antenna, which was impractical in the application environment, and too short read range restricted the use of these systems in this application.

In 2002 a research project called Electronic Supply Chain Identification with Passive RFID Systems (eSCID) was started at Tampere University of Technology, Department of Electronics. One of the main research topics of this project was paper reel identification with passive UHF RFID systems. The research was started by studying the identification of broadband tags through a paper layer [9]. Promising results were achieved and the tag antennas were further developed with modeling and measurements. The results also showed that reading a passive UHF RFID tag through a thick paper layer with sufficient read ranges is possible.

However, the biggest challenge – developing an omnidirectional tag – was still unsolved. Idea of a tag antenna which would be mounted around the reel core lead to breakthrough in development of the omnidirectional tag. The original idea was C-330 tag. The name of the tag was based on its shape: it was to cover 330 degrees of perimeter of the reel core and its mounted shape resembled a letter C. However, in the early stage of the research work the results were not as good as expected. Therefore, the tag antenna design was further developed and the C-180 tag antenna was the result of this research work. It covers 180 degrees of perimeter of the reel core. The first

omnidirectional reading of a paper reel with the C-180 tag took place in 2005. This breakthrough proved that passive UHF RFID systems can be used in paper reel identification.

In 2006 a new research project, Global Paper Reel RFID (PapeRFID) was started with a wide support from Finnish paper industry. In this project, C-tag has been further developed to meet the requirements of the application, which are presented in Section III. In addition, other suitable tag antenna geometries have also been studied. For example, an array tag antenna for paper reels has been studied together with the University of Mississippi RFID research group. PapeRFID project was finished in April 2009. During this project, the C-tag has been tested within paper reel supply chain in various identification locations (paper mill, sea port, printing house) and with paper reel clamp-integrated reader antennas. In addition, the industrial manufacturing of the C-tag has already begun. The C-tag meets the requirements presented in Section III.

V. MODELING

Communication between an RFID tag and the reader unit is based on modulation of backscattering of the reader's CW signal from a loaded tag antenna. This type of system resembles a radar system with the difference that the echo signal carries object's identification information. Thus the communication principle of an RFID system differs from common wireless communication where the data carrying signal is fed to a transmitting antenna and received at the other end of the link with a receiving antenna.

However, since currently in the passive UHF RFID technology the energy scavenging of the tag limits the detection range, for the design purposes it is sufficient to consider the tag antenna as a receiving antenna, loaded with the impedance of the IC's energy scavenging state's impedance. Consequently the design goal is to tune the antenna impedance to the complex conjugate of the of the load impedance to maximize the power delivery to the IC and thereby to achieve the maximal detection range.

Another goal for the design of the paper reel C-tag, in addition to optimal impedance matching, was to tailor the desired omnidirectional radiation pattern for the antenna when it is attached to the reel core under the paper wrapped on top of it. In

general, when a tag antenna is mounted on an object, its pattern may differ significantly from its free-space pattern depending on the shape and materials of the object. Therefore co-design with the actual object is advisable. This co-design is also advantageous – and often necessary – for impedance matching of the antenna, since the nearby materials affect the antenna current and thus the impedance seen from its input terminals.

Most conveniently the previously discussed design goals are met by first selecting a suitable antenna geometry to produce the desired radiation pattern and then realizing the maximal power delivery to the IC by a matching network embedded in the antenna structure. If the area occupied by the matching network is small enough compared to the radiation elements of the antenna, its contribution to the radiation pattern is insignificant and the pattern adjustment and impedance tuning can be done separately.

The initial stage of the paper reel C-tag design followed the above-explained procedure. First different C-shaped geometries were tried and sufficient matching was found to be realizable with an embedded T-matching. After this initial stage computer simulations were conducted to predict the current distribution in the antenna structure and to characterize its radiation properties as well as to optimize its performance.

For the modeling of the C-tag we have used Ansoft High Frequency Structure Simulator (HFSS), which is a commercially available FEM-based full wave electromagnetic simulator. Results from different models are compared below to demonstrate the importance of an appropriate simulation model to design both, impedance matching and tailored radiation pattern for the tag.

In addition to the simulation of the antenna impedance, accurate knowledge of the load impedance, i.e. the IC's input impedance in its energy scavenging state, is crucial for the realization of the complex conjugate matching. Commonly the front-end section of an UHF RFID IC contains rectifier and voltage multiplication stages. This circuitry consists mainly of capacitors and diodes and consequently the input impedance of the chip is capacitive and depends on the frequency and input power. Typically the chip vendors either list this impedance at a few discrete frequency points in the operation band or provide an equivalent circuit model and related component

values for a continuous impedance model. The development of the C-tag has been done with various ICs, but in this article the design of impedance matching for Alien Higgs-3 IC is studied by simulations.

In this study the antenna is mounted on the reel core and paper is wrapped around it. The reel core itself is composed of dense cardboard and the paper is standard copy paper. In reality the amount of the paper can vary through the life cycle of the reel, but for the simulations 0.3 m paper layer on top of the antenna was assumed. In our case the tag antenna is in immediate contact with only these two materials and in addition to the antenna conductor they are the only materials, which were considered in the simulations.

The electrical parameters of paper are discussed in [27]. For the paper reel C-tag design the dielectric constant of paper and the loss tangent values were set to 3 and 0.01, respectively. Dielectric constant of reel core was assumed to be 4.0 and its loss tangent was set to 0.02. Since the thickness of the conductor layer is very small compared to the reel core and paper layer, it was modeled as finite conductivity boundary with the Copper conductivity $\sigma=58$ MS/m.

The configuration studied in this paper is a 6-inch reel core with radius $r \approx 0.09$, paper layer thickness 0.3 m, which corresponds to value $R \approx 0.39$ m, and paper reel height $H \approx 0.53$ m. All these parameters are shown in Fig. 3.

Figure 4 shows simulated impedance from five different models. First model (M1), with only the planar antenna structure in vacuum, is clearly a non-realistic scenario for our study. In the second model (M2) a finite sized reel core material brick is added as substrate for the antenna. In the third model (M3) a finite sized paper brick is included in the simulation model as a superstrate for the antenna. Fourth model (M4) is the same as the third one, but in this model paper bricks are placed on both sides of the antenna. In the fifth model (M5) the reel core and the paper layer are finite-sized cylinders and the antenna structure is placed on the cylindrical reel core. This model represents the most accurate reproduction of the application's physical setting.

To simplify the design process a planar model would be preferable, since it is faster to simulate and also easier create in any simulation software.

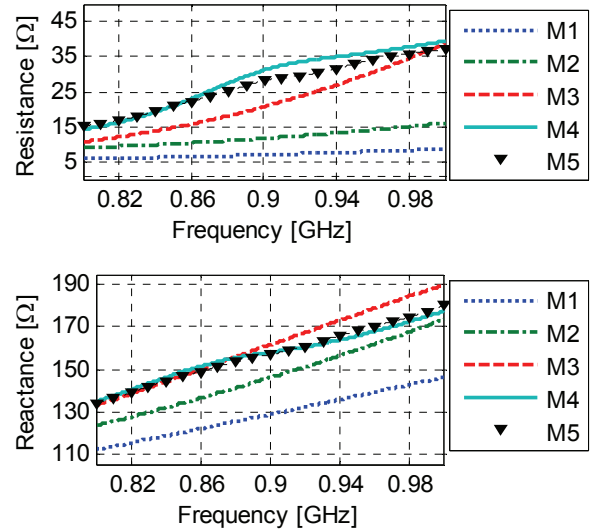


Fig. 4. Simulated antenna impedance from five different simulation setups.

Results in Fig. 4 indicate that only the planar model with reel core material (M4) and paper layers on both sides of the antenna would produce a result, which agrees reasonably well with the cylindrical model (M5).

Using a series equivalent circuit for the antenna and load impedances one can derive the power transmission coefficient τ as

$$\tau = \frac{4R_L R_A}{|Z_L + Z_A|^2}, \quad (1)$$

where $Z_A = R_A + jX_A$ and $Z_L = R_L + jX_L$ and subscripts A and L refer to *Antenna* and *Load* respectively. This quantity is the ratio of power delivered to the load and the power available for the load and it is bounded to the interval $0 < \tau \leq 1$. To predict the power transmission coefficient for the Alien Higgs-3 IC versus frequency we used the equivalent circuit model for the chip impedance provided by the manufacturer's website [0]. The equivalent circuit is a parallel RC-circuit with equivalent input parallel resistance $R_p = 1500 \Omega$ and equivalent input parallel capacitance $C_p = 0.85$ pF. The input impedance of the chip is related to these equivalent quantities through

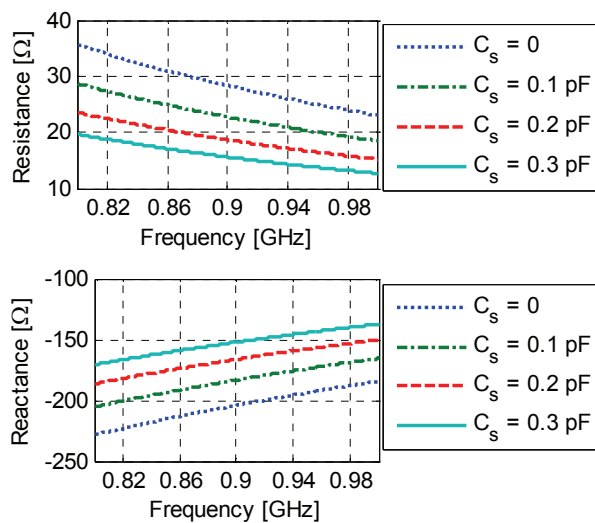
$$Z_{chip}(f) = \frac{1}{j2\pi f C_p + 1/R_p}. \quad (2)$$

This model is given at -14 dBm input power for the frequency range 860 MHz to 960 MHz, but our results are plotted from 800 MHz to 1000 MHz, yet keeping in mind that the prediction may become less reliable towards lower and upper end of the studied frequency band.

During the prototype testing we found that in our case the previous chip impedance model may predict too high operation frequency. Further inspections revealed that in the prototype tag, due to an imperfect connection between the antenna and the IC strap, also additional equivalent parallel stray capacitance (C_s) may be present. Indeed, adding also this effect into the chip impedance model yielded systematically better agreement between the simulations and measurements. In this augmented model the chip impedance is given by

$$Z_{chip2}(f) = \frac{1}{j2\pi f C_s + \frac{1}{Z_{chip1}(f)}}. \quad (3)$$

Figure. 5 shows the chip impedances using the stray capacitance model with different estimates for the capacitance value and Figs. 6 and 7 show the corresponding power transmission coefficients for different simulation schemes and stray capacitance values $C_s = 0$ and $C_s = 0.2$ pF



respectively.

Fig. 5. The effect of the stray capacitance to the input impedance of the IC chip.

Results in Figs. 5, 6, and 7 indicate that only the two most simplistic simulation setups; planar vacuum model and the planar reel core model, predict notably different power delivery compared to the other three setups, which all give quite similar predictions. Another observation is that the impedance model for the IC chip is sensitive for additional parasitic effects related to the chip attachment; in the presented example the augmented model with $C_s = 0.2$ pF shows already 50 MHz frequency shift in the operation frequency of the tag compared to the nominal model.

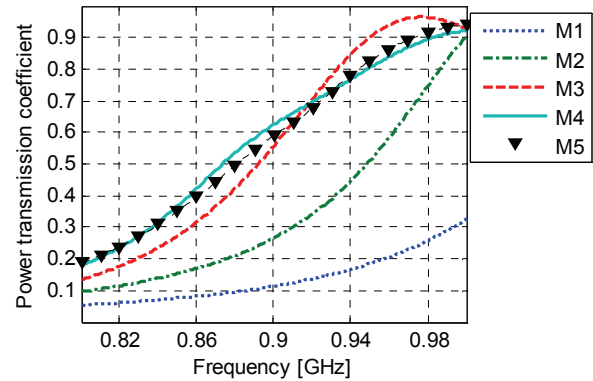


Fig. 6. Power transmission coefficient with an ideal antenna-chip connection ($C_s=0$).

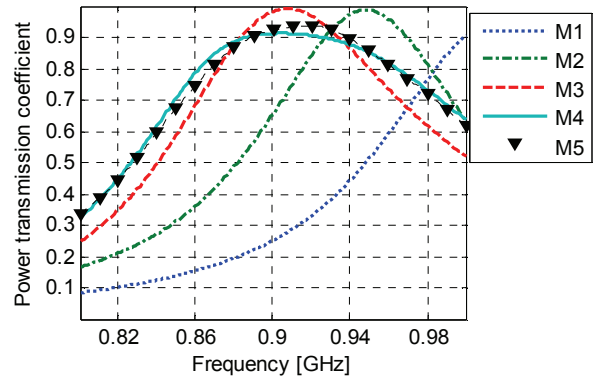


Fig. 7. Power transmission coefficient with stray capacitance value $C_s=0.2$ pF.

Figure 8 shows the simulated directivity pattern at 866 MHz with different simulation setups in the xy-plane as shown in the Fig. 3. 866 MHz frequency was chosen because it is the UHF RFID band center frequency in Europe and therefore suitable for comparison. Results are plotted using standard spherical coordinates, where 0°

corresponds to the direction of the positive x-axis and the angle 90° corresponds to the direction of the positive y-axis. Results in Fig. 8 show more variation between the different simulation setups than the simulated antenna impedances.

The two most simplistic setups; planar vacuum model and the planar reel core model yield an almost omnidirectional pattern cut, which is similar to a dipole H-plane. Planar simulation model with antenna on the reel core material slab and paper layer on top of it (red curve) has distinct maxima near ± 30 degrees and in the region 75 degrees to 285 the pattern oscillates between 0 and -5 dBi. The blue curve is obtained from a similar model as the red one, but in this model the paper layer is on both sides of the tag. This simulation setup does not predict the two maxima like the previously discussed model and the obtained directivities remain between 0 and -5 dBi for almost all observation angles. This result is already quite close to the most realistic scenario with the conformal tag model (black curve), but it can be seen that the result from the conformal model is smoother and predicts greater directivities especially in the forward direction. Therefore, when both the radiation pattern and the impedance matching are considered, the conformal simulation model seems to be a better choice than the other more simplistic models with planar geometry.

To provide an overview of the simulated radiation characteristics of the C-tag in a 6-inch reel core with 30 cm paper layer on the reel, the simulated directivity at four directions around the reel from the conformal model are plotted in the Fig. 9 at three different frequencies in the horizontal plane cut indicated in the Fig. 3. The selected frequencies in Fig. 9 are UHF RFID band center frequencies in Europe, North America and Japan, respectively. The simulated radiation efficiency at all these frequencies is 85%.

Directivity patterns in Figs. 8 and 9 suggest that the readability of the tag around the paper reel remains similar through the global UHF RFID frequencies. At all three frequencies of interest, there seems to be an asymmetry in the patterns, so that more radiation is directed to angles over 180 deg. This is explained by the feed network, which results to a slightly asymmetric current distribution shown in the Fig. 10. According to this result more current concentrates on the antenna structure on

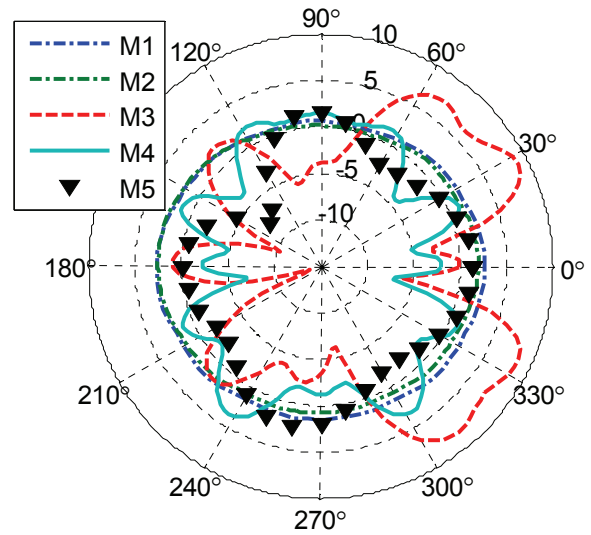


Fig. 8. Directivity [dBi] of the paper reel C-tag at 866 MHz in the xy-plane (as in Fig. 3).

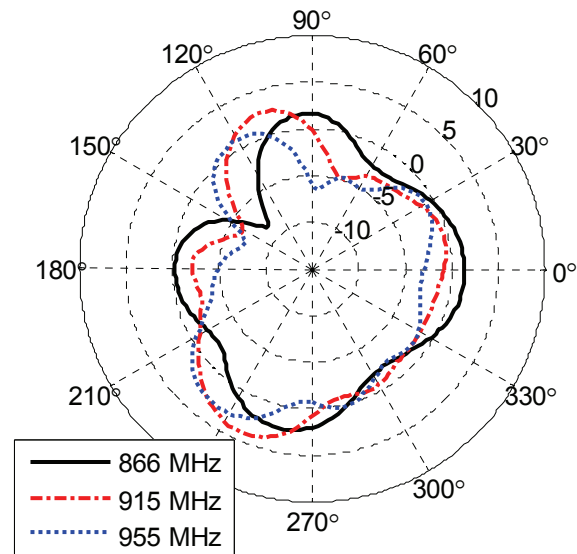


Fig. 9. Directivity [dBi] of the paper reel C-tag, from model M5 in the xy-plane (as in Fig. 3) at three different frequencies.

the feed point side than on the opposite side. Symmetric current distribution could be attained by introducing an asymmetry to the radiating structure on the right hand side of the split plane, or by using a symmetric matching structure instead of the T-matching network.

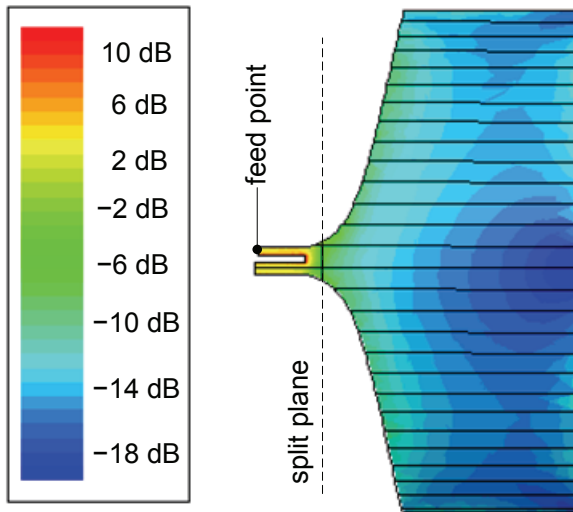


Fig. 10. Maximum surface current density distribution in decibels, normalized to the maximum value on the right hand side of the split plane.

VI. CONCLUSIONS

Requirements, design principles and modeling methods for an RFID tag antenna for industrial paper reel identification were discussed and the history of the C-tag antenna development was summarized. Electromagnetic modeling plays a key-role in the development of tag antennas for challenging objects, such as paper reels. The modeling results from the presented simulation case clearly support a careful co-design with the actual object, in this case mounting the antenna on a curved surface. Mounting and nearby materials affect the radiation pattern of the tag antenna. In addition, the realization of the chip-antenna connection can not be neglected in the design of the impedance matching.

ACKNOWLEDGMENT

This research has been funded by TEKES and the Academy of Finland.

REFERENCES

- [1] L. Ukkonen, L. Sydänheimo, and M. Kivikoski, "Identification of industrial paper reels with passive UHF RFID," *Proc. Pervasive 2006 Workshop "Pervasive Technology Applied - Real-World Experiences with RFID and Sensor Networks*, pp. 333 – 340, May 2006.
- [2] C. A. Balanis, *Advanced Engineering Electromagnetics*, John Wiley & Sons, USA, 1989.
- [3] A. Lehto, J. Nummela, L. Ukkonen, L. Sydänheimo, and M. Kivikoski, "Passive UHF RFID in Paper Industry: Challenges, Benefits and the Application Environment", *IEEE Transactions on Automation Science and Engineering*, vol. 6, no. 1., pp.66-79, 2009
- [4] C.-C Yen, A. E. Gutierrez, D. Veeramani, and D. van de Weide, "Radar cross-section analysis of backscattering RFID tags", *IEEE Antennas and Wireless Propagation Letters*, vol. 6, pp. 279-281, 2007.
- [5] L. Sydänheimo, J. Nummela, L. Ukkonen, J. McVay, A. Hoorfar, and M. Kivikoski, "Characterization of passive UHF RFID tag performance", *IEEE Antennas and Propagation Magazine*, vol. 50, no. 3, pp. 207-212, 2008.
- [6] M. Keskilammi, P. Salonen, L. Sydänheimo, and M. Kivikoski, "Antenna Demands for RFID Interface in Paper Reel Supply Chain", *Proc. IASTED International Conference on Robotics and Manufacturing*, pp. 99-104, May, 2001.
- [7] L. Ukkonen, L. Sydänheimo, and M. Kivikoski, "Radar Cross Section Modelling of RFID Tag Antennas for Paper Reel Identification", *Proc. 2nd European Conference on Antennas and Propagation*, November 2007.
- [8] J. Kataja, L. Ukkonen, M. Schaffrath, L. Sydänheimo, and M. Kivikoski, "Modelling the Effects of Stacked Paper on the Radiation Pattern of Bow-Tie RFID Tag Antennas", *Proc. IEEE Antennas and Propagation Society International Symposium with USNC/URSI National Radio Science and AMEREM Meetings*, pp. 3225-3228, July 2006.
- [9] M. Schaffrath, L. Ukkonen, L. Sydänheimo, and M. Kivikoski, "RFID Antenna Designs for Paper Industry Applications: Passive Bow-Tie-Transponder Performance Analysis", *Proc. 2nd IASTED International Conference on Antennas, Radar, and Wave Propagation*, pp. 348-353, July 2005.
- [10] http://www.epcglobalinc.org/tech/freq_reg/, last accessed July 2, 2009

- [11] Alien Technology, Higgs-3 RFID IC's datasheet, http://www.alientechnology.com/docs/products/DS_H3.pdf, last accessed July 2, 2009
- [12] M. Keskilammi, L. Sydänheimo and M. Kivikoski, "Radio wave propagation modeling in paper reel for novel radio frequency identification system JamC," Proc. IEEE on, August 2000.
- [13] M. Keskilammi, L. Sydänheimo and M. Kivikoski, "Modeling Electromagnetic Wave Propagation in Paper Reel for UHF RFID System Development", Proc. International Conference on Machine Automation (ICMA 2004), pp. 565-568, November 2004.
- [14] T. Varpula, "UHF, the new technology of remote identification", VTT Technical Research Center of Finland, <http://www.uudenmaanosaamiskeskus.fi/rfid/VTT%20VarpulaRFID%20Mikrotekniikka%202003b.pdf>, last accessed May 13 2009
- [15] IPICO Inc. Paper Reel Identification with IPICO's IPX DF Tags and Readers – Application Note, http://www.ipico.com/site/ipico/assets/pdf/PAPER_REEL_APPLICATION_NOTE_22_april_1.pdf, May 6, 2009.
- [16] PowerID Ltd. PowerR Datasheet, http://www.powerid.com/Data/pdf/PowerR_March09.pdf, accessed May 7, 2009.
- [17] M. Schaffrath, L. Ukkonen, L. Sydänheimo, and M. Kivikoski, "Novel Skew Bow-Tie, Skew Patch and Skew Sandglass Tag Antennas for RFID in Paper Reel Logistics", Proc. IEEE Antennas and Propagation Society International Symposium with USNC/URSI National Radio Science and AMEREM Meetings, pp. 3221-3224, July 2006.
- [18] M. Schaffrath, J. Kataja, L. Ukkonen, L. Sydänheimo, and M. Kivikoski, "Spread Bow-Tie Tag Antenna for Passive UHF RFID of Paper Reels", Proc. 2006 IEEE Antennas and Propagation Society International Symposium with USNC/URSI National Radio Science and AMEREM Meetings, pp. 3217-3220, July 2006.
- [19] L. Ukkonen, A. Yu, L. Sydänheimo, F. Yang, M. Kivikoski, and A. Elsherbeni "Analysis of Bow Tie Array RFID Tag Antenna for Paper Reel Identification", *Proc. IEEE Antennas and Propagation Society Symposium*, pp. 2745 – 2748, June 2007.
- [20] J. Nummela, L. Ukkonen, L. Sydänheimo, and M. Kivikoski, "Exploiting passive UHF RFID in paper industry - case study: end user", Proc. IEEE Conference on Automation Science and Engineering CASE 2008, pp. 436-441, August 2008.
- [21] J. Nummela, L. Ukkonen, and L. Sydänheimo, "Automatic Reel Identification in Paper Reel Supply Chain in Paper Mill and Sea Port Environments by Means of Passive RFID", *International Journal of RF Technologies*, ACCEPTED.
- [22] P. V. Nikitin, K. V. S. Rao, "Antennas and Propagation in UHF RFID Systems," RFID, 2008 IEEE International Conference on, pp.277-288, April 2008.
- [23] S. R. Saunder and A. Aragón-Zavala, *Antennas And Propagation for Wireless Communication Systems*, John Wiley & Sons, England, 2007.
- [24] G. Marrocco, "The art of UHF RFID antenna design: impedance-matching and size-reduction techniques," *IEEE Antennas and Propagation Magazine*, vol. 50, no. 1, pp.66-79, Feb. 2008.
- [25] <http://www.ansoft.com/products/hf/hfss/>, July 2, 2009.
- [26] G. De Vita and G. Iannaccone, "Design criteria for the RF section of UHF and microwave passive RFID transponders," *IEEE Transactions on Microwave Theory and Techniques*, vol. 53, no. 9, pp. 2978-2990, Sept. 2005.
- [27] S. Simula, S. Ikäläinen, K. Niskanen, T. Varpula, H. Seppä, and A. Paukku, "Measurement of the dielectric properties of paper", *The Journal of Imaging Science and Technology*, vol. 43, no.5, pp. 472-477, 1999.
- [28] K. V. S. Rao, P. V. Nikitin, and S. F. Lam, "Impedance matching concepts in RFID transponder design," 4th IEEE Workshop on Automatic Identification Advanced Technologies, pp. 39-42, Oct. 2005.



Leena Ukkonen received the M.Sc. and Ph.D. degrees in electrical engineering from Tampere University of Technology (TUT) in 2003 and 2006, respectively. She is currently working at the TUT Department of Electronics as Senior Research Scientist,

leading the RFID research group. She has authored over 60 publications in the field of RFID antenna design and industrial RFID applications.

Her research interests are focused on passive UHF radio frequency identification (RFID) antenna development for tags and readers.



Toni Björninen received the M.Sc. degree in electrical engineering from Tampere University of Technology (TUT) in 2009. He is now working as a researcher in the RFID research group at TUT Department of Electronics and studying towards his

Ph.D. degree in electrical engineering. His research interests include antenna technologies for RFID applications and modeling of electromagnetics. He has authored publications on passive RFID tags and application of printable electronics microwave applications.



Lauri Sydänheimo received the M.Sc. and Ph.D. degrees in electrical engineering from Tampere University of Technology (TUT). He is currently a Professor with the Department of Electronics, TUT, and works as the Research Director of Tampere University of

Technology's Rauma Research Unit. He has authored over 120 publications in the field of RFID tag and reader antenna design and RFID system performance improvement. His research interests are focused on wireless data communication and radio frequency identification (RFID).



Atef Elsherbeni is a Professor of Electrical Engineering and Associate Dean for Research and Graduate Programs, the Director of The School of Engineering CAD Lab, and the Associate Director of The Center for Applied Electromagnetic Systems

Research (CAESR) at The University of Mississippi. In 2004 he was appointed as an adjunct Professor, at The Department of Electrical Engineering and Computer Science of the L.C. Smith College of Engineering and Computer Science at Syracuse University. On 2009 he was selected as Finland Distinguished Professor by the Academy of Finland and TEKES. Dr. Elsherbeni has conducted research dealing with scattering and diffraction by dielectric and metal objects, finite difference time domain analysis of passive and active microwave devices including planar transmission lines, field visualization and software development for EM education, interactions of electromagnetic waves with human body, RFID and sensors development for monitoring soil moisture, airports noise levels, air quality including haze and humidity, reflector and printed antennas and antenna arrays for radars, UAV, and personal communication systems, antennas for wideband applications, antenna and material properties measurements, and hardware and software acceleration of computational techniques for electromagnetics. Dr. Elsherbeni is the co-author of the book "*The Finite Difference Time Domain Method for Electromagnetics With MATLAB Simulations*", SciTech 2009, the book "*Antenna Design and Visualization Using Matlab*", SciTech, 2006, the book "*MATLAB Simulations for Radar Systems Design*", CRC Press, 2003, the book "*Electromagnetic Scattering Using the Iterative Multiregion Technique*", Morgan & Claypool, 2007, the book "*Electromagnetics and Antenna Optimization using Taguchi's Method*", Morgan & Claypool, 2007, and the main author of the chapters "*Handheld Antennas*" and "*The Finite Difference Time Domain Technique for Microstrip Antennas*" in Handbook of Antennas in Wireless Communications, CRC Press, 2001. Dr. Elsherbeni is a Fellow member of the Institute of

Electrical and Electronics Engineers (IEEE) and a Fellow member of The Applied Computational Electromagnetic Society (ACES). He is the Editor-in-Chief for ACES Journal and an Associate Editor to the Radio Science Journal.



Fan Yang received the B.S. and M.S. degrees from Tsinghua University in 1997 and 1999, and the Ph.D. degree from University of California, Los Angeles (UCLA) in 2002. From 1994 to 1999, he was a Research Assistant in the State Key Laboratory of Microwave and Digital Communications, Tsinghua University, China. From 1999 to 2002, he was a Graduate Student Researcher in the Antenna Lab, UCLA. From 2002 to 2004, he was a Post-doc Research Engineer and Instructor in the Electrical Engineering Department, UCLA. In August 2004, he joined the Electrical Engineering Department, The University of Mississippi as an Assistant Professor and was promoted to Associate Professor in 2009.

Dr Yang's research interests include antenna theory, designs, and measurements, electromagnetic band gap (EBG) structures and their applications, computational electromagnetics and optimization techniques, and applied electromagnetic systems such as the radio frequency identification (RFID) system and concentrating solar energy system. He has published over 100 technical journal articles and conference papers, five book chapters, and two books entitled *Electromagnetic Band Gap Structures in Antenna Engineering* and *Electromagnetics and Antenna Optimization Using Taguchi's Method*.

Dr. Yang is a Senior Member of IEEE and was Secretary of IEEE AP Society, Los Angeles chapter. He is also a Full Member of URSI/USNC. Dr. Yang serves as the Associate Editor-in-Chief of the Applied Computational Electromagnetics Society (ACES) Journal. He is also a frequent reviewer for over twenty scientific journals and book publishers, and has chaired numerous technical sessions in various international symposiums. Dr. Yang was a Faculty Senator at

The University of Mississippi, and currently is a Member of the University Assessment Committee.

For his contributions, Dr. Yang has received several prestigious awards and recognitions. In 2004, he received the *Certificate for Exceptional Accomplishment in Research and Professional Development Award* from UCLA. Dr. Yang was the recipient of *Young Scientist Award* in the 2005 URSI General Assembly and in the 2007 International Symposium on Electromagnetic Theory. He was also appointed as The University of Mississippi *Faculty Research Fellow* in year 2005 and 2006. In 2008, Dr. Yang received the *Junior Faculty Research Award* from The University of Mississippi. In 2009, he received the inaugural IEEE Donald G. Dudley Jr. Undergraduate Teaching Award.

Space-Filling Curve Radio Frequency Identification Tags

John A. McVay¹, Ahmad Hoorfar² and Nader Engheta³

¹Eureka Aerospace
Pasadena, CA, 91067

²Department of Electrical and Computer Engineering
Villanova University, Villanova, PA 19085

³Department of Electrical and System Engineering,
University of Pennsylvania, Philadelphia, PA 19104

Abstract- Two different concepts for the use of resonant space-filling curves (SF-curves) elements as RFID tags are proposed. In the first concept the space-filling curve geometries such as Hilbert and Peano curves are studied with respect to the creation of an ultra-passive type of RFID in which an array of space-filling curve elements, scaled to resonate at different and particular frequencies, are used to provide a backscattered signal, in which information can be embedded. Using both numerical simulations and RCS measurement, it is shown that these electrically compact resonators could produce relatively large scattered fields over an inherently narrow frequency band at their corresponding fundamental resonant modes. The performances of these tags are also investigated when placed near a typical inventory objects, such as paper rolls. In the second concept, an SF-curve antenna is used above an SF-curve high impedance surface to develop an RFID tag that is well-suited for tagging of conducting objects.

Index Terms- RFID, passive tags, SF curves.

I. INTRODUCTION

In recent years, there has been considerable interest in the area of Radio Frequency Identification (RFID) and Radio Frequency Tagging (RFTAG). This emerging area of technology has a wide range of applications that include commercial inventory control in warehouses, supermarkets, hospitals as well as in military friend/foe identification to name but a few [1-2]. Most of these applications require low cost, thin-film printed antennas and sensors. The current

technology can be broken down into two main groups, namely passive and active RFID tags. In general, both active and passive tags utilize integrated circuits, with active tags utilizing a source, such as a battery. In passive RFID tags, the electrical current induced in the antenna by the incoming radio frequency signal provides just enough power for the integrated circuit (IC) in the tag to power up and transmit its response. Most passive tags emit signal by backscattering the carrier signal from the reader. This means that the antenna has to be designed to collect its power from the incoming signal as well as transmit the response signal. The lack of an onboard power supply means that the device can be quite small. Passive tags have practical read distances ranging from about 2 mm up to a few meters depending on the radio frequency and antenna design, type and/or size. Passive RFID tags can be much smaller and cheaper to manufacture than their semi-passive, which uses a small battery, and active counterparts and can have an almost unlimited life span. Majority of RFID tags in existence are of the passive variety.

This work explores the potential for utilizing the electrically small, resonant characteristics of space-filling curves (SF-curves) [3] for RFID technologies. An interesting property of a space-filling curve, such as Peano and Hilbert curves, shown in Fig. 1, is that, as the higher iteration-orders, n , of this curve are considered, a long "line" can be compacted into a small "surface" area. In general, the expressions relating total lengths, S_H and S_P , of the Hilbert and Peano curves to their corresponding side dimension, L , are:

$$S_H = \left(\frac{2^{2n} - 1}{2^n - 1} \right) L ; S_P = \left(\frac{3^{2n} - 1}{3^n - 1} \right) L . \tag{1}$$

From an electromagnetic point of view, such a curve may provide a structure that, although small in its footprint, can be resonant at a wavelength much longer than its footprint. Such a “compact resonator” can be quite useful in various applications in radiation and scattering problems. For instance, this feature is of interest to antenna designers since it provides a planar resonant radiator that can have a very small footprint as one considers the higher orders in iterative filling of a 2-D region [4-8]. These curves have also been utilized as inclusions to form high impedance ground-planes (HIGP), also known as artificial magnetic conductors (AMC) [11, 12].

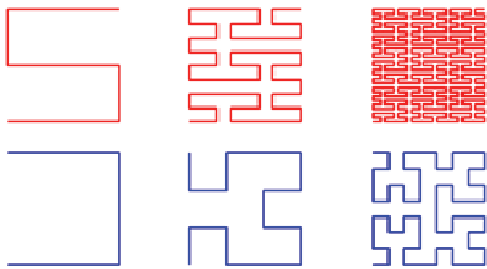


Fig. 1. First three orders of Peano (top) and Hilbert (bottom) space-filling curves.

In particular, we present two different concepts for the use of the SF-curves as RFID tags. In the first concept the space-filling curve geometries are studied with respect to the creation of an ultra-passive type of RFID in which an array of space-filling curve elements, scaled to resonate at different and particular frequencies, are used to provide a backscattered signal, in which information can be embedded. In the second concept, an SF-curve antenna [6, 8] is used above an SF-curve high impedance surface, or artificial magnetic conductor (AMC) [11, 12] to develop a tag that is well-suited for tagging of conducting objects, which, as it is well known, causes very poor performance when conventional RFID tags are used. Previous works [6, 8, 11, 12] have shown that for a given footprint the Peano of order 2 and the Hilbert of order 3, resonate approximately at

the same fundamental resonant frequency with a similar relative bandwidth, which is why, in this work, these two orders are often compared side-by-side.

II. PRINTED PEANO AND HILBERT ARRAYS FOR RFID TAGS

The “compact resonator” behavior of the Peano and Hilbert curves may allow for relatively small resonant passive tags with comparably large scattering characteristics. The relatively narrow bandwidth inherent to these geometries may prove useful in allocating the narrow resonances as the “spectral ID”. To investigate the scattering characteristics of these curves, a single element Peano curve of order 2 and single element Hilbert curve of order 3, both contained within a 30 mm x 30 mm footprint (linear side-dimensions), were studied in free-space under the influence of a normally-incident, uniform plane-wave excitation with varying frequency, utilizing a method of moments (MoM) code, NEC-4. The corresponding mono-static radar cross-section (RCS), as a function of frequency, and the scattering RCS patterns are shown in Figs. 2 and 3, for the Peano curve and the Hilbert curve element, respectively. Two different polarizations were studied corresponding to polarizations in the x and y-directions, E_x and E_y , respectively. As can be seen, both curves possess resonances dependent on the polarization of the excitation, and at the resonances, the scattering from the curves behave like resonant dipoles, and yet the 30 mm x 30 mm footprint which encloses these curves is electrically very small with respect to the resonant wavelengths. For the fundamental resonance corresponding to the y-polarized excitation, both the Peano and Hilbert curves have electrical footprints on the order of 0.07λ . Since the curves are smallest with respect to this first resonance, corresponding to the y-polarized electric field excitations, the primary focus of the work presented here will focus on this lowest resonance.

We now consider the space-filling curve geometries in creation of an ultra-passive type of RFID in which an array of space-filling curve elements, scaled to resonate at different and particular frequencies, are used to provide a backscattered signal, in which information can be embedded.

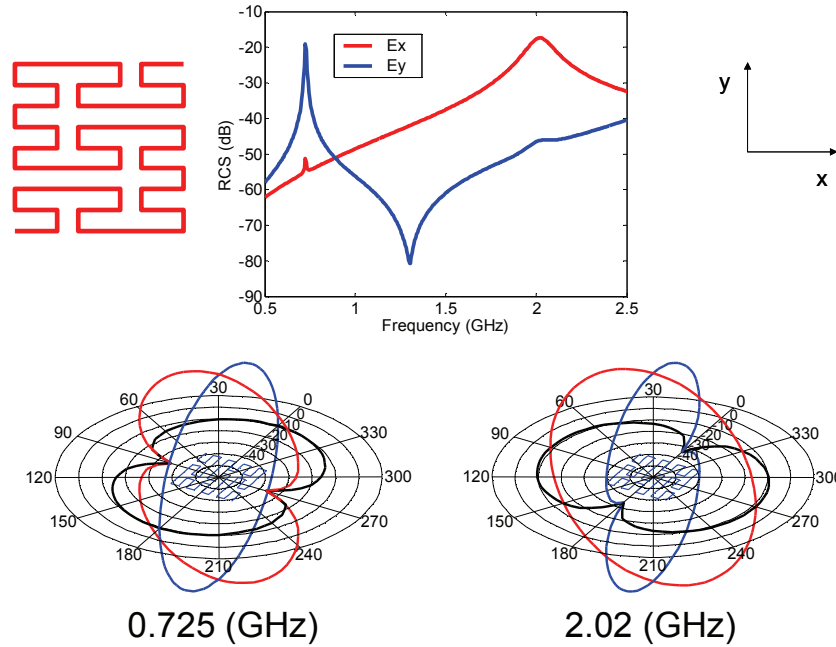


Fig. 2. Results of numerical simulations for scattering from a single Peano of order 2 element.

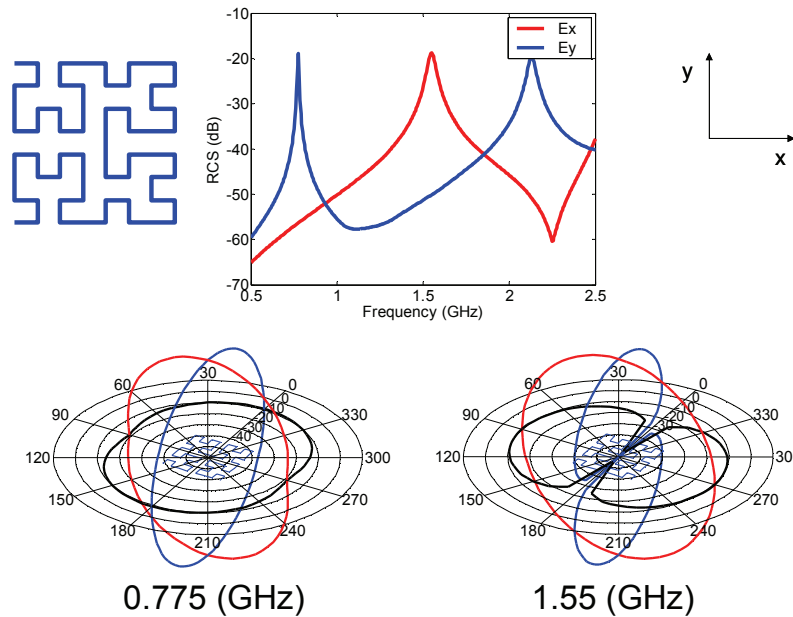


Fig. 3. Results of numerical simulations for scattering from a single Hilbert of order 3 element.

To illustrate a potential RFID tag application, a 5-element array of Peano and Hilbert curve scatterers, shown in the insets of Figs. 4-5 (Peano) and 6-7 (Hilbert), are examined, respectively. For the case of the Peano array, each element consists of a Peano curve of order 2 while in the cases of the Hilbert array, each element consists of a

Hilbert curve of order 3. Each element within the array is scaled to 95% of the physical size (e.g. footprint) of the element to its left and by using this scaling factor, each element in the array is designed to resonate at a separate and particular frequency. When illuminated with a normally incident plane-wave excitation, polarized in the x

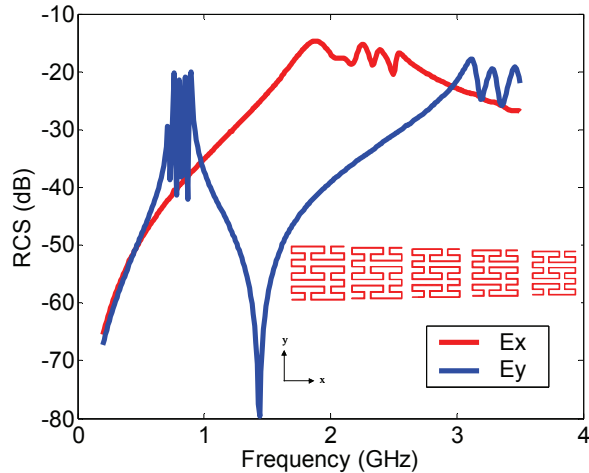


Fig. 4. Frequency signature for 5-element Peano RFID tag (inset) for both polarization excitations.

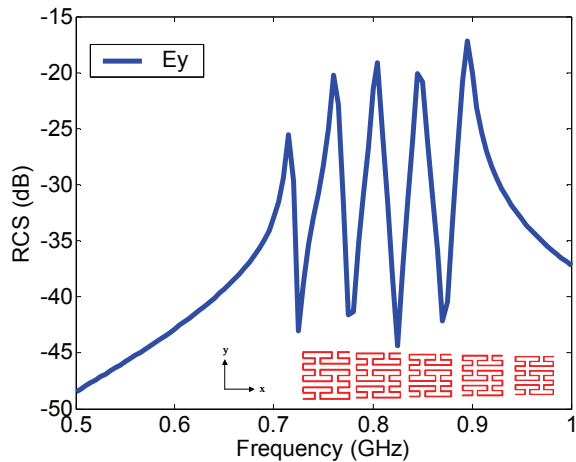


Fig. 5. Expanded (zoomed in) E_y frequency signature for 5-element Peano RFID tag, shown in inset.

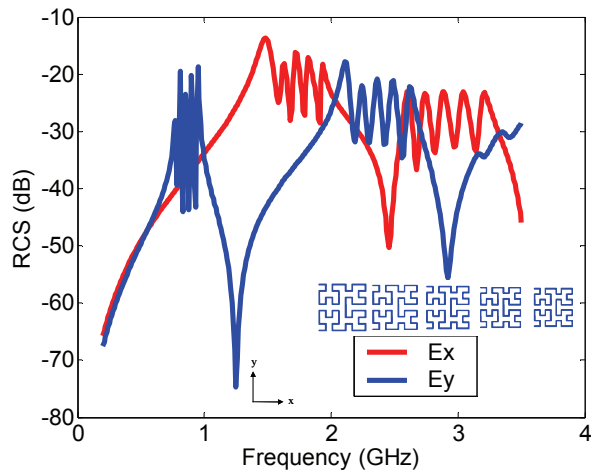


Fig. 6. Frequency signature for 5-element Hilbert RFID tag (inset) for both polarization excitations.

and y-directions separately (see Figs. 4 (Peano) and 6 (Hilbert)), these geometries give rise to the scattering shown in the respective figures. Multiple peaks in the Radar Cross Section (RCS) are evident and each peak corresponds to the resonance of a different element within the array. For this illustration, the arrays were designed to produce a mono-static RCS representative of the binary number 11111, where a peak in the RCS refers to a binary 1. It is in this manner that the Peano and Hilbert arrays are acting like a barcode, as is used in the optical regime, but instead the information is contained within the frequency response of the tag.

From Figs. 4 and 6 it is noted that the frequency response is different for both of these arrays, for the x-polarized and y-polarized incident fields used to excite these structures. For the x-polarized case, the elements in the arrays achieve resonance at higher frequencies and thus the element sizes are larger with respect to the operational wavelength. Also, since the higher order resonances possess a larger relative bandwidth, the total frequency spectrum occupied by the RFID tag is greater (e.g. less compact).

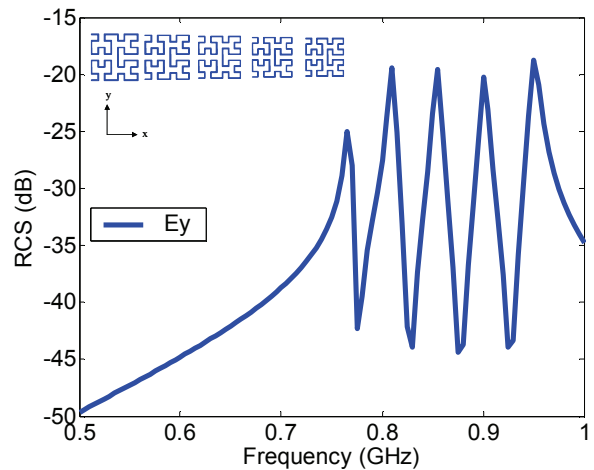


Fig. 7. Expanded (zoomed in) E_y frequency signature for 5-element Hilbert RFID tag, shown in inset.

III. POLARIZATION INDEPENDENT TAGS

To address the issue of the polarization dependence on such tags, the geometry shown in the inset of Fig. 8 is considered. In this geometry, consisting of Hilbert curves of order 3, each

element within the previous array is replaced with 4-elements, identical in size with the original, 2 of which are rotated by 90° with respect to the original element. This process is repeated for each element and again the 95% scaling factor is applied to each super-element. In the case shown in Fig. 8, again a 5-element array was assumed and then the second and fourth elements were removed to produce a signature of 10101. This frequency signature is now obtained regardless of the polarization of the incoming excitation albeit at the expense of tag elements which are larger in size. Due to coupling among the elements, the frequency response is not completely independent on polarization, but the dependence on polarization has been significantly reduced.

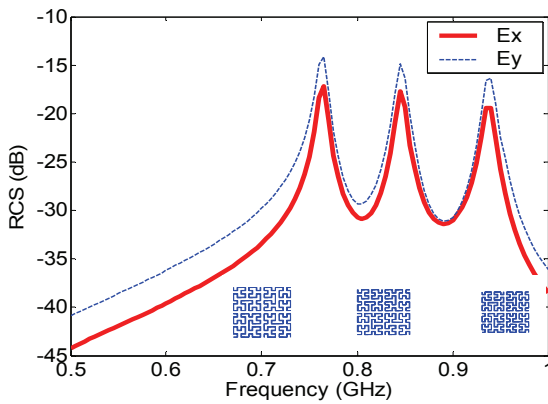


Fig. 8. Frequency signature for a Hilbert RFID tag with reduced polarization sensitivity.

IV. PEANO RFID TAG ON A DIELECTRIC AND METALLIC CYLINDER

To investigate the performance of the proposed space-filling RFID tags when placed near a typical inventory object, Finite Element Method (FEM) based HFSS software was used to numerically model the radar cross-section (RCS) of the 5-element array of Peano-curve elements of 2nd order on a paper roll (see Fig. 9). The paper roll was assumed to have $\epsilon_r = 2.6$, $\tan\delta = 0.08$ as given as appropriate values in [9]. The 5-element Peano array is identical to the previously studied case (see Figs. 4 and 5) however now the array is considered as printed on a Duroid substrate with a thickness of 1.575 mm which accounts for a slight shift in frequency as compared to the free-space case considered previously in Fig. 5. Various radii

of the paper roll were considered to investigate the performance of the RFID tag in the presence of both large and small inventory objects. The height of the paper roll was fixed at 210 mm for all cases and the electric field of the incident plane-wave was polarized in the direction of the cylinder axis.

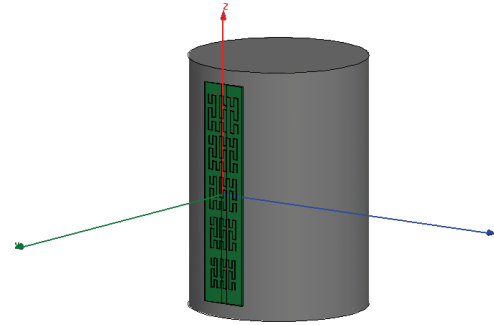


Fig. 9. The Peano-curve array placed on a paper roll of height 21 cm and radius r .

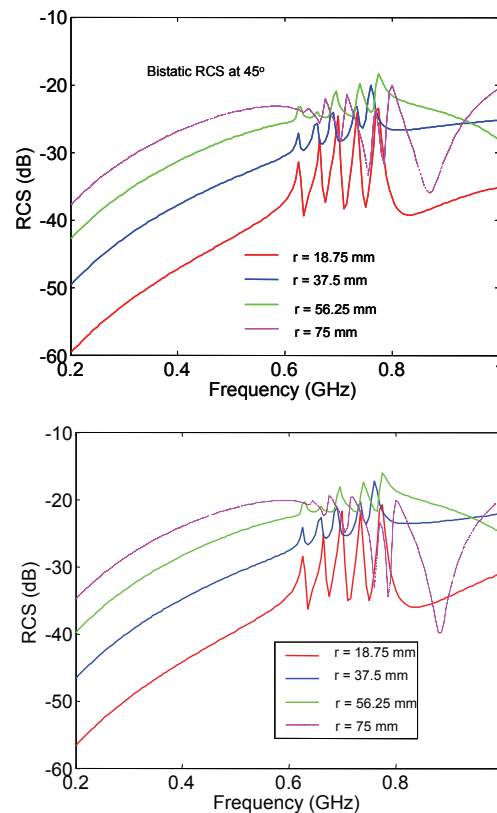


Fig. 10. Results of numerical simulation for the RCS of the Peano-curve RF tag near a paper roll for different radius values.

The monostatic and bistatic RCS results for the paper rolls of various radii are plotted in Fig.

10. The backscattered and the bistatic results at 45 degrees are very similar, due to the dipolar scattering pattern associated with these elements, as shown in Fig. 11 for the resonance at 0.76GHz.. For the cases of $r = 18.75$ mm and $r = 37.5$ mm, one can clearly see the peaks corresponding to the resonant frequencies of the Peano curve elements, and hence the RFID tag frequency signature. As the radius of the paper roll increases, however, the resonant peaks become less pronounced due to the increased contribution of the paper roll to the overall RCS of the combined geometry.

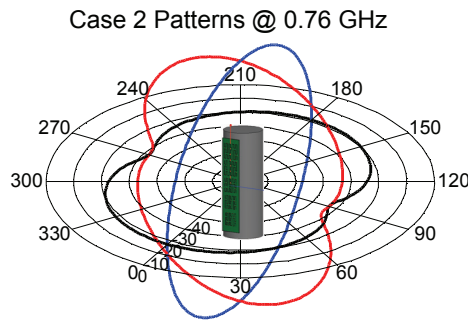


Fig. 11. Scattering Patterns of the Peano-curve RFID tag on a paper roll of 37.5mm radius at 0.76GHz.

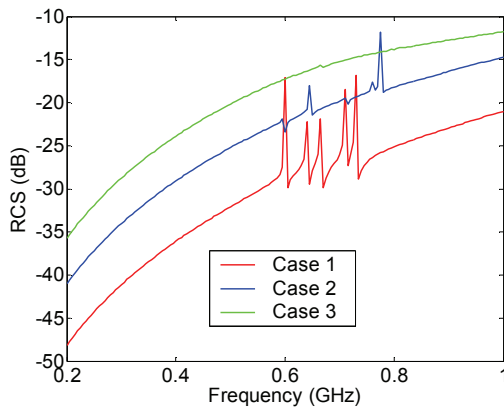


Fig. 12. Monostatic frequency signatures for cases shown in Fig. 8.6 but when the cylinder is considered as metallic (radii = 18.75 mm (case 1), 37.5 mm (case 2) and 56.25 mm (case 3).

This effect was also found, and even more pronounced when a metallic cylinder made of aluminum was considered in place of the paper roll cylinder. The scattering for the case when the cylinder is metallic is shown in Fig. 12. For this case, it can be seen that the scattering from the

tagged object, namely the metallic cylinder, completely dominates the return by the third case studied. To this end, the possibilities into the use of space-filling curve RFID tags for tagging large metallic objects are investigated in a later section. Background subtraction or other appropriate signal processing algorithms may also potentially be used to enhance the peaks in the received RCS spectrum.

IV. EXPERIMENTAL RESULTS

In order to experimentally confirm the overall space-filling curve RFID tag concept, a set of 3-element arrays, corresponding to the Peano order 2 and Hilbert order 3 geometries, and a 5 element array of 3rd order Hilbert curve elements were fabricated (see Fig. 13 insets). In both the Peano and Hilbert RFID tag cases the largest tag element was scaled such that the lowest resonant frequency was within the frequency range of the available horn antennas (1-12.4 GHz) utilized for the measurement and as such, the dielectric substrate effects were also taken into account in the design. The largest element size for both the Peano and Hilbert tag arrays is about 7 mm. The subsequent elements were then scaled using a 95% scaling factor as was previously discussed. The arrays were fabricated on DUROID 5870 ($\epsilon_r=2.33$) and measured. The measurement setup consisted of two H-1479 horns, one for transmit and one for receive, with a 267 mm separation distance between them. The RFID tags were placed, separately, 122 cm downrange. The RCS was collected utilizing an Agilent E-5071B vector network analyzer and some absorbing material was utilized to reduce noise and reflections within the room. Measurements were taken both in the absence of and in the presence of the RFID tags in order to perform background subtraction. The RCS results are plotted in Fig. 13, for both tags utilized. The peaks corresponding to the resonant frequencies, f_1 , f_2 and f_3 , of the space-filling curve elements can be seen. A similar 5-element Hilbert array was also fabricated and its measured RCS is shown in Fig. 14.

V. LOCATING MULTIPLE NEARBY TAGS

One potential pitfall for this type of ultra-passive tag would be the ability to identify

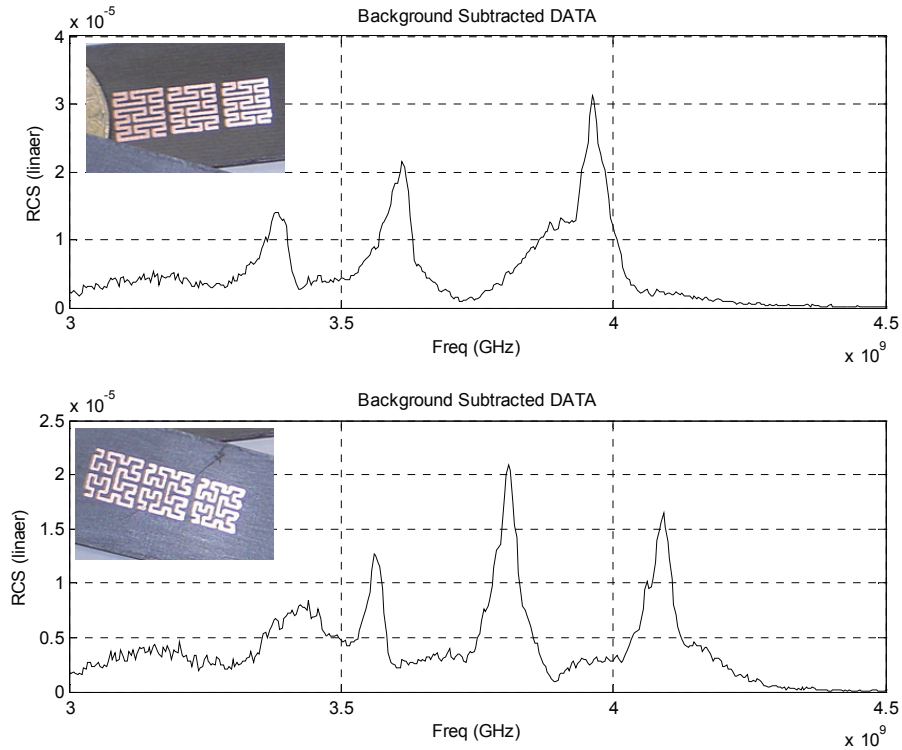


Fig. 13. Measured frequency signature for 3-element Peano and Hilbert RFID tags.

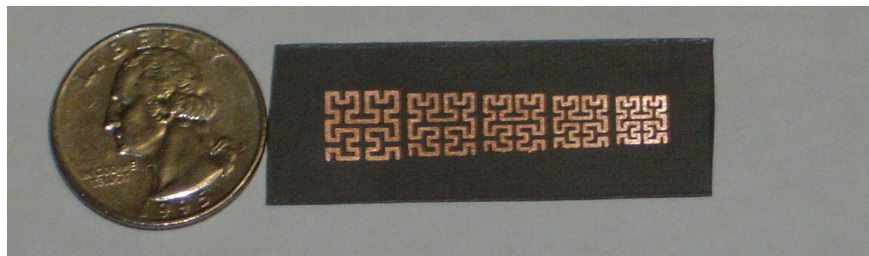
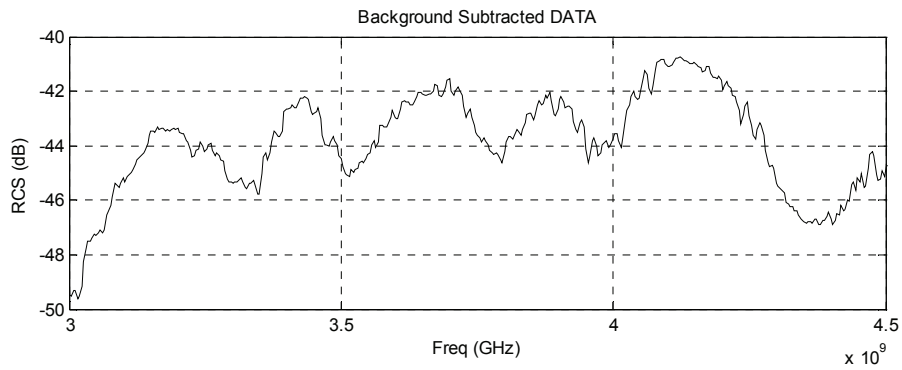


Fig. 14. Measured frequency signature for 5-element Hilbert RFID tag.

multiple tags located within close proximity to one another. Passive and active tags offer the advantage that a given tag can be “silenced” while

another tag is “interrogated”. However, in this section delay and sum beamforming is explored as an approach that may allow for the frequency

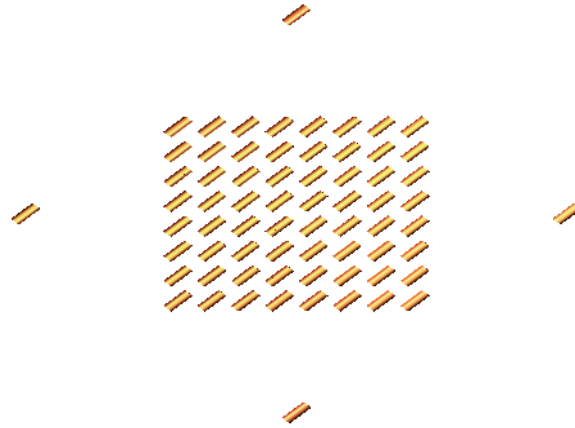


Fig. 15. Rectangular array of dipole elements; 64 receive elements and 4 transmit elements.

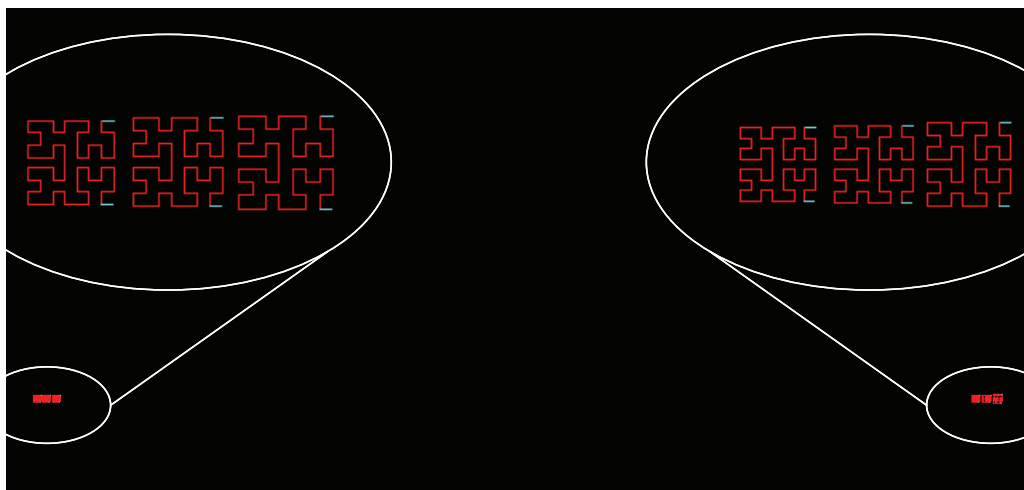


Fig. 16. Two separate Hilbert curve RFID tags.

signature of multiple tags within close proximity to be extracted.

Using Method of Moment based NEC-4, a receive array consisting of a rectangular array of 64 dipole elements is numerically modeled. Four transmit dipole elements are placed near the receive array. The geometry of the array is shown in Fig. 15. The elements in the receive array are spaced $\frac{1}{2} \lambda$ apart (at 2.5 GHz) and are $\lambda/2$ dipoles. The 45 degree rotation of the elements is to avoid contact between the elements. The transmit elements are placed 4.5 times the separation distance of the receive elements, away from the rectangular array sides. This particular set-up was chosen to correspond to a particular array, in use for another unrelated radar project that has been proven effective in imaging of nearby objects in a cluttered environment [10].

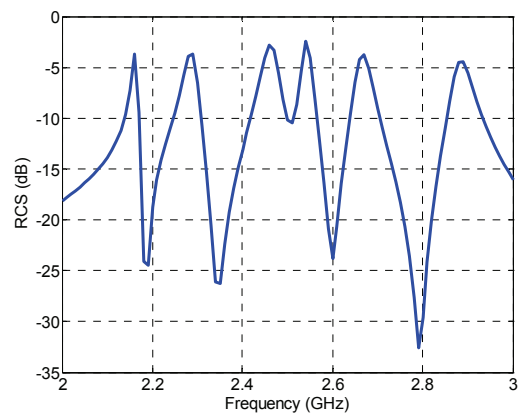


Fig. 17. Numerically calculated received signal without delay and sum beamforming.

Two separate 3-element space-filling curve tags were then modeled and placed 3.2 meters

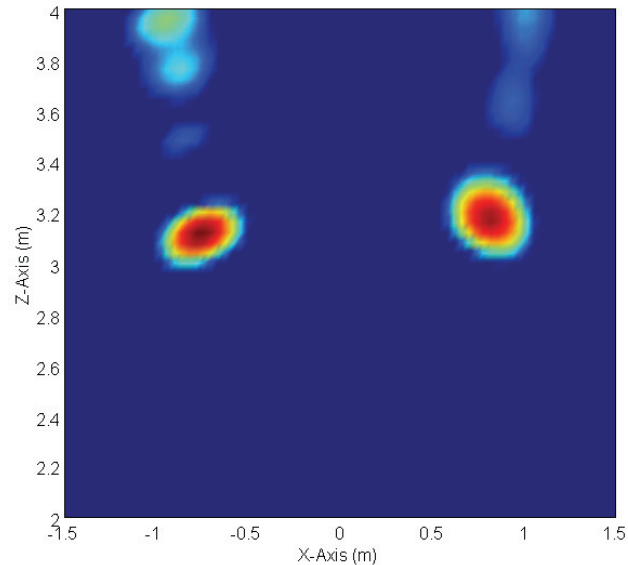


Fig. 18. Results of numerical simulations for the output of the beamformer in the area of interest. The “hot spots” correspond to the returns from the space-filling curve RFID tags.

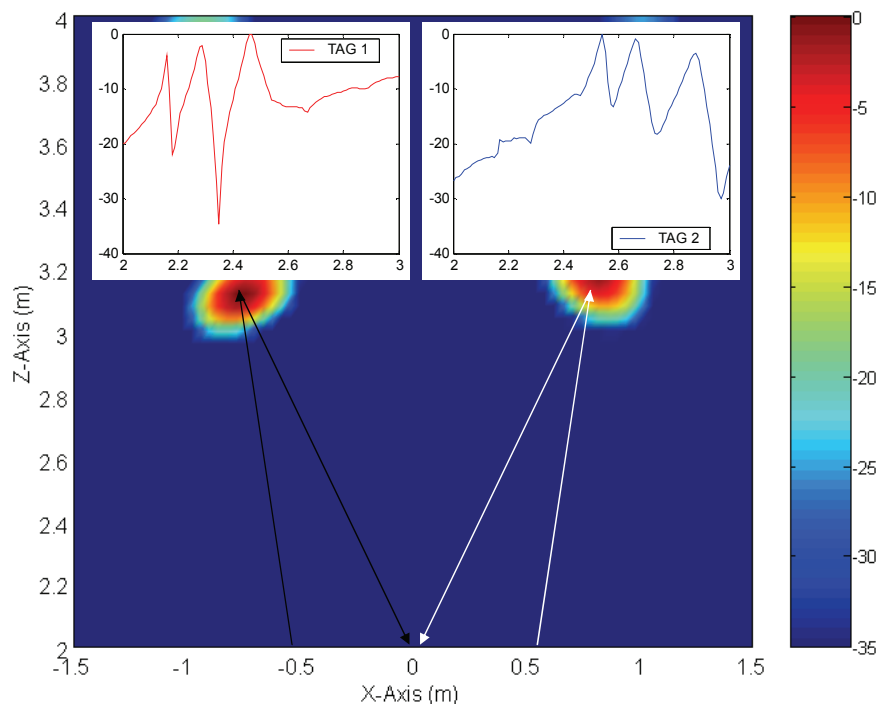


Fig. 19. Simulation results: Application of the proper phase delays in the directions of the targets to obtain the frequency content at the desired locations. Insets show the frequency content of the individual tags, separated by the process described in the text.

downrange of the array. The model for the tags is shown in Fig. 16.

The numerically calculated received signal without any processing is shown in Fig. 17. As can be seen, 6 peaks are present, however it is not

evident which peak corresponds to which tag. Beamforming is then implemented over the frequency range from 1 to 3 GHz. To implement the beamformer, the delay path for a single transmit/receive path was calculated and applied

for each transmit/receive pair, for all the pixels within the space being imaged. The space imaged was 3 meters by 3 meters with a separation of 0.04 m between the individual (pixel) locations being imaged in both x and y directions. The standard beamforming equation is given by:

$$I(l, m, n) = \sum_{p=1}^P \sum_{q=1}^Q \sum_{k=1}^K R_{pq}(\omega_k) e^{j\omega_k \tau_{pq}(l, m, n)}, \quad (2)$$

where $I(l, m, n)$ is the total power received at the pixel location (l, m, n) , k corresponds to the sum across the frequency range, p and q correspond to the transmit receive pair, respectively and the

exponential term $e^{j\omega_k \tau_{pq}(l, m, n)}$ gives the focusing delay for the location (l, m, n) at the k^{th} frequency for the pq receive pair, where $\tau_{pq}(l, m, n)$ is the phase delay between the pq receive pair to the location (l, m, n) . R_{pq} is the received signal from the p th transmitter to the q th receiver.

The resulting output of the beamformer is shown in Fig. 18. The “hot spots” shown correspond to the locations of the two separate tags.

In order to obtain the separate frequency responses, the S-parameter data collected in the above procedure can then be focused in the direction of one particular tag and the sum over the frequency range in (2) can be omitted in order to obtain frequency information content from that particular location, while simultaneously spatially filtering out signals arriving from other locations. Applying this procedure for each of the “hot spots” in Fig. 18, the frequency content is extracted and shown in Fig. 19.

VI. HILBERT-CURVE RFID ANTENNA ABOVE HILBERT-CURVE HIGH-IMPEDANCE GROUND-PLANE

It is well known that a horizontally polarized radiating element will not radiate efficiently when placed horizontally above and within close proximity to a good conductor. If however an artificial magnetic conductor could be realized, it could be used to enhance the radiation characteristics of the radiating element. In this section we study the potential of utilizing the electrically small SF-curve radiating elements, above the high impedance ground-planes (HIGP),

also known as artificial magnetic conductors (AMC) made of space-filling curve inclusions [11, 12]. In such a process, it may be possible to have an electrically small yet resonant, horizontal, dipole-like element within close proximity to a conductive ground-plane, while maintaining a matched system with gain values greater than that of the free-space counterparts. Such a scheme may particularly be useful when these antennas are used in RFID tagging of conducting objects in either passive or an active RFID application.

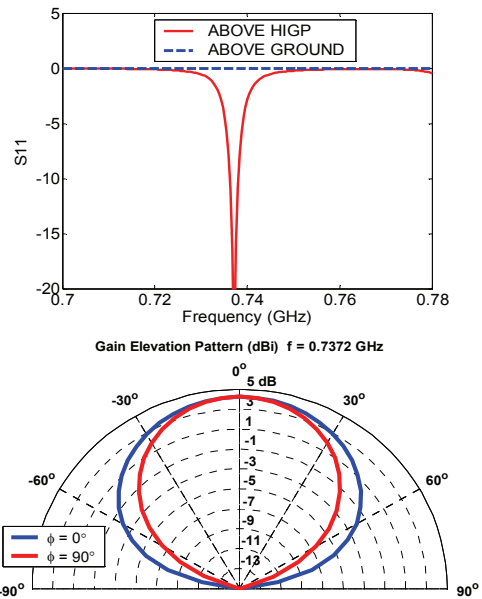
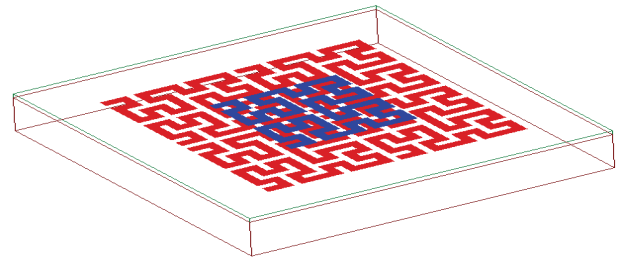


Fig. 20. Hilbert RFID tag utilizing a Hilbert HIGP (AMC) for enhanced radiation performance.

As an example we consider the case shown in Fig. 20. It consists of a Hilbert curve of order 3 antenna, matched in free-space to a 50Ω source by judiciously choosing its feed location [6]. When placed at a height of 15 mm above a conductive ground, of infinite extent, it gives rise

to the return loss (S_{11}) shown in Fig. 20 (blue, dashed line). As can be seen, in the presence of the metallic ground, the match to the $50\ \Omega$ source is lost, due to the small value of radiation resistance when in close proximity to the conductive backing. When a 2 by 2 array, also consisting of Hilbert curves of order 2, acting as a high-impedance ground-plane is inserted between the antenna and the ground plane, at a height of 13.425 mm, the radiation resistance is restored as is the $50\ \Omega$ source match as is evident in the return-loss values plotted in Fig. 20, as a function of frequency, for the antenna above the high-impedance ground plane. The gain elevation pattern, corresponding to the resonance is also shown in Fig. 20 and it is noted that the pattern is similar to a dipole pattern, in the presence of a conductive ground of infinite extent and that the gain of the antenna, in the presence of the AMC is on the order of 4.26 dBi.

In order to provide an experimental verification of the proposed space-filling curve dipole antenna above the corresponding high-impedance ground-plane, a realistic feed system must first be considered. In the numerical modeling, one can simply assume a $50\ \Omega$ gap-source, while in practice; this requires a bit more thought. Since this system has a ground-plane, a coaxial-probe fed system is considered, as is utilized in many patch antenna designs. Since this design consists of 3 layers, a ground-plane, a high-impedance surface and a dipole layer, it will be necessary to feed a probe up from the ground-plane to the antenna layer. A commonly used SMA probe diameter is 1.27 mm. In order to feed the probe through the surface without making an electrical connection, the inclusions on the high-impedance surface must be scaled such that a 1.27 mm probe can fit in between the distances between the inclusions' microstrip lines.

An SMA coaxial probe is grounded to the ground-plane while the probe center comes up through the high-impedance surface and connects to the antennas' $50\ \Omega$ free-space feed location. The numerical model of the coaxial-fed antenna is shown in Fig. 21. The shaded areas correspond to the 1.575 mm thick Duroid ($\epsilon_r=2.2$) substrates which were also considered in the modeling process. We note that for a passive tag when an IC chip is connected in place of the probe, the

antenna should be matched to the input-impedance of the chip by choosing an appropriate feed-point location on its trace.

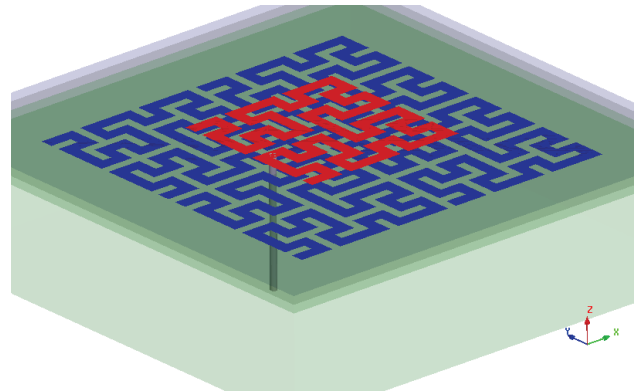


Fig. 21. Simulated model of the probe-fed Hilbert dipole antenna above a 4 element Hilbert high-impedance ground-plane.

The fabricated design is shown in Fig. 22. It should be noted that due to the Duroid substrate of the antenna, the 4-element high impedance surface is not visible in the figure. The return loss (S_{11}) results of the numerical model and the experimental prototype are shown in Fig. 23. As can be seen there is a very close agreement between the two. An additional drop is seen in the return loss of the prototype at 650 MHz, which is most likely due to some fabrication or construction flaw. This additional drop is still not in the matched range where the return loss is less than -10 dB. The resonance of interest here is the resonance which is closely correlated between both results, both in the resonant frequency and in the level of the return loss, at 700 MHz. As was previously mentioned, the antenna was designed around this 700 MHz frequency region such that the probe diameter could be inserted through the high-impedance surface level. Due to the fact that the frequency range of this design, falls outside that of our laboratory's anechoic chamber, which has a lower cut-off of 2.0 GHz, pattern measurements were not possible. The simulated gain patterns however indicated a dipolar radiation pattern, as expected, with a gain of 4.22 dBi and a bandwidth of about 0.3%. These values all correspond very closely to the values in the previous section, which assumed a perfect gap-source and identical dimensions.



Fig. 22. Prototype of the probe-fed Hilbert antenna above a 4-element Hilbert high-impedance ground-plane.

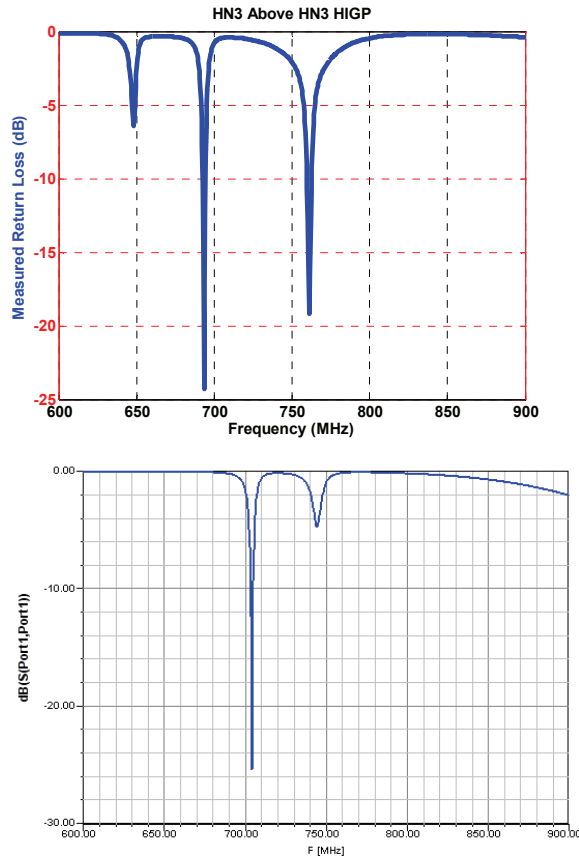


Fig. 23. Measured and simulated return loss of the fabricated Hilbert antenna above Hilbert high-impedance ground-plane.

VII. CONCLUSIONS

Arrays of Peano and Hilbert space-filling curve elements are proposed for potential use as RFID tags. Using both numerical simulations and RCS measurement, it was shown that these electrically compact resonators could produce relatively large scattered fields over an inherently narrow frequency band at their corresponding fundamental resonant modes. These tags were also investigated in terms of their performances when placed near a typical inventory objects, such as paper rolls. In addition, the use of a Hilbert-curve antenna above Hilbert AMC ground-plane was investigated for tagging of metallic objects, where it was shown that a such a configuration could provide a compact, low-profile and highly efficient technique for RFID tagging in presence of conducting surfaces.

REFERENCES

- [1] J. Landt, "The History of RFID", *IEEE Potentials*, vol. 24, no. 4, pp. 8-11, Nov. 2005
- [2] R. Weinstein, "RFID: A technical overview and its application to the enterprise", *IT Professional*, vol. 7, no. 3, pp. 27-33, June 2005.
- [3] H. Sagan, *Space-Filling Curves*, Springer-Verlag, 1994.
- [4] K. J. Vinoy, K. A. Jose, V. K. Varadan, and V. V. Varadan, "Hilbert curve fractal antenna: A small resonant antenna for VHF/UHF applications," *Microwave and Optical Technology Letters*, vol. 29, no. 4, pp. 215-219, May 2001.
- [5] S. R. Best, "A comparison of the performance properties of the Hilbert curve fractal and meander line monopole antennas," *Microwave and Optical Technology Letters*, vol. 35, no. 4, pp. 258-262, November 20, 2002.
- [6] J. Zhu, A. Hoorfar, and N. Engheta, "Bandwidth, cross-polarization, and feed-point characteristics of matched Hilbert antennas," *IEEE Antennas and Wireless Propagation Letters*, vol. 2, pp. 2-5, 2003.
- [7] D. H. Werner and S. Ganguly, "An Overview of Fractal Antenna Engineering Research," *IEEE Antennas & Propagation Magazine*, vol. 45, no. 1, pp. 38-56, February 2003.

- [8] J. Zhu, A. Hoorfar, and N. Engheta, "Peano antennas," *IEEE Antennas and Wireless Propagation Letters*, vol. 3, pp. 71-74, 2004.
- [9] R. Olmi, M. Tedesco, C. Riminesi, and A. Ignesti, "Thickness independent measurement of the permittivity of thin samples in the X band," *Measurement Science and Technology*, vol. 13, pp. 503-509, 2002.
- [10] J. A. McVay, K. M. Yemelyanov, A. Hoorfar, and N. Engheta, "Through-the-Wall Imaging and Sensing: An Electromagnetic Perspective," *IEEE Workshop on Signal Processing Applications for Public Security and Forensic (SAFE-2007)*, April 2007.
- [11] J. McVay, N. Engheta, and A. Hoorfar, "High Impedance Metamaterial Surfaces Using Hilbert-Curve Inclusions," *IEEE Microwave and Wireless Components Letters*, vol. 14, no. 3, March 2004.
- [12] J. McVay, A. Hoorfar, and N. Engheta, "Peano High Impedance Surfaces," *Radio Science*, vol. 40, pp. 1-9, September 2005.

Compact Metamaterial-Based UHF RFID Antennas: Deformed Omega and Split-Ring Resonator Structures

Benjamin D. Braaten¹, Robert P. Scheeler¹, Michael Reich², Robert M. Nelson³,
Cherish Bauer-Reich⁴, Jacob Glower¹ and Gregory J. Owen¹

¹ Department of Electrical and Computer Engineering
North Dakota State University, Fargo, ND, 58102, USA
benbraaten@ieee.org

² Center for Nanoscale Science and Engineering (CNSE)
North Dakota State University, Fargo, ND, 58102, USA

³ Engineering and Technology Department
University of Wisconsin - Stout, Menomonie, WI, 54751, USA

⁴ Department of Geology and Geophysics
University of Minnesota – Twin Cities, Minneapolis, MN, USA

Abstract – Over the past decade, researchers have shown significant advances in the area of radio frequency identification (RFID) and metamaterials. RFID is being applied to a wide spectrum of industries and metamaterial-based antennas are beginning to perform just as well as existing larger printed antennas. This paper presents two novel metamaterial-based antennas for passive ultra-high frequency (UHF) RFID tags. It is shown that by implementing omega-like elements and split-ring resonators into the design of an antenna for an UHF RFID tag, the overall size of the antenna can be significantly reduced to dimensions of less than $0.15\lambda_0$, while preserving the performance of the antenna.

Index Terms- Metamaterial, RFID, meander-line, split-ring resonator, printed antenna, passive tag.

I. INTRODUCTION

The use of radio frequency identification (RFID) has grown substantially in recent years [1-4]. RFID has been applied to many different industries such as supply chain management [5], disease prevention [6-7], security [8] and road-tolling [9]. Because of these applications significant research is being conducted in the areas of antenna design [10], environmental effects on RFID systems [11] and novel reader applications [12].

The two major characteristics that distinguish different types of RFID systems are the power source of the tag and the frequency of operation [1]. An excellent review on the characteristics of different types of RFID systems can be found in [1]. A passive RFID system uses the energy from the field radiated by the reader to completely power the tags. A tag in this type of system usually has an antenna attached to a rectifier circuit. This rectifier circuit then provides a voltage and current that will be used to power the tag circuitry. At Ultra-high frequencies (UHF) it is the relation between the input impedance of the rectifier circuit and the antenna impedance and gain that will determine the maximum read range of the tag [6], [10].

When designing a passive RFID tag, it is clear that the antenna is a major component of the overall size [6]. This is because it is difficult to attain an inductive input reactance and a suitable gain of an electrically small antenna. A new and rapidly emerging field of research based on metamaterial inspired antennas [13-16] is showing that antennas with small physical size can have impedance and radiation properties comparable to existing larger antennas such as rectangular microstrip and meander-line (space-filling) antennas. In particular research in the area of metamaterials has resulted in recent advances in optics [17], filters [18], novel resonator structures [19-20], novel transmission lines [21-23] and new compact power dividers [24].

Many advances in metamaterial research have represented very significant steps in the area of antenna and microwave engineering. But, many of the structures introduced so far are very complicated, and in some cases this is a significant drawback. When designing metamaterial-based antennas, many different conducting planes, vias and special ground planes are required. These complicated structures are not easily applied to passive RFID antenna designs. This is because many passive RFID antenna designs are placed on single conducting layers with one or two different dielectric layers. In fact, very little work exists on strictly planar-based metamaterial transmission lines [25].

Recently, several initial studies have been conducted on using metamaterials to enhance the performance of passive RFID tags [26-27]. These studies have shown promising results but several drawbacks of these studies have also been observed. For example, the designs are placed above special ground planes, the feed networks can be complicated and a clear design process for using these antennas is not presented. Since typical antennas printed on passive RFID tags are placed on a single conducting layer, it may be desirable not to have a ground plane, have a simple feed network and have a very useful and clear set of design guidelines to result in a simple and desirable printed antenna.

In this paper, two different metamaterial-based designs for passive UHF RFID antennas are presented. The first design is based on the deformed omega structure presented in [28] and the second design is based on the split-ring resonator structure (SRR) [29]. Several advantages of the designs presented in this paper are that these antennas 1) do not need a ground plane; 2) are on a single conducting layer; 3) have a single dielectric substrate; 4) have simple feed networks; 5) are up to 50% smaller than commercially available passive RFID tags; 6) are comparable to the performance of commercially available passive RFID tags; 7) are simple to design; and 8) are easy to manufacture. Many different layouts with different material properties are studied. These different cases are extensive and presented here to clearly show how various dimensions and substrate values can be used to lead to a successful antenna design. It is believed that by using the results presented in this

paper, an antenna designer will avoid costly simulation times as well as less than desirable performance from manufactured antennas. This is especially important during the usually extensive antenna design process.

This paper is organized in the following manner. Section II introduces the deformed omega structure-based meander-line RFID antenna. Within this section simulations from commercial software are compared to measurements for accuracy and various configurations of the printed antenna are modeled to illustrate the characteristics of the antenna. Section III introduces the SRR-based RFID antenna. Within this section various configurations are modeled with commercial software and the characteristics of these designs are presented. These sections are followed by a conclusion in section IV.

II. DEFORMED OMEGA STRUCTURE-BASED MEANDER-LINE RFID ANTENNA

A. The Three Different Meander-Line Geometries

The first antenna presented is a meander-line antenna with metamaterial elements. These elements are based on the left-handed deformed omega structure presented in [28]. A typical element of a deformed omega structure is shown in Fig. 1. Several meander-line sections are also shown with s denoting the trace width, a denoting the element width, k denoting the width between the traces, p denoting the trace width of the deformed omega element, m denoting the overall width of the antenna, Δ denoting the height of the deformed omega element and δ denoting the height of the meander-line sections.

Three different versions of the antenna in Fig. 1 were evaluated. These three versions are shown in Fig. 2. Fig. 2 (a) is the meander-line antenna with zero ($N = 0$) deformed omega elements, Fig. 2 (b) is the meander-line antenna with two ($N = 2$) deformed omega elements and Fig. 2 (c) is the meander-line antenna with four ($N = 4$) deformed omega elements. These three different designs were studied to determine how the introduction of the deformed omega elements into the meander-line layout would affect the input impedance and gain of the antenna. This information provides useful guidelines for antenna designers.

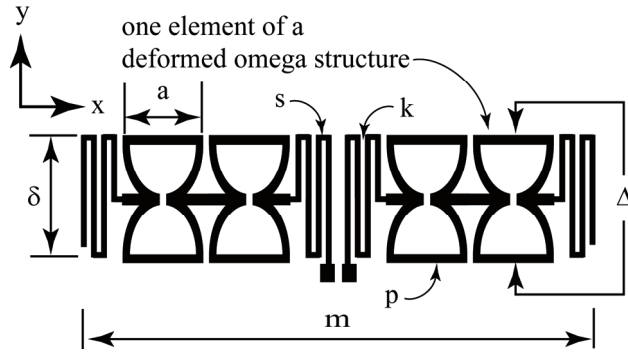


Fig. 1. Deformed omega structure-based meander-line RFID antenna dimensions [28].

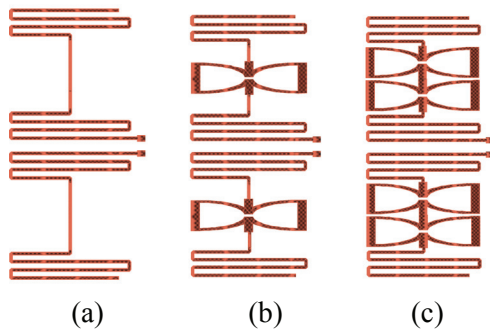


Fig. 2. (a) Layout of the omega structure with no deformed omega elements ($N = 0$); (b) layout of the omega structure with two deformed omega elements ($N = 2$); (c) layout of the omega structure with four deformed omega elements ($N = 4$).

B. Validation of the Numerical Results with Measurements

The first step in modeling the antennas in this paper was to compare the simulated values with measurements. To do this, the printed antenna in Fig. 3 was manufactured on FR4 ($\epsilon_r = 3.75$ measured) with a thickness of $d = 0.787$ mm. The input impedance was measured with a network analyzer in an anechoic chamber (Fig. 4) using a balanced probe [30] and was compared to the simulation results from the commercial software Advanced Design System (ADS) [31] by Agilent Technologies. The results from these measurements and simulations are shown in Fig. 5 (a). Figure 5 shows good agreement between the measurements and simulations. The magnitude of the electric field in the y - z and x - z planes is also shown in Fig. 5 (b) and (c), respectively, along with the simulated current distribution in part (d). This

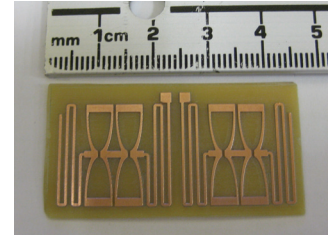


Fig. 3. Omega structure-based meander-line RFID antenna ($s = 0.5$ mm, $k = 1.0$ mm, $m = 42.2$ mm, $a = 5.0$ mm, $p = 0.86$ mm, $\delta = 4.0$ mm, $\Delta = 18.8$ mm, $\epsilon_r = 3.75$ (measured) and $d = 0.787$ mm).

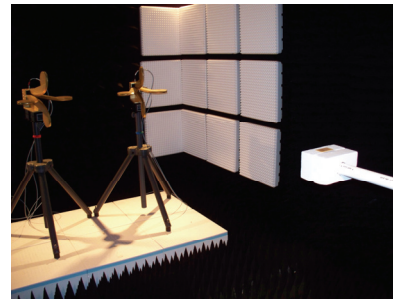


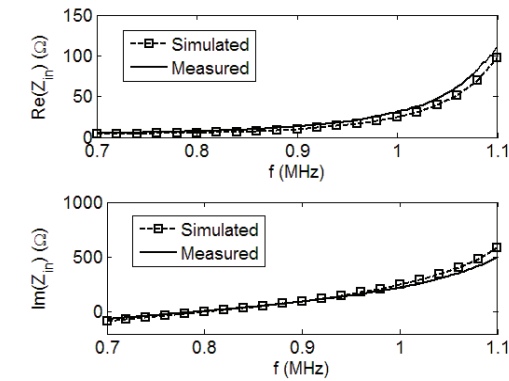
Fig. 4. Measuring the tag in an anechoic chamber.

shows that ADS is an accurate tool and can be used to model the printed antennas investigated in this paper. Therefore, because of the large number of different designs in the following sections, ADS will be used exclusively to determine the characteristics of the novel designs. It should also be noted, that a passive RFID integrated circuit (IC) was attached to the ports of the antenna in Fig. 3 and the performance (i.e., experimental read range) of this tag was determined in an anechoic chamber (Fig. 4). The read range was 4.5 m and was comparable to commercially available tags that were twice as large.

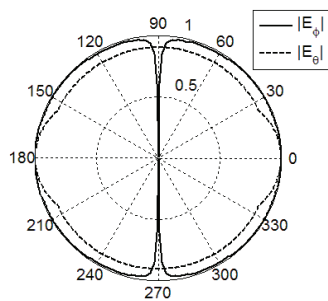
C. Results for Various Values of Substrate Permittivity

The next step is to determine the characteristics of the layout in Fig. 3 (or Fig. 1) for various values of substrate permittivity. The results from these simulations are shown in Figs. 6 - 8 for various values of ϵ_r .

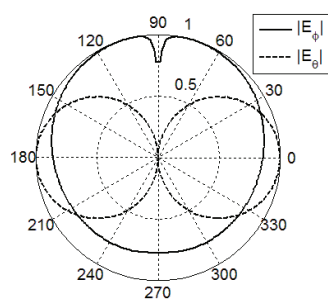
The results in Figs. 6 and 7 show that the radiation resistance increases and the resonant frequency decreases for larger values of ϵ_r . Figure 8 shows that the gain is only slightly reduced for higher values of ϵ_r . This is desirable, because



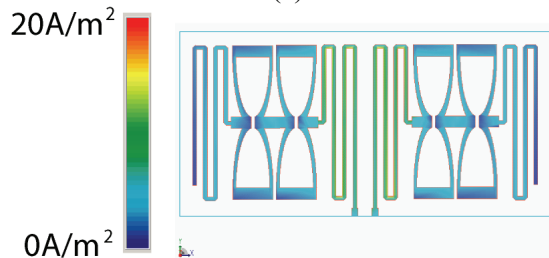
(a)



(b)



(c)



(d)

Fig. 5. (a) Measured and simulated input impedance of a deformed omega structure-based meander-line RFID antenna; (b) simulated pattern in the y - z plane; (c) simulated pattern in the x - z plane; (d) simulated surface current at 920 MHz.

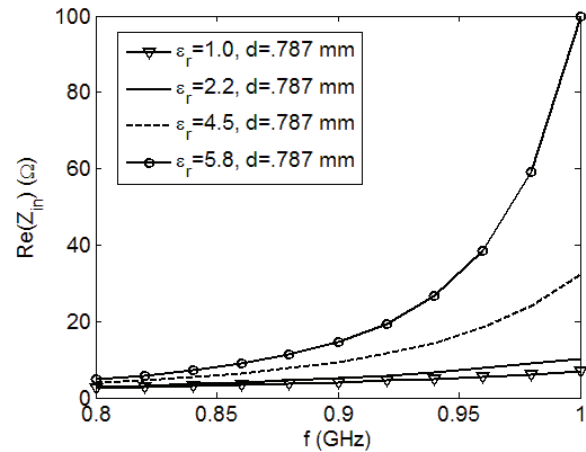


Fig. 6. Input resistance of the omega structure for various values of ϵ_r .

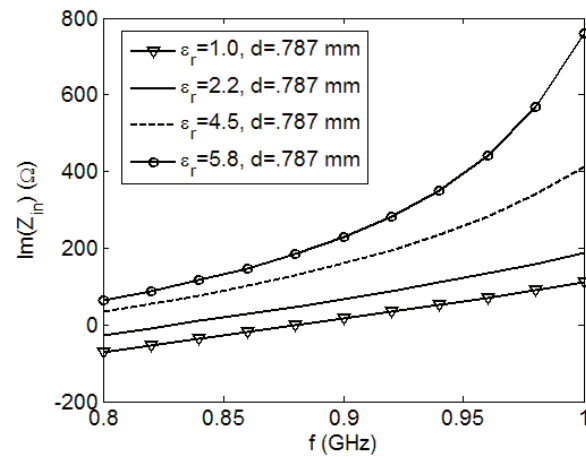


Fig. 7. Input reactance of the omega structure for various values of ϵ_r .

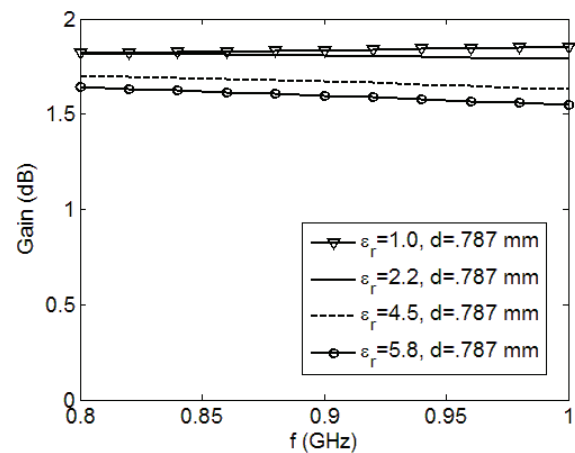


Fig. 8. Gain of the omega structure for various values of ϵ_r .

typically electrically small antennas are very capacitive and have a very small input resistance below resonance. By increasing ϵ_r the antenna can obtain useful input impedance values (approximately $10+j139 \Omega$ [6]) and the gain is only reduced slightly.

D. Results for Various Values of Substrate Thickness

The next step is to determine the characteristics of the layout in Fig. 3 for various values of substrate thickness d . The results from these simulations are shown in Figs. 9 - 11 for various values of d .

The results in Fig. 9 show that the radiation resistance increases slightly for larger values of d while the results in Fig. 10 show that the input reactance can be significantly affected by d . Fig. 11 shows that the gain is only slightly reduced for higher values of d . This is very useful information to have, especially if it is anticipated that the RFID tag will be placed on many different types of materials and thick surfaces.

E. Results for Various Values of Deformed Omega Elements

The next step is to determine the characteristics of the layouts in Fig. 2 (a) – (c) for various values of Δ and number of deformed omega elements N . These layouts had the following dimensions: $s = 0.5 \text{ mm}$, $k = 1.0 \text{ mm}$, $m = 42.2 \text{ mm}$, $a = 5.0 \text{ mm}$, $p = 0.86 \text{ mm}$, $\delta = 4.0 \text{ mm}$, $\epsilon_r = 2.2$ and a substrate thickness of $d = 0.787 \text{ mm}$.

The results from these simulations are shown in Figs. 12 - 14 for various values of N and Δ . The results in Fig. 12 show that the radiation resistance is reduced as more deformed omega elements are removed as well as for smaller values of Δ . In Fig. 13 it is shown that the resonant frequency is significantly reduced as deformed omega elements are added to the design and for larger values of Δ . Finally, Fig. 14 shows the gain is almost unaffected by the different values of N and Δ .

F. Discussion and Design Guidelines

Several important comments can be made about the results in Figs. 5 – 14.

1) In Figs. 6 – 7 and 9 – 10 it is shown that the antenna resonates at a lower frequency for larger values of ϵ_r and d , and that the input impedance can be easily controlled with ϵ_r and d .

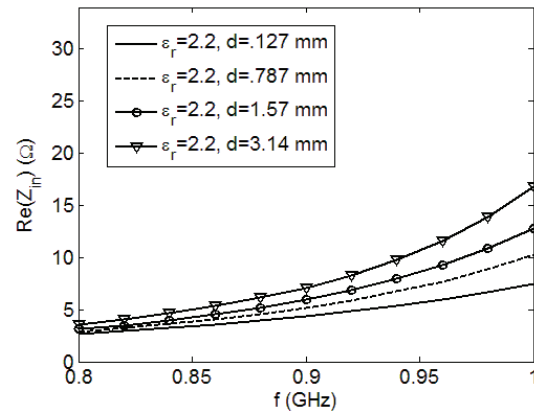


Fig. 9. Input resistance of the omega structure for various values of substrate thickness.

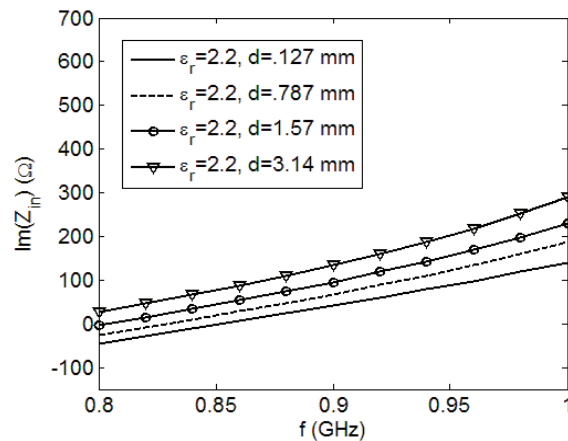


Fig. 10. Input reactance of the omega structure for various values of substrate thickness.

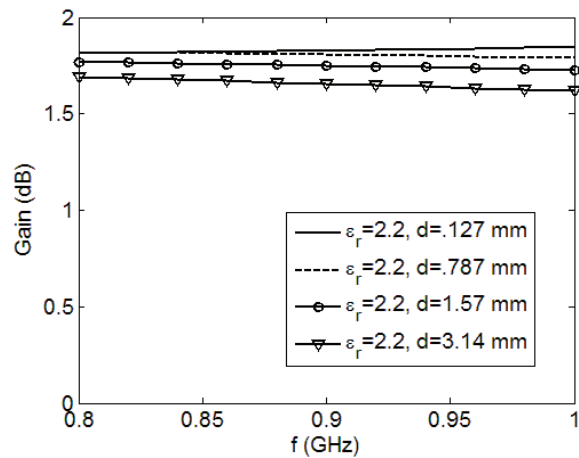


Fig. 11. Gain of the omega structure for various values of substrate thickness.

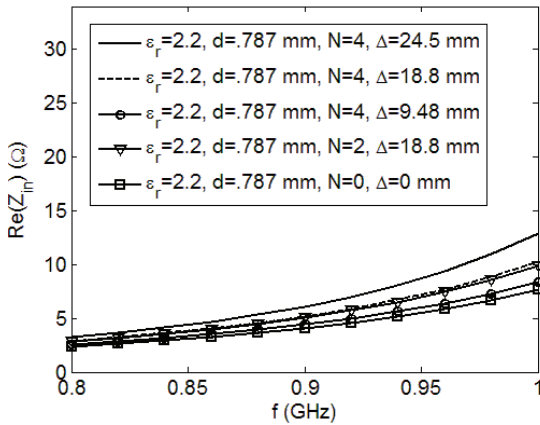


Fig. 12. Input resistance of the omega structure for various values of N and Δ for the deformed omega elements.

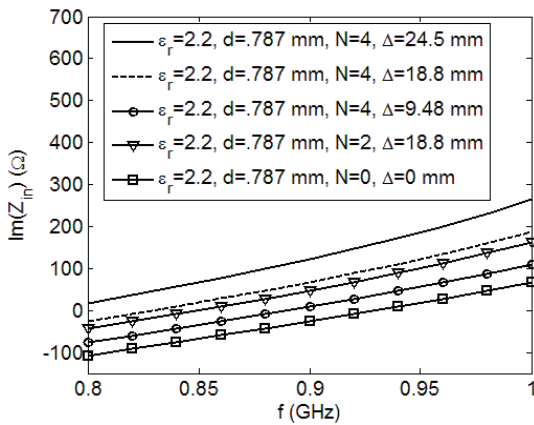


Fig. 13. Input reactance of the omega structure for various values of N and Δ for the deformed omega elements.

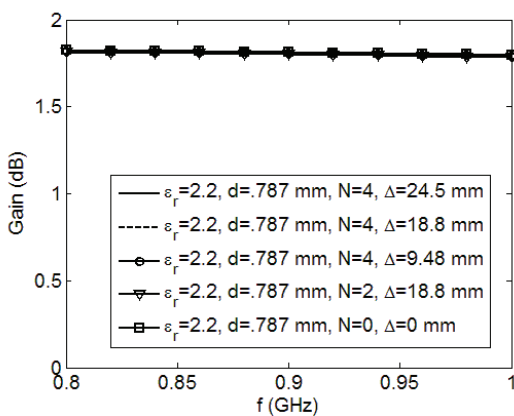


Fig. 14. Gain of the omega structure for various values of N and Δ for the deformed omega elements.

2) From the results in Figs. 12 – 13 it can be concluded that by adding more deformed omega elements to the meander-line antenna, the input resistance is only slightly changed but the resonant frequency is significantly reduced.

3) In Figs. 8, 11 and 14 it is shown that the gain is consistent for the various configurations.

4) The printed antenna design in Fig. 3 resonates at a width of $m = 0.112\lambda_0$ where λ_0 the free space wavelength of the source.

5) Fig. 5 shows the largest gain is broadside to the antenna.

These results show the antenna in Fig. 1 can have many different values of input impedance while maintaining a consistent gain. This can be very useful in many design situations. Typically, when the dimensions of an antenna are changed or the antenna is placed on many different substrates, both the input impedance and gain of the antenna are significantly affected. This then requires a new design with both the input impedance and desired gain in mind. The design in Fig. 1 reduces this design effort by providing a good gain in all the cases above with flexible impedance values.

It is shown in Fig. 13 that the input impedance of the layout in Fig. 2 (b) is more inductive (i.e., resonates at a lower frequency) than the layout in Fig. 2 (a). The layout in Fig. 2 (b) is a meander-line antenna with a single deformed omega element. The impedance of each deformed omega element can be approximated as two loops with a constant current connected in parallel. This impedance can be approximated for small values of ϵ_r with the following equation [32]:

$$Z_a \approx \frac{1}{2} j\omega\mu_0 a \left[\ln\left(\frac{8a}{p}\right) - 2 \right] \Omega \quad (1)$$

where a and p are defined in Fig. 1. By using (1) a designer can approximate the impact of introducing the deformed omega structure to an antenna design.

III. SPLIT-RING RESONATOR-BASED RFID ANTENNA

The next antenna discussed is the split-ring resonator-based RFID antenna shown in Fig. 15. This antenna has two SRRs attached to each side of the RFID IC. The radius of the inner ring is denoted as r , the width of each ring is denoted as t , the gap between the rings is denoted as g , the gap on either end of the rings is denoted as w and the gap between the ports as h . For this section, the

thickness of the substrate is again denoted as d . The layout in Fig. 15 is used in all the simulations, but the dimensions are scaled and the substrate characteristics are changed to determine the behavior of the input impedance and gain of the antenna. Figure 16 (a) shows a manufactured version of the SRR antenna in Fig. 15. The magnitude of the electric field in the y - z plane is also shown in Fig. 16 (b) along with the simulated current distribution in Fig. 16 (c).

It should also be mentioned that the design in Fig. 16 a) had a max read range 1.5 m. It is anticipated that by placing the design on a substrate with a smaller value of ϵ_r , a smaller value of d and appropriate dimensions, the read range could be greatly improved.

A. Results for Various Values of Substrate Permittivity

The next step is to determine the characteristics of the layout in Fig. 16 (a) for various values of substrate permittivity. The results from these simulations are shown in Figs. 17 - 19 for various values of ϵ_r .

The results in Fig. 17 show that the radiation resistance increases for larger values of ϵ_r while the results in Fig. 18 show that the resonant frequency significantly reduces for larger values of ϵ_r . Figure 19 shows that the gain varies only slightly for various values of ϵ_r . The characteristics of the input impedance observed in Figs. 17 - 18 are very desirable. In particular, Fig. 18 shows that the resonance of the antenna in Fig. 16 can be below 800 MHz. This lower resonance is very significant because the antenna is resonating at an overall length that is a fraction ($q < .15\lambda_0$) of the free-space wavelength of the source. This then results in an inductive input reactance for frequencies above resonance, which are desirable for appropriate matching to RFID ICs [6], [10], [26].

B. Results for Various Values of Substrate Thickness

The next step is to determine the characteristics of the layout in Fig. 16 (a) for various values of substrate thickness. The results from these simulations are shown in Figs. 20 - 22 for various values of d .

The results in Figs. 20 and 21 show the input impedance can be significantly affected by the substrate thickness. In particular, Fig. 21 shows the

antenna resonates at a lower frequency for thicker substrates. Similarly, the gain plot in Fig. 22 shows a larger gain is achieved for smaller values of d . Therefore, this type of antenna may be best suited for being printed on thin dielectric adhesives.

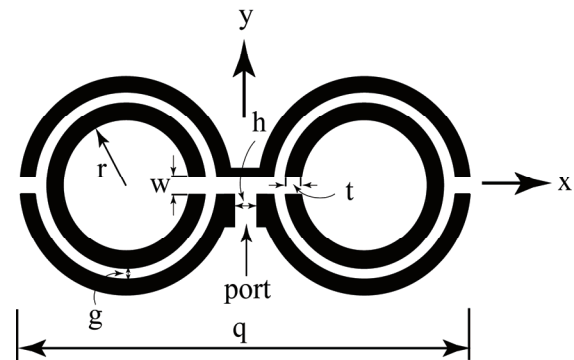


Fig. 15. Dimensions of the split-ring resonator-based RFID antenna.

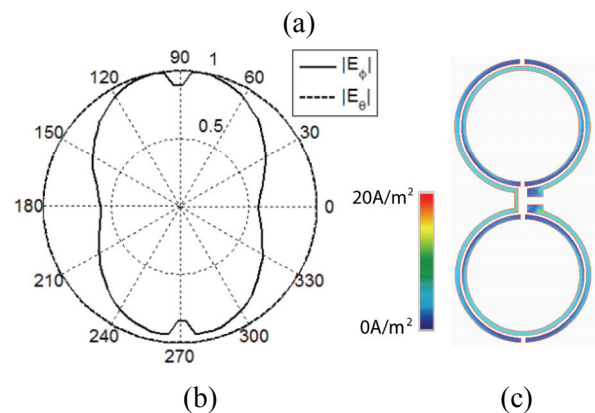
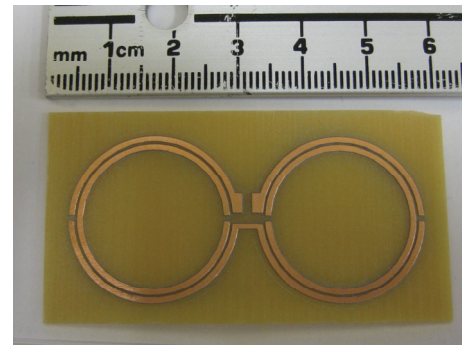


Fig. 16. (a) Manufactured split-ring resonator-based RFID antenna ($r = 11.135$ mm, $t = 0.89$ mm, $g = 0.44$ mm, $q = 56.28$ mm, $w = 0.89$ mm, $h = 1.54$ mm, $\epsilon_r = 3.75$ (measured) and $d = 0.787$ mm); (b) simulated pattern in the y - z plane; (c) simulated surface current at 920 MHz.

C. Results for Various Values of r

The next step is to determine the characteristics of the layouts in Fig. 15 for various overall dimensions. This was done by scaling the following dimensions by 0.95 and 1.05: $r = 11.135$ mm, $t = 0.89$ mm, $g = 0.44$ mm, $q = 56.28$ mm, $w = 0.89$ mm, $h = 1.54$ mm and $\epsilon_r = 3.75$. The results from these simulations are shown in Figs. 23 - 25.

The results in Figs. 23 and 24 shows a slightly larger or smaller scale can significantly impact the input impedance. Finally, Fig. 25 shows that the gain is generally improved with a larger antenna.

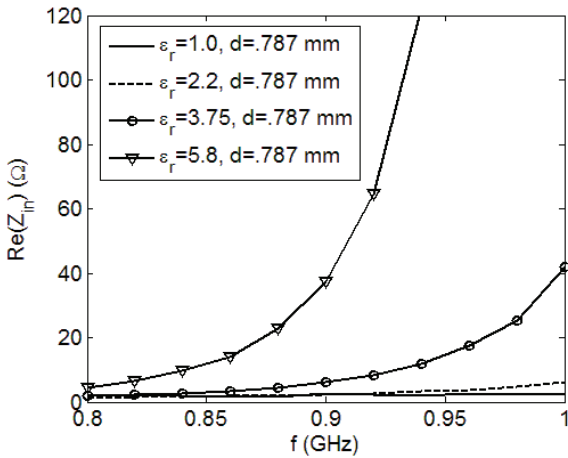


Fig. 17. Input resistance of the SRR structure for various values of ϵ_r .

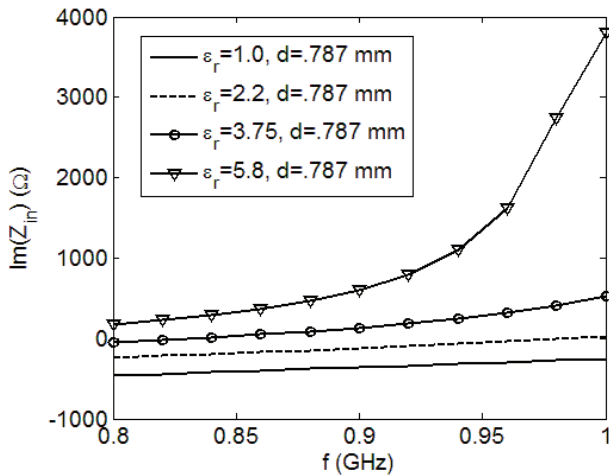


Fig. 18. Input reactance of the SRR structure for various values of ϵ_r .

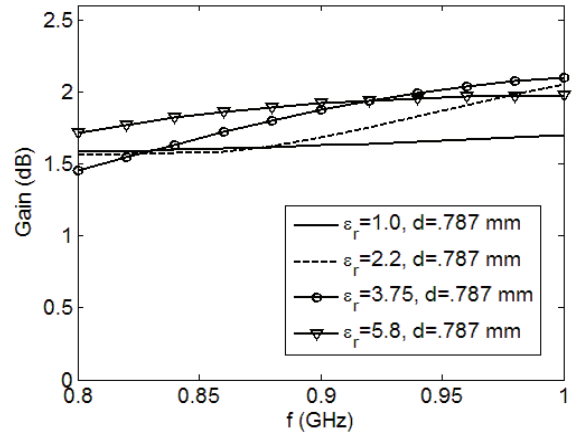


Fig. 19. Gain of the SRR structure for various values of ϵ_r .

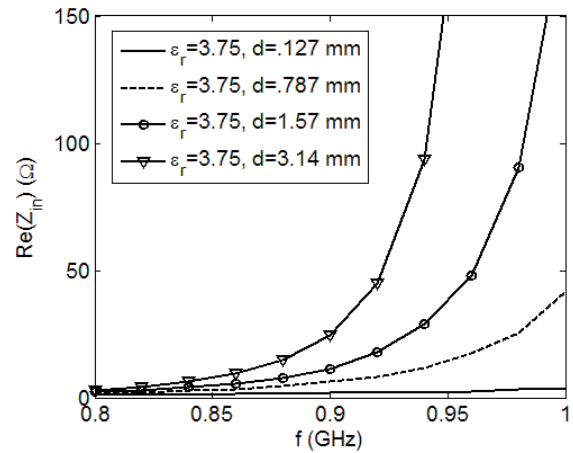


Fig. 20. Input resistance of the SRR structure for various values of substrate thickness.

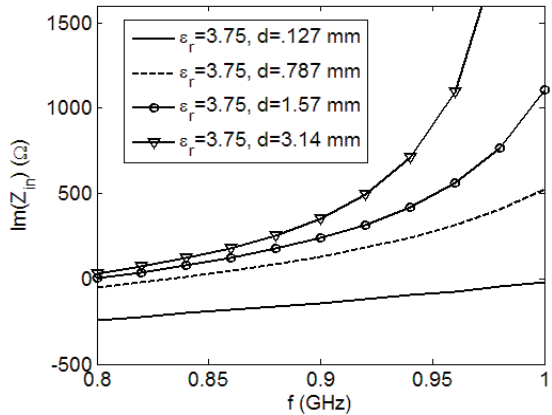


Fig. 21. Input reactance of the SRR structure for various values of substrate thickness.

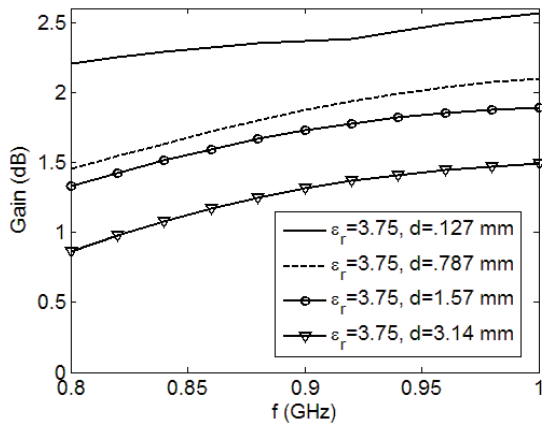


Fig. 22. Gain of the SRR structure for various values of substrate thickness.

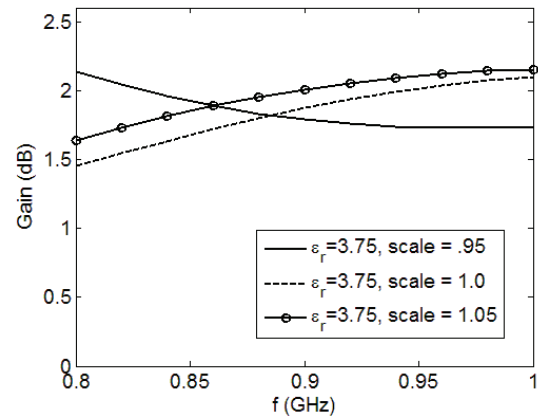


Fig. 25. Gain of the SRR structure for various scale values.

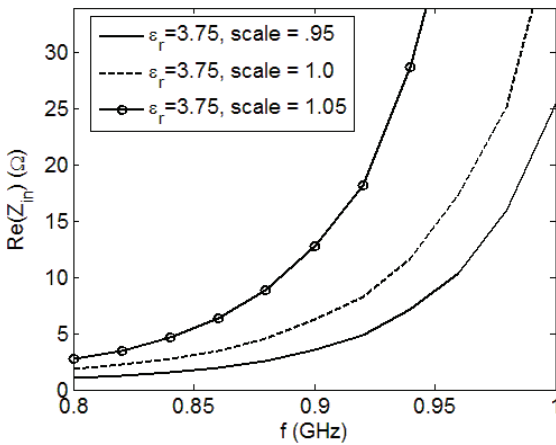


Fig. 23. Input resistance of the SRR structure for various scale values.

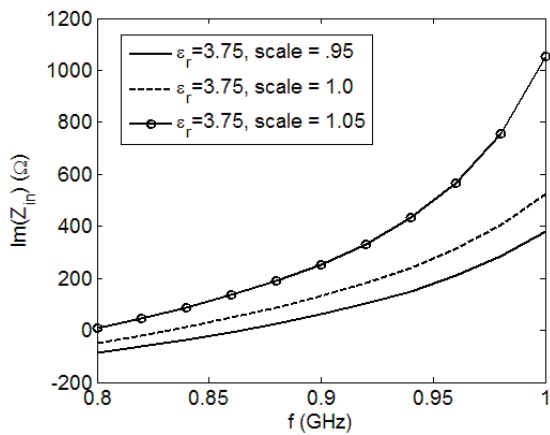


Fig. 24. Input reactance of the SRR structure for various scale values.

D. Discussion and Design Guidelines

Several important comments can be made about the results in Figs. 16 – 25.

- 1) In Figs. 17 – 18 and 20 – 21 it is shown that the antenna resonates at a lower frequency for larger values of ϵ_r and d , and that the input reactance can be controlled with these values.
- 2) In Figs. 19 and 22 it is shown that the gain of the SRR-based antenna can be significantly impacted by the larger values of ϵ_r and d .
- 3) It can be concluded from Figs. 23 – 25 that scaling the antenna can affect both the gain and input impedance of the antenna.
- 4) The layout in Fig. 16 resonates at a width of $q = 0.138\lambda_0$.
- 5) In Fig. 16 it is shown that the largest gain is broadside to the antenna.

The previous results show that the antenna in Fig. 15 can have many different values of input impedance and gain. In particular, Fig. 22 shows that the SRR has the largest gain for smaller dielectric substrates. This can be very useful in many design situations such as using RFID tags to track hospital records. In this situation RFID tags are placed on each individual folder of information, which can be represented as a very thin dielectric.

IV. CONCLUSION

Two novel compact metamaterial-based antenna designs for UHF RFID tags are presented. The first design is based on a deformed omega structure found in left-handed designs and the second design is based on SRRs which are used in the designs of left-handed material. For both

designs the value of the permittivity was varied, the substrate thickness was varied and several different layouts were investigated. This resulted in a very thorough understanding of the characteristics of both designs. It has been shown that the deformed omega-based antenna is more suitable for an application on a thicker substrate while the SRR-based antenna is more suitable for applications with thin adhesive type substrates. Finally, in all cases the antennas presented here are very simple to design, very simple to manufacture, resonate at dimensions less than $0.15\lambda_0$ and are comparable to the performance of commercially available passive RFID tags with larger overall dimensions.

ACKNOWLEDGMENTS

The authors would like to thank Aaron Reinholz, the Associate Director for Electronics Technology, at the Center for Nanoscale Science and Engineering (CNSE), North Dakota State University, for supporting various aspects of this project.

This material is based on research sponsored by the Defense Microelectronics Activity under agreement number H94003-08-2-0804. The United States Government is authorized to reproduce and distribute reprints for government purposes, notwithstanding any copyright notation thereon.

REFERENCES

- [1] K. Finkenzeller, *RFID Handbook: Radio-Frequency Identification Fundamentals and Applications*, John Wiley and Sons, 2002.
- [2] E. Cooney, *RFID+: The Complete Review of Radio Frequency Identification*, Cengage Delmar Learning, 2006.
- [3] D. Paret, R. Riesco and R. Riesco, *RFID and Contactless Smart Card Applications*, John Wiley and Sons, Inc., 2005.
- [4] V. D. Hunt, A. Puglia, and M. Puglia, *RFID - A Guide to Radio Frequency Identification*, John Wiley and Sons, Inc., 2007.
- [5] E. W. Schuster, S.J. Allen, and D.L. Brock, *Global RFID: The Value of the EPCglobal Network for Supply Chain Management*, Springer-Verlag New York, LLC, 2006.
- [6] B. D. Braaten, G. J. Owen, D. Vaselaar, R. M. Nelson, C. Bauer-Reich, J. Glower, B. Morlock, M. Reich, and A. Reinholz, "A printed rampart-line antenna with a dielectric superstrate for UHF RFID applications," *IEEE International Conference on RFID*, April 16-17, 2008.
- [7] M. L. Ng, K. S. Leong, D. M. Hall, and P. H. Cole, "A small passive UHF RFID tag for livestock identification," *IEEE International Symposium on Microwave, Antenna, Propagation and EMC Technologies for Wireless Communications*, vol. 1, pp. 67-70, Aug. 8-12, 2005.
- [8] B. Rosenberg, *RFID: Applications, Security, and Privacy*, Pearson Education, 2006.
- [9] P. Blythe, "RFID for road tolling, road-use pricing and vehicle access control," *IEE Colloquium on RFID Technology (Ref. No. 1999/123)*, pp. 811-816, Oct. 1999.
- [10] K. V. S. Rao, P. V. Nikitin, and S. F. Lam "Antenna Design for UHF RFID Tags: A Review and a Practical Application," *IEEE Transactions on Antennas and Propagation*, vol. 53, no. 12, pp. 3870-3876, December 2005.
- [11] H. -J. Li, H. -H. Lin, and H. -H. Wu, "Effect of antenna mutual coupling on the UHF passive RFID tag detection," *IEEE Antennas and Propagation Society International Symposium*, Jul. 2008.
- [12] X. Qing and Z. N. Chen, "Proximity effects of metallic environments on high frequency RFID reader antenna: study and applications," *IEEE Transactions on Antennas and Propagation*, vol. 55, no. 11, pp. 3105-3111, Nov. 2007.
- [13] R. W. Ziolkowski and C. -C. Lin, "Metamaterial-inspired magnetic-based UHF and VHF antennas," *IEEE Antennas and Propagation Society International Symposium*, July 2008.
- [14] C. -J. Lee, K. M. K. H. Leong, and T. Itoh, "Composite right/left-handed transmission line based compact resonant antennas for RF module integration," *IEEE Transactions on Antennas and Propagation*, vol. 54, no. 8, pp. 2283-2291, August 2006.
- [15] C. -J. Lee, K. M. K. H. Leong, and T. Itoh, "Design of resonant small antenna using composite right/left-handed transmission line," *IEEE Antennas and Propagation Society International Symposium*, pp. 218-221, July 2005.
- [16] I. O. Mirza, S. Shi, C. Fazi, and D. W. Prather, "Stacked patch antenna

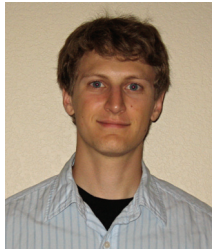
- miniaturization using metamaterials,” *IEEE Antennas and Propagation Society International Symposium*, July 2008.
- [17] A. V. Kildishev and U. K. Chettiar, “Cascading optical negative index metamaterials,” *ACES Journal*, vol. 22, no. 1, pp. 172-183, March 2007.
- [18] A. Ali and Z. Hu, “Metamaterial resonator based wave propagation notch for ultra-wideband filter applications,” *IEEE Antennas and Wireless Propagation Letters*, vol. 7, pp. 210-212, 2008.
- [19] J. Bonache, M. Gil, I. Gil, J. Garcia-Garcia, and F. Martin, “On the electrical characteristics of complementary metamaterial resonators,” *IEEE Microwave and Wireless Components Letters*, vol. 16, no. 10, pp. 543-545, October 2006.
- [20] N. T. Messiha, A. M. Ghuniem, and H. M. El-Hennawy, “Planar transmission line medium with negative refractive index based on complementary omega-like structure”, *IEEE Microwave and Wireless Components Letters*, vol. 18, no. 9, pp. 575-577, September 2008.
- [21] G. V. Eleftheriades, “Analysis of bandwidth and loss in negative-refractive-index transmission-line (NRI-TL) media using coupled resonators”, *IEEE Microwave and Wireless Components Letters*, vol. 17, no. 6, pp. 412-414, June 2007.
- [22] G. V. Eleftheriades, “A generalized negative-refractive-index transmission-line (NRI-TL) metamaterial for dual-band and quad-band applications”, *IEEE Microwave and Wireless Components Letters*, vol. 17, no. 6, pp. 415-417, June 2007.
- [23] Y. -H. Ryu, J. -H. Lee, J. -Y. Kim and H. - S. Tae, “DGS dual composite right/left handed transmission line,” *IEEE Microwave and Wireless Components Letters*, vol. 18, no. 7, pp. 434-436, July 2008.
- [24] R. Islam and G. V. Eleftheriades, “Compact corporate power divider using metamaterial NRI-TL coupled-line couplers,” *IEEE Microwave and Wireless Components Letters*, vol. 18, no. 7, pp. 440-442, July 2008.
- [25] S. -G. Mao, Y. -Z. Chueh, and M. -S. Wu, “Asymmetric dual-passband coplanar waveguide filters using periodic composite right/left-handed and quarter-wavelength stubs,” *IEEE Microwave and Wireless Components Letters*, vol. 17, no. 6, pp. 418-420, June 2007.
- [26] J. Dacuna and R. Pous, “Miniaturized UHF tags based on metamaterials geometries,” *Building Radio Frequency Identification for the Global Environment*, www.bridge-project.eu, July 2007.
- [27] M. Stupf, R. Mittra, J. Yeo, and J. R. Mosig, “Some novel design for RFID antennas and their performance enhancement with metamaterials,” *Microwave and Optical Technology Letters*, vol. 49, no. 4, pp. 858-867, February 2007.
- [28] D. Mishra, D. R. Poddar and R. K. Mishra, “Deformed omega array as LHM,” *Proceedings of the International Conference on Recent Advances in Microwave Theory and Applications*, pp. 159-160, Nov. 2008.
- [29] M. Shamonin, E. Shamonina, V. Kalinin, and L. Solymar, “Resonant frequencies of a splitting resonator: analytical solutions and numerical simulations,” *Microwave and Optical Technology Letters*, vol. 44, no. 2, pp. 133-136, January 2005.
- [30] K. D. Palmer and M. W. van Rooyen, “Simple broadband measurements of balanced loads using a network analyzer,” *IEEE Transactions on Instrumentation and Measurement*, vol. 55, no. 1, pp. 266-272, February 2006.
- [31] Agilent Technologies, www.agilent.com
- [32] Y. Feng, B. D. Braaten, and R. M. Nelson, “Analytical expressions for small loop antennas – with application to EMC and RFID Systems,” *IEEE International Symposium on Electromagnetic Compatibility*, August 2006.



Benjamin D. Braaten received the B.S., M.S. and Ph.D. degrees in electrical engineering from North Dakota State University, Fargo, in 2002, 2005 and 2009, respectively. He is currently an assistant professor in the electrical and computer engineering department at North Dakota State University. His research interests include antennas, radio frequency identification, complex radiation

problems, methods in computational electromagnetics, source modeling, electromagnetic compatibility and harmonic analysis.

Dr. Braaten is a member of the Applied Computational Electromagnetic Society (ACES), Institute of Electrical and Electronics Engineers (IEEE) and the national mathematics honor society Pi Mu Epsilon.



Boulder.

Robert P. Scheeler received the B.S. degree in electrical engineering at North Dakota State University, Fargo, ND in 2008. He is currently working towards the Ph.D. degree in electrical engineering at the University of Colorado at



Michael Reich received the B.S. degree from North Dakota State University, Fargo, ND, in 1990, the M.S. degree from The Pennsylvania State University, State College, PA, in 1998, and the Ph.D. from North Dakota State University, Fargo, ND, in 2009, all in electrical engineering. He is currently employed by the Center for Nanoscale Science and Engineering at North Dakota State University, Fargo, ND, where he has been a Research Engineer since 2005. At the Center he has been involved in a number of projects revolving around wireless sensors, RFID systems, and antennas. He also manages the Center's RFID and Wireless Sensor Laboratory. Prior to joining the Center for Nanoscale Science and Engineering, he was employed by Phoenix International Corp. from 1997 to 2005 and by the Naval Undersea Warfare Center Division Keyport from 1990 to 1997. In these positions, he performed a wide range of activities, including embedded software development, project management, production test, and electromagnetic compatibility. His research interests include antennas (analysis, synthesis, and measurement), computational electromagnetics, RFID systems, and RF system design.

Dr. Reich is a member of the Institute of Electrical and Electronics Engineers.



Robert M. Nelson is currently a Professor and Program Director (of the Computer Engineering Program) at the University of Wisconsin – Stout in Menomonie, WI. Dr. Nelson received a B.A. degree in mathematics from Northland College, Ashland, WI in 1977, the M.S.E.E. degree from Washington State University, Pullman, WA in 1981, and the Ph.D. from NDSU in 1987. He has been a member of the technical staff of Bell Telephone Laboratories, has served on the faculty of the University of Idaho, and at North Dakota State University, has consulted with Michigan Technological University and Lawrence Livermore National Labs; NDSU Center for Nanoscale Science and Engineering (CNSE); Sverdrup Technology (Eglin Air Force Base); Otter Tail Power Company; and the Naval Undersea Warfare Center, New London, CT. Dr. Nelson has been working (teaching and research) in the area of applied electromagnetics, including antennas, transmission lines, microwave engineering, and EMI/EMC since 1981.



Cherish Bauer-Reich received the B.S. degree in physics (2003) and the M.S. degree in electrical engineering (2008) from North Dakota State University in Fargo, ND. She is currently pursuing a Ph.D. in geophysics from the University of Minnesota – Twin Cities in Minneapolis, MN. Her research interests involve modeling a wide variety of electromagnetic phenomena. She is a member of the Institute of Electrical and Electronics Engineers, American Geophysical Union, and American Physical Society.



Jacob Glower received the B.S., M.S. and Ph.D. degrees in electrical engineering from The Ohio State University in 1982, 1985 and 1988, respectively. He is currently an associate professor in the electrical and computer engineering department at North Dakota State University. His research interests include radio frequency identification, embedded

system design, adaptive controls and impedance controls.



Gregory J. Owen received the B.S. and M.S. degrees in electrical engineering at North Dakota State University, Fargo, ND in 2007 and 2009, respectively. He is currently an electrical engineer for Sebesta Blomberg and Associates in

Fargo ND. His research interests include radio frequency identification, power quality and power system protection.

UHF-HF RFID Integrated Transponder for Moving Vehicle Identification

Alberto Toccafondi¹, Cristian Della Giovampaola¹, Paolo Braconi², Alessio Cucini²

¹ Department of Information Engineering,
University of Siena, Via Roma 56, 53100 Siena, Italy
albertot@dii.unisi.it

² Wavecomm S.r.L.,
Loc. Belvedere, 53034 Colle Val d'Elsa, Siena 53100 Italy
cucini@wavecomm.it

Abstract — This paper presents a passive HF-UHF RFID integrated transponder for the identification of a moving vehicle. It consists of a single ISO 7810 ID-1 Card where both a UHF meander dipole antenna and an ISO 15693 commercial tag are arranged. The UHF antenna is designed by using a parametric analysis of the optimal shape of the meanders to obtain a proper conjugate matching between the antenna and the RFID microchip. A single-lane identification scenario is presented and simulated. The effects of the electromagnetic reflection and diffraction on the reading range as well as on the identification operations of a tagged vehicle are also investigated. Numerical simulations and experimental results on a prototype of the conducted transponder confirm the possibility of using this technology for the identification of a moving vehicle approaching a road-toll system with a relatively slow speed.

Index Terms — RFID, UHF tag, HF tag, integrated transponder, moving vehicle.

I. INTRODUCTION

Radio Frequency Identification (RFID) is a recent outstanding technology which permits the identification and tracking of objects by using wireless data exchange between a reader station and small transponders or tags located on the objects to be identified [1]. Typically these RFID tags are composed of an integrated microchip and an electromagnetic coupling element or antenna. The identification process takes place through an RFID reader which interrogates a specific volume

and collects information about the objects, exchanging wireless data with the object's tags located in the mentioned volume. RFID systems may be active or passive depending on whether the tags have their own power supply.

RFID systems operating at HF band (13.56 MHz) are widely used in the areas of ticketing, personnel access control and object tracking. These systems employ the near field inductive coupling to transfer energy and binary data between the reader and the tags. They are characterized by an excellent immunity to environmental noise and electrical interference and exhibit a minimal shielding effect from adjacent objects and human body. However, limits are imposed on the permitted magnetic field strength due to country regulations. This limitation has resulted in the maximum achievable reading range of approximately 1 m.

RFID systems operating at higher frequencies, especially at the UHF band, allowing us to obtain middle to long range wireless links combined with good reliability of the communication. Passive RFID systems at UHF (865-868 MHz in Europe, 902-928 MHz in North and South America and 950-956 MHz in Japan) and microwave (2.45 GHz) bands use the modulated scattered technique to establish a radio link between the reader and the tags. Here, the reflected signal from the tag is modulated by an integrated microchip (IC) directly connected to the antenna. As a consequence, RFID transponder performances are strongly affected by the frequency-dependent impedance match between antenna and IC. However, in these frequency ranges it is possible to resort to antennas

with far smaller dimensions and greater efficiency than that employed at frequency ranges below 30 MHz. Depending on the IC sensitivity and on the tag antenna performances, typical ranges of 4-6 m can now be achieved using passive UHF backscatter transponders. Typical applications of these RFID systems are in logistic as well as access control services.

The continuous growing of the market demand has promoted intense research on RFID systems for non conventional applications. Among which significant efforts have been made in developing RFID tags and intelligent transponders for vehicle to road-side communications to automate vehicular control access and road-tolling operations [2], [3]. Moving vehicles are typically identified by active tags due to their largely extended communication range and high operational efficiency [4]. However, the use of active tags presents some impairments, such as the high cost for mass production when compared to passive ones, and the life expectancy of the battery. Moreover, the long reading distance may cause some problems in controlling the reader detection volume, which may result in possible wrong detections by the reader when it operates in a multi-lane identification environment. The use of passive tags is more advantageous due to their low cost, compactness and maintenance free nature.

This paper presents and analyzes an RFID passive integrated HF-UHF tag for the identification of moving vehicles within a mono-lane scenario. It is found that this type of transponder may be used in all the multi-service applications where a high level of interoperability between different systems is required [5], [6]. The integrated UHF-HF RFID passive tag is composed of a UHF meander dipole antenna operating at the European band (865-870 MHz) and an HF (13.56 MHz) ISO 15693 commercial tag arranged in two separate sections on an equivalent ISO 7810 ID-1 card space. The UHF antenna has been designed to provide small size and proper conjugate matching to the high-capacitive input impedance of the tag IC. The antenna design has been optimized, taking into account both the presence of the commercial ISO 15693 tag located in the HF section and the presence of the car windshield. UHF antenna characteristics, including both the return loss with respect to the IC input impedance and radiation pattern, are investigated. In order to assess the

effects of the various reflection and diffraction contributions originated by the presence of the car body, which may reach the passive tag, a single-lane vehicle identification scenario is also simulated and analyzed. It is found that in some conditions the presence of multiple paths tends to enhance the minimum field intensity required to activate a passive tag, thus improving the achievable reading distance. Finally, a prototype of the integrated transponder printed on FR4 substrate has been developed and tested in a real scenario. Experimental tests have shown a good overall performance of the transponder, and have confirmed a possible increase of the tag performances in terms of reading distance in presence of the car body.

II. TRANSPONDER STRUCTURE

One of the main challenges of this work is to accommodate two different passive tags operating at HF and UHF bands, with their own radiating structures on a single ISO 7810 ID-1 Card. Typical dimensions of an ISO 7810 ID-1 Card are 85.72 x 54.03 mm which also represent the space available to integrate the two tags. During the design process, it is essential to find the best tradeoff between the space occupied by the tags and the desired operational requirements. Moreover, the final layout has to satisfy the typical RFID requirements in terms of flexibility and low cost for mass production. The above requirements can be achieved by designing a UHF uniplanar single-layered dipole-type antenna with reduced size to take advantage of the common PCB techniques as well as the low cost. In addition, to improve the transponder performance, a correct conjugate impedance matching between antenna and tag IC has to be obtained. Passive ICs are intrinsically highly reactive because of the necessary power to bias the IC front-end, which is delivered through electromagnetic coupling. In this case, due to the low input resistance and the relatively high capacitive reactance of the IC, antennas with a low resistive and highly inductive input impedance have to be designed to achieve a conjugate match the IC. A simple way to reduce the size of a dipole antenna and to obtain both a relatively high inductive input impedance and reliable radiation characteristics is to resort to a T-match dipole antenna with meandered arms [5],[7],[8]. The antenna layout is shown in Fig. 1

where the geometrical parameters of the antenna are also indicated.

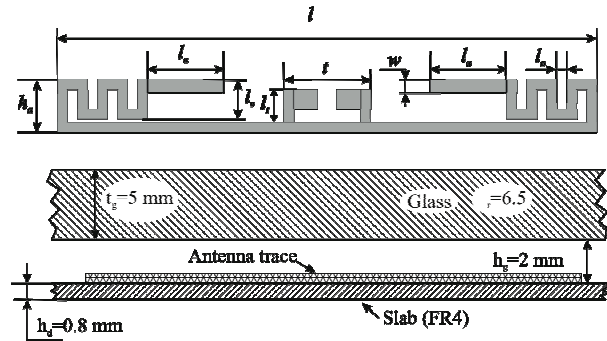


Fig. 1. UHF tag antenna layout and simulation model.

The RFID chip chosen to connect to the prototype antenna is a UHF Gen2 Strap kindly provided by Texas, with an estimated packaged chip input impedance of $Z_c = (11 - j63) \Omega$ and a power sensitivity $P_{th} = -13$ dBm at $f = 867$ MHz.

In RFID systems operating at HF band (13.56 MHz), the tag coupling element is typically constituted by a planar coil antenna that may be built at low cost using etching or common screen printing technique. Concerning the HF section, due the wide availability of commercial inlays, we chose to resort to a commercial ISO 15693 Tag constituted by a copper wire deposited antenna coil connected to a Philips I-Code RFID chip. This commercial Tag is 52 mm x 41 mm thus leaving an available space of about 81 mm x 12 mm for the UHF antenna. However, to take into account the presence of the HF antenna coil while designing the UHF tag, a 6-turn rectangular loop coil is considered in the numerical simulations, as illustrated in Fig. 2. The prototype transponder has been derived on a single grounded low cost FR4 dielectric slab ($\epsilon_r = 4.4$, $h = 0.8$ mm) and has been design to operate at the European licensed UHF band (center frequency $f = 867$ MHz). The proposed arrangement provides a satisfactory overall tag performance with respect to other conceivable layouts.

III. UHF ANTENNA DESIGN AND ANALYSIS

The UHF antenna has been designed and optimized using a commercial electromagnetic simulation software. The main goal of the design has been to tune the antenna input impedance in

such a way to be the conjugate of the microchip characteristic impedance when the tag is in the operative environment. Numerical simulations are first carried out by modeling the presence of the car windshield near the tag antenna. The glass has been modeled as a planar dielectric layer of thickness $t_g = 5$ mm, with relative dielectric permittivity $\epsilon_r = 6.5$ located at a distance $h_g = 2$ mm from the antenna, as shown in the second part of Fig. 1.

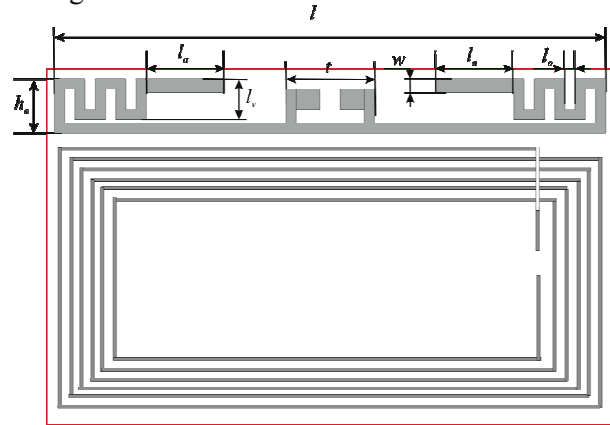


Fig. 2. UHF-HF integrated transponder layout.

A. Return Loss

As mentioned above, a proper impedance match between the antenna and the IC is very important in order to maximize the tag performances. In RFID tags, the antenna is directly connected to the chip, which typically exhibits a high-capacitive input impedance. To obtain a better conjugate impedance match, it is important to minimize the Kurokawa's power reflection coefficient $|s|^2$ [9], [10], where s is defined by

$$s = \frac{Z_c - Z_a^*}{Z_c + Z_a} \quad (1)$$

where Z_a is the complex antenna impedance and Z_c is the complex IC input impedance. The maximum reading range D_{max} of an RFID system is directly affected by the power reflection coefficient and can be computed using the Friis free-space formula as

$$D_{max} = \frac{\lambda}{4\pi} \sqrt{\frac{P_{erp} G_r}{P_{th}} p(1 - |s|^2)} \quad (2)$$

where λ is the wavelength, P_{erp} is the equivalent

isotropic radiated power transmitted by the reader, G_r is the tag antenna gain, P_{th} is the minimum power required to activate the chip, and p is the polarization loss factor.

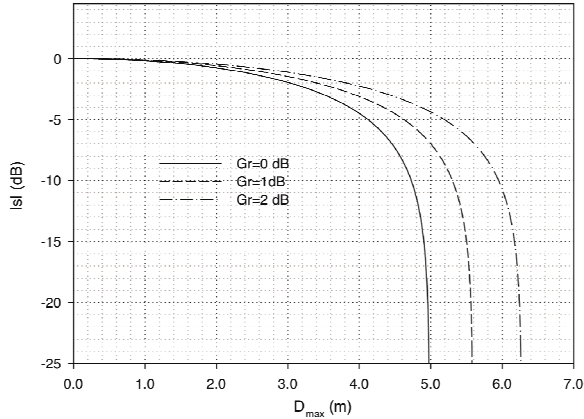


Fig. 3. Return loss as a function of the maximum achievable reading range for different tag antenna gain ($P_{th} = -13$ dBm, $p = 0.5$, $f = 867$ MHz, $P_{eirp} = 35.16$ dBm).

In Fig. 3 the return loss as a function of the maximum achievable reading range, for a given antenna gain G_r , is reported. Calculations are made for a chip sensitivity $P_{th} = -13$ dBm, frequency $f = 867$ MHz, polarization loss factor $p = 0.5$, and for the maximum allowed P_{eirp} by the European regulations ($P_{eirp} = 35.16$ dBm). It is shown that for a given EIRP tag antenna gain, the reading range may not be significantly increased by increasing the return loss over about -15dB to -17dB. These return loss values can be considered as the impedance match requirements in order to obtain good tag performance.

Among all the geometrical parameters considered in the design process, the key ones are the vertical l_v and the horizontal l_o length of the meander line branches, as well as the length l_a of the final arms. As is well known, the length of a resonating dipole must be approximately half of the wavelength at the operational frequency. The geometrical dimensions of the T-match, which comprise the two parameters t and l_t , have been dictated by the size of the chip pads. As a first step, the design parameters were set such that the

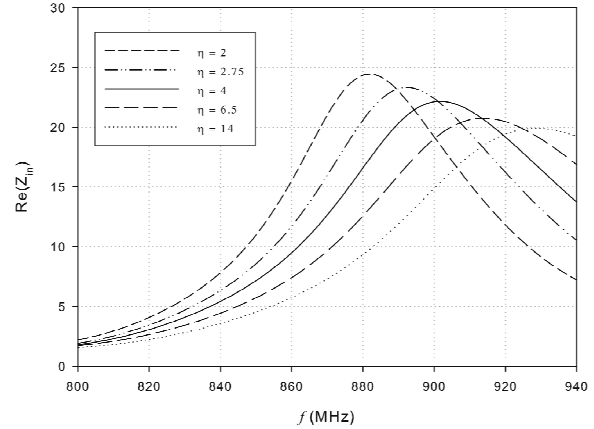


Fig. 4. Real part of the antenna input impedance for different values of $\eta = l_v / l_o$.

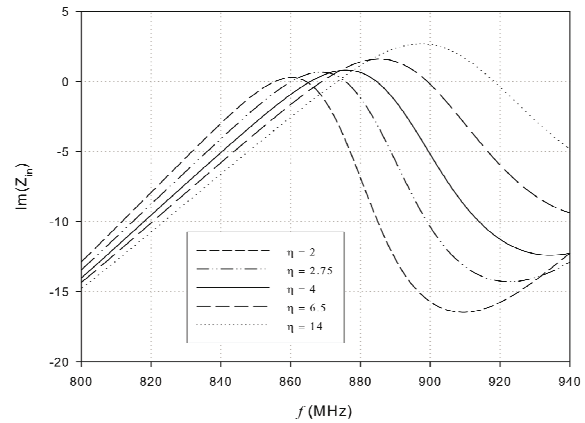


Fig. 5. Imaginary part of the antenna input impedance for different values of $\eta = l_v / l_o$.

total length of the dipole measured at the median line was half wavelength at $f = 867$ MHz, provided that the dipole could fit the space available for the UHF section. The length of the final arm l_a was initially chosen between the maximum and minimum values feasible. This allows us to tune the antenna around the desired frequency. A capacitor connected in series to the feeding port of the antenna has been used in the simulations to take into account the capacitive part of the microchip impedance. Concerning the shape of the meanders, there is not a unique choice for l_v and l_o . To better select these values, once the total length of the dipole is fixed, we analyzed the behavior of the antenna input impedance for several ratios $\eta = l_v / l_o$. Figures 4 and 5 show the impedance curves for different values of η .

In Fig. 5 we can observe that for every value of η considered in the simulations the dipole is almost resonant within the band of interest, since the imaginary part of the impedance is vanishing. This is because the resonant frequency mostly depends on the length of the dipole, which is kept constant. From Fig. 4 we notice that for $\eta = 4$, the antenna impedance exhibits a real part of about 11Ω at $f = 865$ MHz, thus suggesting a good conjugate matching between antenna and microchip impedance at that frequency. The frequency shift between this result and the initial guess is mainly due to the T-match feeding, since the T-match can modify the electrical length of the dipole. In the last step, the fine tuning to the frequency $f = 867$ MHz can be achieved by modifying the length l_a of the final arms of the dipole without significantly changing the impedance matching between antenna and microchip. The final geometrical dimensions of the meandered dipole antenna are $w = 1.5$ mm, $l = 81$ mm, $h_a = 8$ mm, $l_o = 1.5$ mm, $l_a = 11$ mm, $l_v = 6$ mm, $l_t = 5$ mm, $t = 13.24$ mm.

In Fig. 6, the magnitude of the input reflection coefficient is reported. For this antenna, the -10dB bandwidth is approximately 45 MHz, due to the low input impedance quality factor of the IC (~ 5.8).

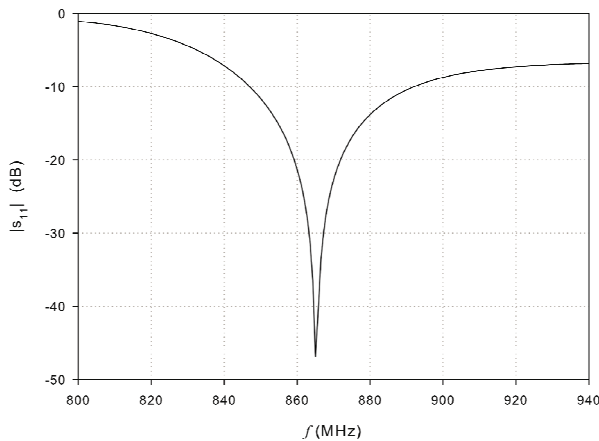


Fig. 6. Antenna input reflection coefficient.

B. Radiation Pattern

The simulated E- and H-plane radiation patterns at $f = 867$ MHz of the co-polar components for the proposed antenna in the final configuration are shown in Fig. 7. These curves

show that the obtained radiation patterns are somewhat similar to that of a typical dipole. It is also observed that the maximum of the radiation pattern in the H-plane plane is slightly tilted towards the side where the HF coil antenna is located. However it is expected that this effect does not significantly influence the overall performance of the transponder in the direction perpendicular to the dipole plane. Simulations have also shown about 1.5 dB antenna gain at the working frequency.

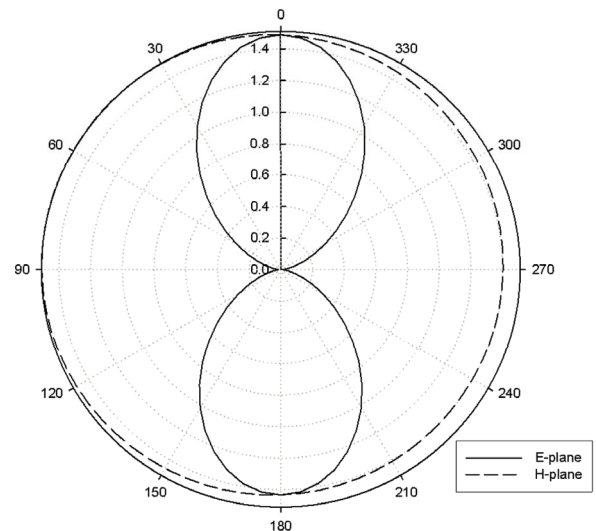


Fig. 7. E-plane (continuous line) and H-plane (dashed line) radiation patterns at 867 MHz.

IV. SINGLE-LANE VEHICLE IDENTIFICATION SCENARIO

In operative conditions the identification of a moving vehicle can be difficult because of multiple path signals that may reach the passive tag during the interrogating operations. Multiple paths are mainly due to reflections and diffractions that occur at the metallic surfaces and edges of the car body. In particular, it is expected that the dominant phenomena are associated with the reflection from the hood of the car and with the diffractions at the surrounding metallic edges of the windshield. To estimate the amount of these interferences and their effects on the performances of the passive tag when located on the windshield of a car, a single-lane identification scenario has been conceived and implemented using a commercial numerical code (Feko). The model implemented consists of a part of the metallic car body with a planar glass windshield illuminated by

a circularly polarized patch antenna operating at 867 MHz, as illustrated in Fig. 8. The antenna is centered with respect to the lane width and the height over the lane is $h_a = 5.5$ m. The beam axis of the antenna is tilted from the horizontal by a $\theta_a = 60^\circ$ angle. The transmitted ERP of the antenna has been set to 2W and, taking into account all the other parameters, the activating electric field intensity for the chosen chip is about 2.5 V/m. In order to limit the computational burden, the car model is constituted of solely the parts that contribute to the reflected or diffracted field at the tag position, as illustrated in Fig. 8. The windshield of the car is modeled by a planar glass of thickness $t_g = 5$ mm and dielectric permittivity $\hat{\epsilon}_g = 6.5$. The total electric field has been observed on a rectangular plane located inside the car parallel to the windshield at a distance of about 2 mm. By symmetry the observation plane is taken to be half of the windshield, with the origin of the x-axis corresponding to the centre of the lower-edge of the windshield and marching towards the lateral edge of the windshield on the x-axis.

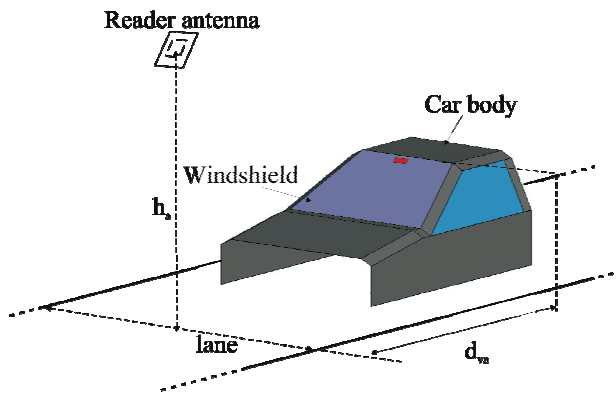


Fig. 8. Simulated single-lane vehicle identification scenario.

As an example, the simulated total electric field intensity at the observation plane for a distance $d_{va} = 2$ m has been reported in Figs. 9 and 10.

The case of free space, where both the car and lane are not present, is shown in Fig. 9. It is observed that the field footprint is dictated by the radiation pattern of the antenna, and that the field intensity in the most part of the windshield is very

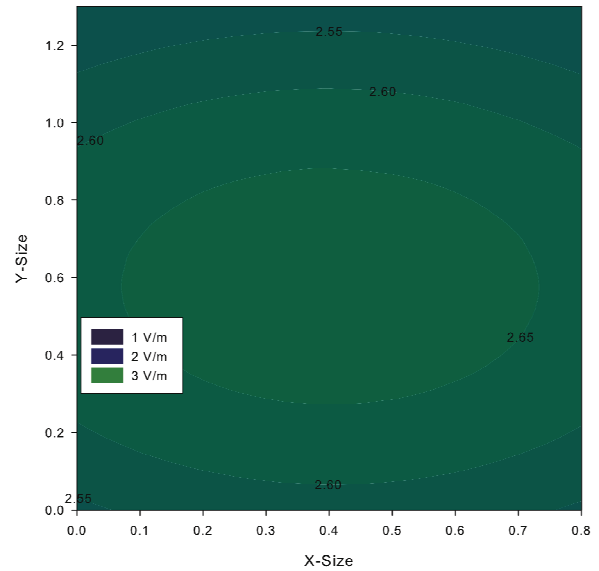


Fig. 9. Electric field intensity at the observation plane without the car body.

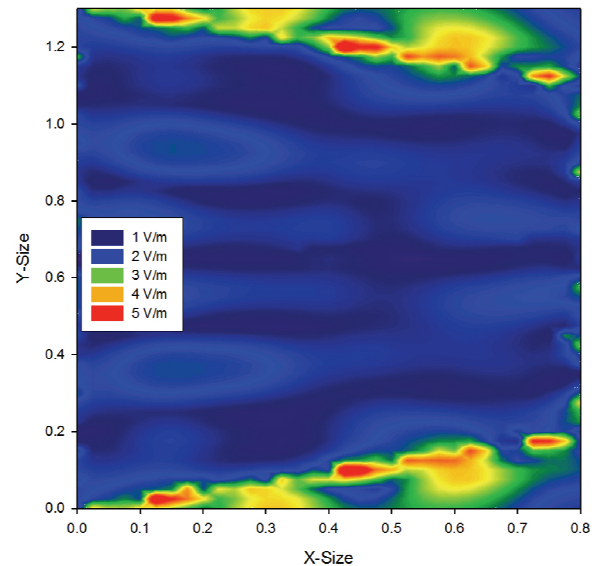


Fig. 10. Electric field intensity (V/m) at the observation plane in presence of the car body.

close to the activation threshold. A completely different situation is shown Fig. 10 where the car body is present.

It is shown that diffractions and reflections by the car body can cause an enhancement of the field intensity in regions near the upper portion of the glass. In these parts of the windshield the total electric field intensity may be significantly higher than the activation threshold. Moreover, due to the

particular geometry configuration, these effects tend to remain rather constant also when the car is moving inside the beam footprint. As a result, the physical gate useful for radio communications that is created with the combination of these effects can be quite large and permits the implementation of a non-stop tolling system.

V. EXPERIMENTAL RESULTS

A prototype of the integrated transponder at the European band ($f_o = 867$ MHz) with the proposed antenna has been built using FR4 ($\epsilon_r = 4.4$, thickness $h = 0.8$ mm) as a substrate and copper for the traces.

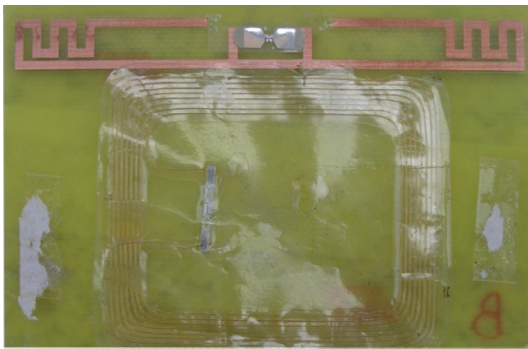


Fig. 11. Prototype of the integrated transponder.

A picture of the prototype is shown in Fig. 11. As mentioned above, the commercial ISO 15693 Tag consists of a copper wire antenna coil deposited on a plastic flexible substrate, which can be easily placed next to the UHF tag antenna. The reading range for the tag has been measured by using a setup composed of a UHF Reader and circularly polarized antenna with gain $G_r = 9$ dBc.

In order to test the maximum reading range of the integrated transponder when placed on the windshield, the reader antenna was first positioned in front of the car under test, such that the tag was illuminated directly by the reader antenna beam. Table 1 shows the measured maximum reading distance of the UHF tag of the integrated transponder when it is equipped with the HF tag.

Table 1: Maximum reading distance.

	Position A	Position B
Car type 1	9.1 m	8.5 m
Car type 2	7.6 m	8.9 m

Test results have been obtained for two different types of car and two different positions of the transponder on the windshield. The two positions A and B refer to an upper central and upper lateral position of the transponder on the windshield, respectively, and are illustrated in Fig. 12.



(a) Upper central position (A)



(b) Upper central position (B)

Fig. 12. Tag position on the windshield during the tests.

It is found that the maximum reading distance is significantly higher than the one expected in free space, thus substantiating an enhancement of the field intensity near the glass-metal junction of the windshield. An uninterrupted reading capability is observed when reducing the distance as the vehicle moves. The measurements show that the presence of the HF coil does not significantly degrade the tag performance. Finally, preliminary tests have also been conducted in a real scenario to establish the number of times a vehicle is identified while approaching a portal-frame equipped with an overhead reader set-up. Test results show that the car type 1 equipped with the proposed tag in position A can be identified at least 2 times, up to a vehicle speed of about 40 Km/h.

VI. CONCLUSION

In this paper an RFID passive integrated HF-UHF tags for the identification of moving vehicles within a mono-lane system for road-toll operations has been presented and analyzed. The passive transponder operates within the European band (865-870 MHz) and it consists of both a UHF tag and an ISO 15693 commercial tag, arranged in

two separate sections on a single ISO 7810 ID-1 card. A design process of the UHF tag antenna which allowed us to obtain a relatively small antenna with proper conjugate matching to the capacitive input impedance of the chosen tag IC has been presented. Simulation results have shown an antenna gain of about 1.5 dB and a power reflection coefficient with a -10 dB bandwidth of about 45 MHz. The radiation patterns produced by the simulations agree with the ones of a typical planar dipole antenna. A single-lane identification scenario has also been conceived and simulated, with the aim of analyzing the effects of the various reflection and diffraction phenomena originating at the car body on the identification operations. Simulation results have shown that, for the chosen configuration of the set-up, multiple path phenomena may cause an enhancement of the field intensity near the upper glass-metal junction of the windshield. This phenomenon may be used to obtain a reading zone useful for the identification of a moving vehicle approaching a road-toll system with a relatively slow speed. A prototype of the integrated transponder has been built and tested in a real scenario. Test results have confirmed the good performance of the integrated transponder and have shown an uninterrupted identification capability of a tagged-car up to distances greater than the ones expected for a free space scenario.

ACKNOWLEDGMENT

The authors wish to express their appreciation to Ing. P. Ceseri for the stimulating discussions and useful support.

REFERENCES

- [1] K. Finkenzeller, *RFID Handbook*, Wiley & Sons, Second Edition, 2003.
- [2] D. L. Almanza-Ojeda, A. Hernandez-Gutierrez, and M. A. Ibarra-Manzano, "Design and implementation of a vehicular access control using RFID," *Multiconference on Electronics and Photonics (MEP 2006)*, Guanajuato, Mexico, pp. 223-225, 2006.
- [3] A. G. Foina, S. E. Barbin, and F. J. Ramirez, "A new approach for vehicle access control using active rfid tags," *SBMO/IEEE MTT-S International Microwave and Optoelectronics Conference, IMOC 2007*, pp. 90-93, 2007.
- [4] P. Blythe, "RFID for road tolling, road-use pricing and vehicle access control," *IEE Colloquium on RFID Technology*, pp. 8/1-8/16, 1999.
- [5] A. Toccafondi and P. Braconi, "Compact meander line antenna for hf-uhf tag integration," *Proc. of IEEE AP-Symposium*, June 2007.
- [6] M. Hirvonen, N. Pesonen, O. Vermesan, C. Rusu, and P. Enoksson, "Multi-system, multi-band rfid antenna: Bridging the gap between hf- and uhf-based rfid applications," *European Conference on Wireless Technology*, pp. 346-349, 2008.
- [7] G. Marrocco, "Gain-optimized self-resonant meandered line antennas for RFID applications," *IEEE Antennas and Wireless Propagation Letters*, vol. 2, pp. 302--305, 2003.
- [8] K. V. Seshagiri Rao, P. V. Nikitin, and S. F. Lam, "Antenna design for UHF-RFID tags: a review and a practical application," *IEEE Transactions on Antennas and Propagation*, vol. 53, no. 12, pp. 3870-3876, Dec. 2005.
- [9] K. Kurokawa, "Power waves and the scattering matrix," *IEEE Transactions on Microwave Theory and Techniques*, vol. 13, no. 3, pp. 194-202, Mar. 1965.
- [10] P. V. Nikitin, K. V. S.Rao, S. F. Lam, V. Pillai, R. Martinez, and H. Heinrich, "Power reflection coefficient analysis for complex impedance in RFID tag design," *IEEE Transactions on Microwave Theory and Techniques*, vol. 53, no. 9, pp. 2721-2725, Sept. 2005.



Alberto Toccafondi was born in Prato, Italy, in 1960. In 1989, he obtained his Laurea degree (cum laude) in Electronic Engineering from the University of Florence, and a Ph.D. in Electromagnetic Engineering from the same University in 1994. In 1995, he joined the Dept. of Information Engineering of the University of Siena, where he is currently an Associate Professor. His research interests are concerned with antennas and microwave devices and with analytic and numerical techniques for electromagnetic scattering and multi-path

propagation prediction. His research activity is mainly focused on the incremental and asymptotic methods applied to the prediction of electromagnetic scattering, as well as to the analysis and design of antennas and passive tags for RFID applications. Dr. Toccafondi is a senior member of the IEEE. From 2002 to 2005 he served as a secretary and treasurer of the Central and South Italy Section as well as of the AP/MTT Joint Chapter of the IEEE. He served as a treasurer (2006-2007) and then as a secretary (2008-2009) of the new IEEE Italy Section.



Cristian Della Giovampaola was born in Chiusi (SI), Italy, in 1981. He received his B.S. degree in telecommunications engineering and his M.S. degree (cum laude) in telecommunications engineering from the

University of Siena, Italy, in 2004 and 2006 respectively. In 2010, he received his Ph.D. degree in Information Engineering from the University of Siena, Italy. From October 2008 to October 2009 he was a visiting scholar at the Electromagnetic Communication Laboratory at Pennsylvania State University, University Park, USA. His research interests include high frequency techniques for electromagnetic scattering and diffraction, numerical methods for solving electrically large electromagnetic problems, and radio frequency identification (RFID) system design.



Paolo Braconi obtained the Laurea degree in telecommunication engineering from the University of Siena, Italy, in 2004. In 2005 he won a scholarship about RFID from the Dept. of Information Engineering

of the University of Siena. From September 2006 to June 2007 he was with Telsa Srl as an antenna designer, working primarily on Wi-Max antennas. In July 2007 he joined WaveComm Srl where he is now working on RFID and antenna systems. His interests are in RFID and WSN systems, RF electronics, and antenna design.



Alessio Cucini was born in Poggibonsi, Italy, in 1973. He received the Laurea degree (cum laude) in telecommunications engineering and the Ph.D. degree in electromagnetic engineering from the University of Siena, Siena, Italy, in 1999

and 2003, respectively. From 2004 to 2008 he has been at the Department of Information Engineering, University of Siena, as a Research Associate. He is presently President of WaveComm S.r.l., a spin-off company of the University of Siena operating in the fields of electromagnetic engineering, antennas, sensors, RF and microwave systems, wireless sensor networks (WSN) and radiofrequency identification (RFID). Since 1999, he has been involved in regional, national and European research projects. His interests are in the area of RFID and WSN technologies, antennas and sensors.

Feasibility of Passive Wireless Sensors Based on Reflected Electro-Material Signatures

Azhar Hasan, Andrew F. Peterson, and Gregory D. Durgin

School of Electrical and Computer Engineering
Georgia Institute of Technology, Atlanta, GA 30332-0250, USA
azhar.hasan@gatech.edu, peterson@ece.gatech.edu, durgin@ece.gatech.edu

Abstract— In this paper, a neural network is applied to reconstruct the permittivity profile of a three-section passive sensor for RFID applications. Input reflection coefficients of the wave backscattered from a RF tag, over the frequency range 1-5 GHz, are used to estimate the material parameters. A neural network incorporating the Levenberg Marquardt algorithm is evaluated in terms of average absolute error, regression analysis and computational efficiency. Suitability of the algorithm is verified using both simulated and measured data, and accurate results are obtained while avoiding computational complexity. The methodology developed in this paper can be successfully used for passive sensing applications involving RFID technology to investigate and reconstruct a material profile altered by environmental variables.

Index Terms— RFID, sensors, neural networks, inverse scattering

I. INTRODUCTION

Radio frequency identification (RFID) has been successfully used across a number of tracking and sensing applications. Recent development of materials whose permittivity parameters can change significantly with environmental conditions suggests the possibility of constructing a passive RFID sensor that can be interrogated remotely to extract data about the environment at the sensor [1]. A simple passive sensor of this type consists of an antenna attached to a microstrip transmission line, which in turn is routed over one or more sections of variable permittivity material before being terminated in a load. In the following, we explore the feasibility of reconstructing the permittivity profile of a three-section sensor of this type by using the backscatter from this sensor over frequencies in the range 1 - 5 GHz. Neural networks are employed to re-create the permittivity profile from the received data.

The problem of identifying medium properties from waves reflected from a device of this type is a form of the classical one dimensional inverse scattering problem. For profile inversion in a lossy inhomogeneous media, analytical techniques are difficult to implement in most practical situations,

and thus various numerical techniques have been investigated [2]. Researchers have been employing methods such as the finite difference time domain technique [3] and 1-port and 2-port measurements [4] for extracting the material properties from the information contained in reflected or transmitted waves. Artificial neural networks have been employed across a wide field of applications, including inverse electromagnetic problems [5], [6], and [7]. Exploiting a priori knowledge of the geometry, neural networks incorporating a backpropagation algorithm were able to retrieve the radius position and dielectric permittivity of a circular cylinder [8]. Neural networks have also demonstrated the ability to reconstruct the permittivity profile of homogeneous cylinders in free space and detecting the position of cylinders [9]. The effective use of neural networks to determine non-smooth, one-dimensional profiles of an inhomogeneous layer has been investigated with noisy data by Yaman and Simcsek [10].

The sensor is explained in the following section. The complex reflection coefficient is calculated using signal flow theory as described in section III. A brief introduction to neural networks, with details on the specific approach used in this investigation, is given in section IV. The feasibility study and results are demonstrated in sections V and VI.

II. REMS SENSOR CONCEPT

A sensor concept based on reflected electro-material signatures (REMS) consists of three distinct components working together to provide passive sensing capability of environment information. The first component is the electro-material line, a chemical strip sandwiched between the ground plane and top trace of an RF tag's microstrip transmission line. The second component, the reflector circuitry, consists of the transmission line itself, the radio-frequency integrated circuit (RFIC) that performs backscatter and identification functions, and any RF tag antennas. Finally, an RF reader must be used to interrogate the REMS sensor as well as performs the signal-processing for data extraction. These components are illustrated in Fig. 1

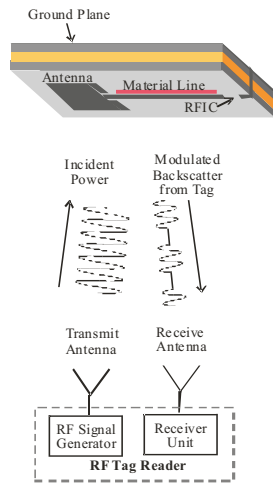


Fig. 1. Components of a REMS Sensor.

Conceivably, the REMS concept could be implemented with existing UHF or microwave passive RFID integrated circuits, greatly lowering cost and allowing passive interrogation of the sensor. In a conventional backscatter RFID system, the signal is reflected from a binary-switched load, providing two potential frequency-dependent measurements for extracting material line parameters [11]. Since an RFID reader filters out unmodulated scatter components, an RFID-based REMS sensor would allow a much more precise measurement compared to other forms of remote sensing.

Any material that has environmental sensitivity to permeability, permittivity, or conductivity may be a candidate for the electro-material line in the REMS sensor. For example, a simple instantaneous temperature sensor could incorporate thermotropic liquid crystals. These types of liquid crystals experience state disordering upon heating, leading to a change in their electrical (and optical) properties [12, 13]. A common, everyday example of these liquid crystals are the disposable thermometer magnets that allow temperature readouts to become visible through a graded liquid crystal film. Another example of candidate material may be a line substrate doped with ferroelectric or super-paramagnetic particles [14]. Such a device could use the nonlinear relationship between field and flux density components to sense external field strengths. The REMS sensor concept may also allow for materials that time-record environmental attributes, thus providing a form of chemical memory rather than electrical memory that would achieve a completely passive sensor. This type of sensor functionality cannot be achieved under today's 'system on a chip' paradigm, which still requires external power supplies for electronic memory recording functions.

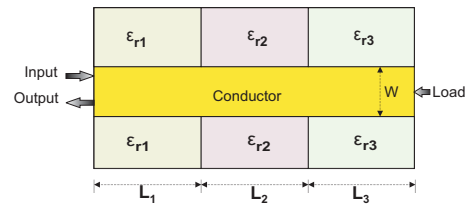


Fig. 2. The microstrip line model with three discrete segments having different permittivity profiles, terminated in a load to emulate a REMS sensor with three wells of sensor material.

III. CALCULATING REFLECTION COEFFICIENT FROM TRANSMISSION LINE MODEL

A REMS reader is an RF transceiver that measures modulated backscatter signals from the RF tag. To test the REMS concept, the sensor is modeled using three cascaded microstrip transmission lines, emulating a three part step discontinuity in the electro-material line. Each cascaded microstrip line is 1.25cm long and 0.5cm wide with a substrate height of 0.05cm. Different dielectric materials in the segments are used to emulate a REMS sensor with three wells of sensor material. The line is terminated in a resistive load. As the transmission line geometry is not specifically designed for a characteristic impedance of 50Ω , this load causes part of the wave to be absorbed and part reflected back. The microstrip line model with three discrete segments having different permittivity profiles is shown in Fig. 2. For the frequency range of 1-5GHz, the relative permittivity, ϵ_r , of each segment was swept across a range of values, and the values of reflection coefficient, Γ_{IN} , at the input of the system were computed. Each transmission line acts as a two port network, and the complete system of the cascaded lines can be analyzed in terms of S-parameters and signal flow graphs [15], using Eq. 1.

$$\Gamma_{IN} = \frac{b_1}{a_1} = S_{11} + \frac{S_{12}S_{21}\Gamma_L}{1 - S_{22}\Gamma_L} \quad (1)$$

The complex-valued reflection coefficient contains information about magnitude as well as phase, and both will be used by the inversion algorithm. To demonstrate how the frequency-swept measurement of an RF reader changes for slight perturbations in the permittivity profiles, the dielectric constant of the second bin was changed for four different values, as illustrated in Fig. 3, and the reflection coefficient was calculated for each case. The effect on magnitude and phase of Γ_{in} , between four values of ϵ_{r2} , with $\epsilon_{r1} = 2.5$ and $\epsilon_{r3} = 3.5$, is shown in Fig. 4 and Fig. 5, respectively. Significant alterations are observed in the magnitude and phase

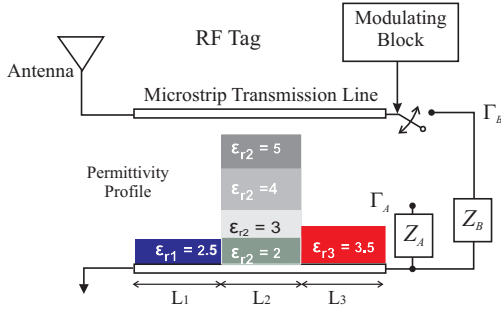


Fig. 3. The transmission line model of the RF tag, illustrating four changing permittivity profiles of the center well of the REMS sensor.

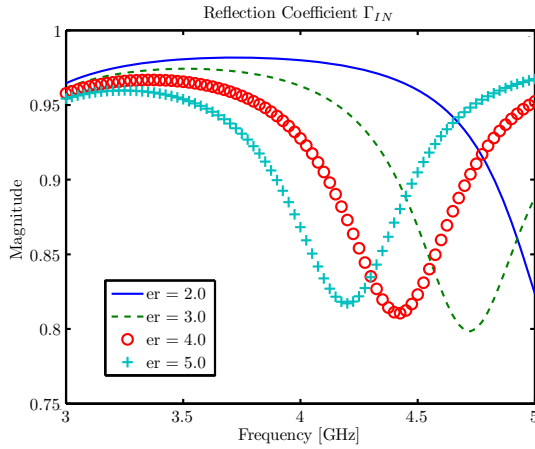


Fig. 4. Magnitude of Γ_{IN} for $\epsilon_{r2} = 2, 3, 4$ and 5 calculated from the signal flow graph.

of the wave scattered out of the tag. Theoretically, every material profile will produce a unique frequency sweep - although designing a wide range of switchable loads (Z_A , Z_B , and possible more) will greatly affect measurement resolution and sensitivity.

IV. NEURAL NETWORK

The idea of neural networks evolved in late 19th century in an attempt to understand how the human brain functions. The concept of decentralized network units (neurons) was introduced in 1943 when McCulloch and Pitts developed the first mathematical model of a neuron [16]. Inspired from brain function, the neural network is generally used to solve artificial intelligence problems without requiring a model of the system. Neural networks are adjusted and trained to solve problems that are difficult to solve using conventional techniques and are extremely useful in pattern recognition and function approximation problems. In this paper, a neural

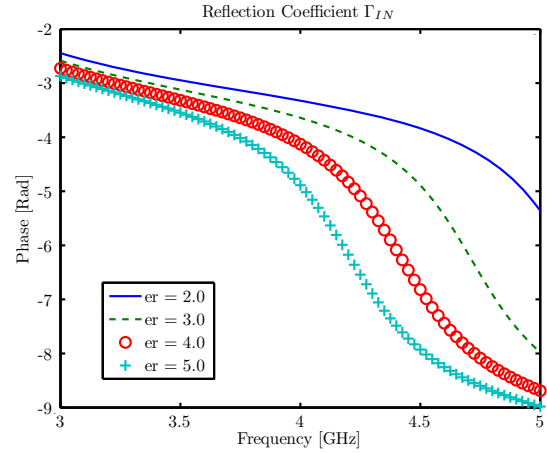


Fig. 5. Phase of Γ_{IN} for $\epsilon_{r2} = 2, 3, 4$ and 5 calculated from the signal flow graph.

network is used to extract the material properties of the microstrip transmission line structure based on the reflection coefficient of a backscattered wave.

In a typical single neuron having a scalar input p , p is multiplied with a weight w and added to a bias/offset b . A neuron may or may not have the bias/offset. The output n (net input) of the summer forms the argument of an activation function (transfer function) f , whose output a is the output of the neuron. The activation function is chosen by the designer, while the weight and bias (if used) are adjusted by some learning rule [17]. The output function is described by Eq. 2.

$$a = f(wp + b) \quad (2)$$

For many systems, one neuron is insufficient and therefore multiple neurons and multiple neuron layers are used, as depicted in Fig. 6. For one such layer comprising S neurons, there may be an arbitrary number of inputs R , each connected to all S neurons. The resulting weight matrix has dimension $S \times R$. The number of neurons is independent of the number of rows and columns [17]. All neurons usually have the same transfer function, although this is not always the case [17]. In the event that one layer of multiple neurons is inadequate, a network with additional (hidden) layers can be used. Each layer has its own weight matrix W , bias vector b , net input vector n and output vector a . For R inputs and S^1 neurons in the first layer, the second layer can be considered as a layer with S^1 inputs, S^2 neurons and a weight matrix of order $S^1 \times S^2$. Input to the second layer is a^1 and its output is the input to the next layer. The final output, a^3 , is given by

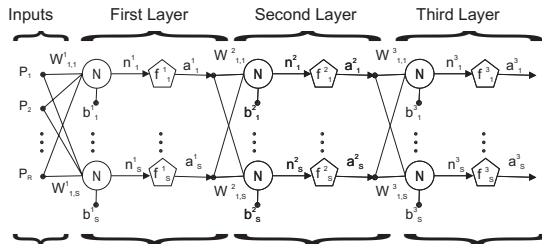


Fig. 6. Three layers of multiple neurons.

Eq. 3.

$$a^3 = f^3(W^3 f^2(W^2 f^1(W^1 p + b^1) + b^2) + b^3) \quad (3)$$

The transfer function may be linear or nonlinear depending upon the problem. The three most commonly used transfer functions are the *hardlimit* transfer function, the *linear* transfer function, and *logsigmoidal* transfer function [16]. The logsigmoidal transfer function takes an input from minus infinity to plus infinity and compresses the output into the range 0 to 1 according to the expression in Eq. 4. It is the most typically used transfer function in backpropagation algorithms and is used in this work as well.

$$a = \frac{1}{1 + e^{-n}} \quad (4)$$

A. Training Algorithms

The weights described in the previous section must be determined by a training process that attempts to match the actual output of the neural network with the desired output for a training data set. Function approximation problems are typically solved using backpropagation algorithms, which require the activation function to be differentiable. A common implementation is known as the *delta* rule, given by Eq. 5 for the j^{th} neuron and the i^{th} weight, where α is the constant learning rate, t_j is the target output, y_j is the actual output and $g(x)$ is the activation function.

$$\Delta w_{ji} = \alpha(t_j - y_j)g'(h_j)x_i \quad (5)$$

Eq. 5 provides the adjustment in weights during one step of the training process.

The training algorithm must minimize the error between the desired and actual network outputs as quickly as possible. The learning rate (denoted by α or l_r) is a critical parameter in every algorithm. If l_r is too large, the algorithm may be unstable, and if l_r is too small, the algorithm converges too slowly. A variety of heuristic or numerical optimization algorithms are reported in the literature [17, 18, 19, 20, 21, 22]. Each algorithm has its own merits

and demerits depending upon the type of problem and computing resources. The gradient descent and gradient descent with momentum algorithms are considered too slow for practical problems [17]. Conjugate gradient methods were invented purely for quadratic functions, and some require excessive memory while others require more iterations to converge. Newton's method is an alternative to conjugate gradient methods for fast optimization, and often converges faster than the conjugate gradient method, but it involves the Hessian which is expensive to compute. In the quasi-Newton method, an approximate Hessian is updated at each iteration instead of being recomputed from scratch [17]. The Broyden, Fletcher, Goldfarb, and Shanno (BFGS) algorithm requires more computation and storage than the conjugate gradient algorithm and is not suited to large networks [17]. The one step secant algorithm is an effort to bridge the gap between conjugate gradient and quasi-Newton algorithms. In terms of accuracy (mean square error), speed, and memory requirements, which algorithm performs best depends upon a number of factors including the problem complexity, the number of points in the data set, weights, biases, the desired accuracy, and the type of problem (pattern recognition or function approximation). For a function approximation problem having a network with a few hundred weights, the Levenberg Marquardt (LM) algorithm often converges the fastest [17].

A number of simulations were carried out to determine the best algorithm, with the result that the LM algorithm exhibited superior absolute average error and computation time. The algorithm was designed to approach second order training speed without computing the Hessian H , instead using the approximation $H = J^T J$, where J is the Jacobian containing the first derivative of network errors with respect to weights and biases. The gradient is computed as $g = J^T e$, where e is the vector of network errors [23]. The Jacobian is computed through a standard back propagation technique which is much less complex than computing the Hessian [24]. The algorithm may be written as

$$x_{k+1} = x_k - [J^T J + \mu I]^{-1} J^T e \quad (6)$$

The primary drawback of the Levenberg Marquardt algorithm is that it requires the storage of a relatively large matrix. The size of the Jacobian is $Q \times n$, where Q is the number of training sets and n is the number of weights and biases. The Jacobian can be divided into equal sub matrices, with the Hessian expressed as

$$H = J^T J = J_1^T J_1 + J_2^T J_2 \quad (7)$$

Table 1. Comparison of actual values of $\epsilon_{r1,2,3}$ vs neural network output

	Actual Values	Neural Network output	Error
Set1	4	4.115	0.115
	4	4.024	0.024
	4	3.985	-0.015
Set2	2	2.018	0.018
	2.3	2.334	0.034
	4.8	4.501	-0.299
Set3	3	3.255	0.255
	2.5	2.495	0.005
	4.5	4.238	0.262

Table 2. Dimensions of microstrip transmission lines in experimental setup.

	Trnas Line 1	Trans Line 2	Trans Line 3
Length (L)	1.25 cm	1.25 cm	1.25 cm
Width (W)	0.5 cm	0.5 cm	0.5 cm
Substrate Height	0.127 cm	0.157 cm	0.127 cm
Conductor Thickness	0.0017 cm	0.0017 cm	0.0017 cm
Loss Tangent	0.002	0.0009	0.002
Substrate	RO 3006	RT/Duroid 5880	RO 3006
Dielectric Constant	6.15	2.2	6.15

Table 3. Comparison of values of $\epsilon_{r1,2,3}$ estimated using neural networks against the actual values for frequency range 1-2.5 GHz.

	ϵ_{r1}	ϵ_{r2}	ϵ_{r3}	Average Error
Actual Value	6.15	2.2	6.15	
Estimate 1 using LM Algorithm	5.72	2.73	5.60	
Absolute Error	0.43	0.53	0.55	0.50
Estimate 2 using LM Algorithm	5.72	2.89	5.53	
Absolute Error	0.43	0.69	0.62	0.58
Estimate 3 using LM Algorithm	5.67	2.81	5.69	
Absolute Error	0.48	0.61	0.46	0.51

where J is divided into two equal matrices J_1 and J_2 .

V. APPLICATION OF NEURAL NETWORKS FOR EXTRACTING MATERIAL PROPERTIES (ϵ_R)

As a first step in using a neural network to extract material parameters, the dielectric constant ϵ_{r2} of the center segment of a 3-step microstrip line is varied from 2-8 with a step size of 0.1, while ϵ_{r1} and ϵ_{r3} were fixed at 3 and 3.8, respectively. A data set containing the magnitude and phase of Γ_{in} was generated for frequencies from 5 to 6 GHz with a step size of 100 MHz. The step size of 100 MHz was chosen to keep the data matrix dimensions within the computing capability of a modest desktop computer; it was observed that frequency steps smaller than 100MHz did not increase the accuracy of the results. The magnitude and phase values were combined in the data matrix D , which has the form shown in Eq. 8.

$$D = \begin{bmatrix} |\Gamma| \\ \angle\Gamma \end{bmatrix} \quad (8)$$

For the initial test, $|\Gamma|$ and $\angle\Gamma$ were matrices of dimensions 11×61 , corresponding to 11 frequencies and 61 different values of ϵ_{r2} . A finer increment of the dielectric constant, 0.01 for instance, might improve the accuracy of the network model, but at a cost of increasing each matrix to 11×601 . The neural network with 10 neurons in single layer was trained using ϵ_{r2} in the range from 2-8, and then tested using the phase and magnitude of Γ_{in} corresponding to $\epsilon_{r2} = 2.1$, and 4.75. The network produced estimated values for ϵ_{r2} of 2.1186 and 4.7693, respectively.

As a second test, ϵ_{r1} and ϵ_{r3} were also varied as the frequency was swept across the 5-6 GHz range with a step size of 100 MHz. Values of ϵ_{r1} , ϵ_{r2} , and ϵ_{r3} were varied from 2-5 with a step size of 0.1. The resulting data matrix had dimensions $22 \times 29,971$. After training, the Levenberg Marquardt algorithm

with 10 neurons in a single layer was able to produce relative permittivity values within ± 0.3 of the actual values, as summarized for several examples in Table 1.

The first two tests were carried out with a single neuron layer. Additional tests were carried out with single layer networks with 5, 10, 15, 20 and 25 neurons, and a two layer network with 10 neurons each. The results were compared in terms of error and coefficient of regression analysis. Each network was tested for the set of permittivity values shown in Eq. 9 in matrix T . The rows of T correspond to ϵ_{r1} , ϵ_{r2} and ϵ_{r3} , while the columns show the set of dielectric constants presented to the network at each time. It was observed that a single layer with 20 or 25 neurons is best suited in terms of absolute mean error and computation efficiency. The errors for 20 neurons are shown in matrix E_{20} in Eq. 10.

$$T = \begin{bmatrix} 2.1 & 2.5 & 3.5 \\ 3.5 & 3.5 & 3 \\ 4.9 & 4.5 & 4 \end{bmatrix} \quad (9)$$

$$E_{20} = \begin{bmatrix} -0.097 & -0.026 & 0.005 \\ 0.048 & 0.004 & 0.015 \\ -0.015 & 0.008 & 0.009 \end{bmatrix} \quad (10)$$

To simulate the presence of white Gaussian measurement noise, random numbers were added to the training data. Five different levels of noise corresponding to a 5dB, 10dB, 15dB, 20dB and 30dB signal to noise ratio (SNR) were induced. The system was trained, validated and tested using the LM algorithm, and regression analysis was carried out. The coefficient of correlation from regression analysis for all different levels of SNR is plotted in Fig. 7 where it can be observed that higher SNR corresponds to higher coefficient of regression R and vice versa. The ideal value for R is 1.0.

VI. EXPERIMENTAL MEASUREMENT AND ANALYSIS

To enable measurements, a device was fabricated with three microstrip transmission lines cascaded together in the fashion described in section III, as shown in Fig. 2 and Fig. 8. The dimensions and dielectric properties of the cascaded microstrip lines are tabulated in Table 2. Materials with parameter values of $\epsilon_{r1} = \epsilon_{r3} = 6.15$ and $\epsilon_{r2} = 2.2$ were used. The microstrip line was terminated in a 50Ω load.

A network analyzer was used to record S-parameters over the frequency range 1-5 GHz. A comparison between measured and simulated values of the magnitude and phase of the reflection coefficient are shown in Figs. 9 and 10. There is

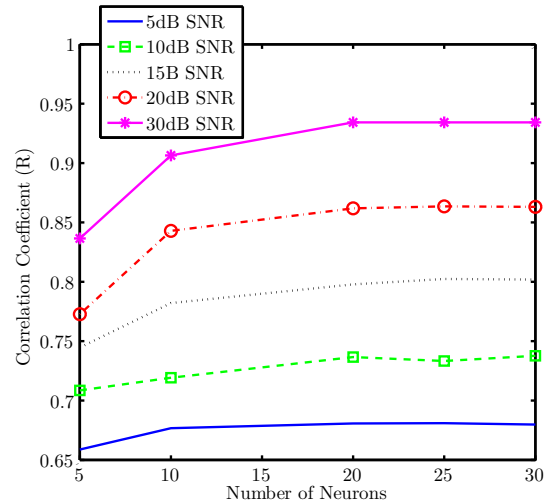


Fig. 7. Correlation coefficient (R) of regression analysis plotted against the number of neurons for a network trained with data having white Gaussian noise. Number '30' on the X-axis represents two hidden layers of 10 neurons each



Fig. 8. Snapshot of microstrip transmission line setup for experimental measurements.

excellent agreement between measured and simulated results in the frequency range 1-2.5 GHz, and reasonable agreement at higher frequencies. Ripples and other deviations are observed for higher frequencies, which can be attributed at least in part to discontinuities introduced by the fabrication technique. The microstrip lines were soldered together horizontally, across the width, which caused a noticeable amount of solder paste to sit on the joints. Moreover, a thin wire was also inserted horizontally to strengthen the solder.

For training purposes, simulated data was generated for ϵ_{r1} and ϵ_{r3} swept across the range from 5 - 8, and for ϵ_{r2} from 1.1 - 3.6. This results in a dataset with $30 \times 25 \times 30 = 22,500$ vectors. The row dimension of the data matrix is determined by frequency range and frequency step size. To limit

Table 4. Comparison of actual values of $\epsilon_{r1,2,3}$ with the neural network results obtained with 1 layer of 20 neurons and trained on data having different levels of white noise, over the frequency range from 1-5 GHz.

	'R'	ϵ_{r1}	ϵ_{r2}	ϵ_{r3}	Average Error
Actual Value		6.15	2.2	6.15	
Estimated with AWGN (30dB SNR)	0.99	5.96	2.56	7.23	
Absolute Error		0.19	0.36	1.08	0.54
Estimated with AWGN (20dB SNR)	0.952	5.91	2.96	6.58	
Absolute Error		0.24	0.76	0.43	0.48
Estimated with AWGN (10dB SNR)	0.956	5.95	2.75	6.20	
Absolute Error		0.20	0.55	0.05	0.27
Estimated with AWGN (05dB SNR)	0.91	6.45	2.75	6.04	
Absolute Error		0.30	0.55	0.11	0.32

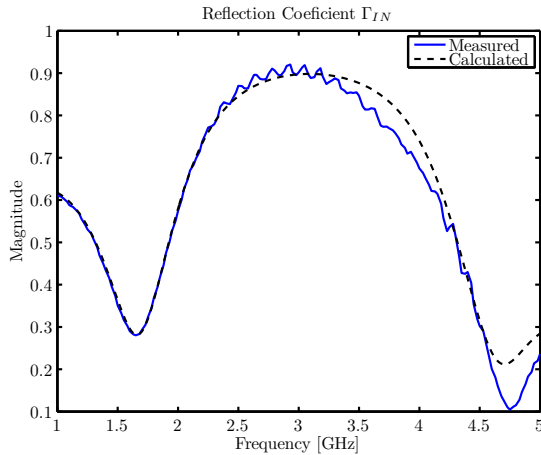


Fig. 9. Comparison between magnitude of measured and calculated reflection coefficient ($|\Gamma_{in}|$).

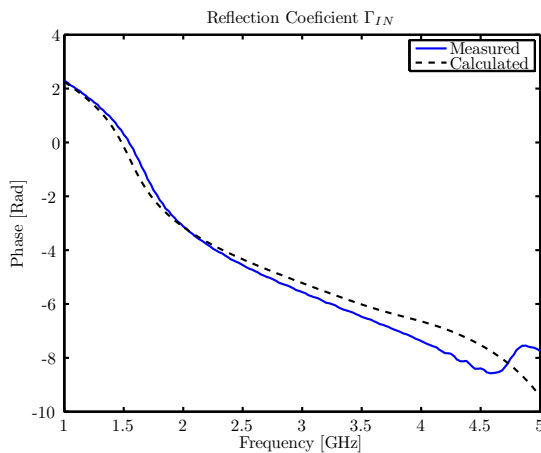


Fig. 10. Comparison between measured and calculated phase of reflection coefficient ($\angle\Gamma_{in}$).

the column length, the frequency range from 1-2.5 GHz was used. A neural network containing a single hidden layer of 20 neurons was trained with data containing white Gaussian noise (10dB SNR). To eliminate the element of coincidence, and verify the robustness of algorithm, the neural network was trained and tested three times on the same data, with different starting weights each time. The three sets of results are tabulated in Table 3. These results exhibit an average absolute error range of ± 0.6 and a coefficient of regression R greater than 0.92.

Additional tests were carried out using the 1-5 GHz frequency range, with a frequency step size of 300 MHz. Using 20 neurons with the LM algorithm, a neural network was trained with simulated data containing white Gaussian noise. In terms of absolute error, the coefficient of regression R was determined to be 0.91, 0.95, 0.95 and 0.99 for an SNR of 5, 10, 20 and 30 dB, respectively. Table 4 shows the estimated values of dielectric constants and their absolute error levels. In this case, the best errors are achieved for a neural network trained with a data set containing white Gaussian noise with an SNR of 10dB. To verify the optimum number of neurons in the hidden layer, the same procedure was repeated for 25 neurons, with similar results for the coefficient of regression as a function of the SNR level. In this case 20 neurons is sufficient for an accurate approximation using a frequency range from 1-5GHz and a step size of 300 MHz.

VII. CONCLUSION

In this feasibility study, neural networks were used to extract material parameter values from reflection coefficient data obtained from an RFID-like sensor. The dielectric constant was varied across each of three lengths of microstrip transmission lines. With a priori knowledge of geometry of the structure and the range of varying dielectric constants, the neural network was trained with data for the magnitude and phase of Γ_{in} across the complete frequency range of interest. The frequency resolution was an important parameter for accu-

racy of results and computational efficiency. It was demonstrated that a frequency step size smaller than 100 MHz does not improve the accuracy of results. Furthermore, for a wide range of frequencies from 1-5 GHz, a frequency resolution of 300MHz is sufficiently dense to keep the results accurate while maintaining the computational efficiency of the algorithm. The Levenberg Marquardt backpropagation algorithm was determined to be well-suited to solve this one dimensional inverse scattering type problem using neural networks. White Gaussian noise with a 10dB SNR was induced in training data to simulate the measurement noise. The architecture of the neural network is an important parameter for any problem, and it was demonstrated that one hidden layer of 20 or 25 neurons enables optimum performance of the network in terms of average absolute error and computational efficiency. With the application of a neural network based on the LM backpropagation algorithm with one hidden layer of 20 neurons, the dielectric constant of a three cascaded microstrip transmission line system was estimated with absolute average error less than ± 0.5 . We note that this one dimensional inverse scattering problem would be more challenging to investigate with non deterministic boundaries and for material properties that vary across a greater range.

REFERENCES

- [1] G. Durgin, "Reflected Electro-Material Signature (REMS) Sensor," Provisional Patent filed on June 2008.
- [2] C. Q. Lee, "Wave propagation and profile inversion in lossy inhomogeneous media," *Proceedings of the IEEE*, vol. 70, no. 3, pp. 219–228, Mar. 1983.
- [3] H. W. Yang and R. S. Chen, "FDTD analysis on the effect of plasma parameters on the reflection coefficient of the electromagnetic wave," *Optical and Quantum Electronics*, vol. 39, no. 15, pp. 1245–1252, Dec. 2007.
- [4] E. Kemppinen, "Effective permittivity and attenuation coefficient of microstrip transmission line determined by 1-port and 2-port measuring methods," *Measurement Science and Technology*, vol. 11, pp. 38–44, 2000.
- [5] S. Ratnajeevan and H. Hoole, "Artificial neural networks in the solution of inverse electromagnetic field problems," *IEEE Trans. on Magnetism*, vol. 29, no. 2, pp. 1931–1934, Mar. 1993.
- [6] I. Elshafiey, L. Udpa, and S. S. Udpa, "Application of Neural Networks to Inverse Problems in Electromagnetics," *IEEE Trans. on Magnetism*, vol. 30, no. 5, pp. 3629–3632, Sep. 1994.
- [7] C. Christodoulou and M. Georgiopoulos, *Application of Neural Networks in Electromagnetics*, Boston, London: Artech House, 2001.
- [8] S. Caorsi, and P. Gamba, "Electromagnetic detection of dielectric cylinders by a neural-network approach," *IEEE Trans. on Geo Science and Remote Sensing*, vol. 37, no. 2, pp. 820–827, Mar. 1999.
- [9] E. Bermami, S. Caorsi, and M. Raffetto, "Microwave detection and dielectric characterization of cylindrical objects from amplitude-only data by means of neural networks," *IEEE Trans. on Antennas and Propagation*, vol. 50, no. 9, pp. 1309–1314, Sep. 2002.
- [10] F. Yaman and S. Simsek, "Neural network approach to determine nonsmooth one-dimensional profiles in inverse scattering theory," *Microwave and Optical Technology Letters*, vol. 49, no. 12, pp. 3158–3162, Sep. 2007.
- [11] J. D. Griffin and G. D. Durgin, "Complete Link Budgets for RFID and Backscatter Radio," *IEEE Antennas and Propagation Magazine*, vol. 51, no. 2, pp. 11–25, April 2009.
- [12] S. Chandrasekhar, *Liquid Crystals, 2nd Ed.*, Cambridge: Cambridge University Press, 1992.
- [13] P. J. Collings and M. Hird, *Introduction to Liquid Crystals*, Bristol, PA: Taylor & Francis, 1997.
- [14] R. C. O'Handley, *Magnetic Materials: Principles and Applications*, Wiley-Interscience, 1999.
- [15] D. M. Pozar, *Microwave Engineering, 3rd Ed.*, John Wiley and Sons- New York, 2005.
- [16] K. Mehrotra, S. Ranka and C. K. Mohan, *Elements of Artificial Neural Networks*, MIT Press, 1996.
- [17] M. T. Hagan, H. B. Demuth and M. Beale, *Neural Network Design*, Boston, MA: PWS Publishing Company, 1996.
- [18] D. G. Luenberger, *Introduction to Linear and Non Linear Programming*, Addison Wesley Pub. Co., 1973.
- [19] M. Powell, "Restart procedures for the conjugate gradient method," *Mathematical Programming*, vol. 12, pp. 241–254, 1977.
- [20] E. M. L. Beale, *A derivation of conjugate gradients in F. A. Lootsma, Ed., Numerical methods for nonlinear optimization*. London Academic Press, 1972.
- [21] M. Moller, "A scaled conjugate gradient algorithm for fast supervised learning," *Neural Networks*, vol. 6, pp. 525–533, 1993.
- [22] R. Battiti, "First- and Second-Order Methods for Learning: Between Steepest Descent and Newton's Method," *Neural computation*,

vol. 4, no. 2, pp. 141–166, Jun. 1992.

- [23] D. W. Marquardt, “An Algorithm for Least-Squares Estimation of Nonlinear Parameters,” *Journal of the Society for Industrial and Applied Mathematics*, vol. 11, no. 2, pp. 431–441, Jun. 1963.
- [24] M. T. Hagan and M. B. Menhaj, “Training feed-forward networks with the Marquardt algorithm,” *IEEE Transactions on Neural Networks*, vol. 5, no. 61, pp. 989–993, Nov. 1994.



Azhar Hasan received his BE and MS degrees in electrical engineering from National University of Sciences and Technology, Pakistan, in 1997 and 2007 respectively. He is currently working pursuing the PhD degree in electrical and computer engineering at Georgia Institute of

Technology, Atlanta.

His research involves computational techniques for passive RFID based sensing applications. He also holds interest in researching passive components for RF/microwave front end applications.



Andrew F. Peterson received the B.S., M.S., and Ph.D. degrees in Electrical Engineering from the University of Illinois, Urbana-Champaign in 1982, 1983, and 1986 respectively. Since 1989, he has been a member of the faculty of the School of Electrical and Computer Engineering at the Georgia Institute of Technology, where he is now Professor and Associate Chair for Faculty Development. He served for six years as a Director of ACES, and is a past President of the IEEE Antennas and Propagation Society. He is a recipient of the IEEE Third Millennium Medal, and is a Fellow of ACES and the IEEE.



Gregory D. Durgin joined the faculty of Georgia Tech’s School of Electrical and Computer Engineering in Fall 2003 where he serves as an associate professor. He received the BSEE (96), MSEE (98), and PhD (00) degrees from Virginia Polytechnic Institute and State University.

In 2001 he was awarded the Japanese Society for the Promotion of Science (JSPS) Post-doctoral Fellowship and spent one year as a visiting researcher with Morinaga Laboratory at Osaka University. In 1998 he received the Stephen O. Rice prize (with coauthors Theodore S. Rappaport and Hao Xu) for best original journal article in the *IEEE Transactions on Communications*. Prof. Durgin also authored *Space-Time Wireless Channels*, the first textbook in the field of space-time channel modeling. Prof. Durgin founded the Propagation Group (<http://www.propagation.gatech.edu>) at Georgia Tech, a research group that studies radiolocation, channel sounding, backscatter radio, RFID, and applied electromagnetics. He is a winner of the NSF CAREER award as well as numerous teaching awards, including the Class of 1940 Howard Ector Outstanding Classroom Teacher Award at Georgia Tech (2007). He is a frequent consultant to industry, having advised many multinational corporations on wireless technology.

Survey of Laboratory Scale Fabrication Techniques for Passive UHF RFID Tags

Tamer Elsherbeni¹, Khaled ElMahgoub¹, Lauri Sydänheimo², Leena Ukkonen², Atef Elsherbeni¹, Fan Yang¹

¹ Center of Applied Electromagnetic System Research (CAESR), Department of Electrical Engineering, University of Mississippi, University, MS 38677-1848, USA
taelsheri@olemiss.edu, kelmahgo@olemiss.edu, atef@olemiss.edu, fyang@olemiss.edu

² Rauma Research Unit, Institute of Electronics, Tampere University of Technology, Kalliokatu 2, Rauma 26100, Finland
lauri.sydanheimo@tut.fi, leena.ukkonen@tut.fi

Abstract— This paper presents an overview of various RFID tag fabrication methods and briefly describes the advantages and disadvantages of each method. The purpose of this paper is to provide the reader with the fabrication techniques that can be applied for RFID fabrication purposes for laboratory scale experiments. This paper will present the performance results of laboratory made RFID tags based on two fabrication methods (etching and screen printing) on multiple substrates (paper, thin transparent film, polyethylene terephthalate (PET), and fabrics). These results will prove the effectiveness of the presented methods for RFID tag fabrication purposes.

Index Terms - Radio Frequency Identification (RFID), etching, screen printing.

I. INTRODUCTION

In today's world the role of radio frequency identification (RFID) has increased considerably. RFID is a technology which uses RF signals for automatic identification of objects. RFID tags are used for many applications in various areas such as electronic toll collection, asset identification, retail item management, access tracking systems and many others. It has many advantages compared to electronic product code (EPC). For example, RFID systems can identify multiple objects simultaneously without a direct line of sight [1].

An RFID system consists of two basic components, a reader (interrogator) and a tag (transponder). An RFID tag can either be active,

operated by a battery, or passive. A passive tag consists of an antenna and an application specific integrated circuit (ASIC) known as a chip. Passive ultra high frequency (UHF) RFID systems which achieve read ranges longer than 1 meter are defined as long range systems. These systems operate at the UHF center frequencies of 866MHz (Europe), 915MHz (America), and 950MHz (Asia and Australia) [1]. In this paper the fabrication techniques for passive RFID tags will be discussed. Section II will introduce the method of screen printing and etching. The parameters, characteristics, and a step-by-step laboratory procedure will be described for each fabrication method. The advantages and disadvantages of each method will be clearly presented. Section III will convey experimental data of a prototype RFID tag fabricated from the procedure proposed in this paper. Section IV will conclude the effectiveness of the presented methods for RFID tag laboratory scale prototyping.

II. FABRICATION TECHNIQUES

A. Etching Process

The process of etching has been used for hundreds of years. It originated from the custom of making etching designs on armor and was adopted by printmakers as an easy method of engraving. Since then the process of etching has evolved from artistic uses to manufacturing techniques.

The etching processes can be classified into two categories: wet and dry etching. The process of wet etching uses liquid chemicals or etchants to remove metallic substrates. The function of the photoresist mask is to prevent the removal of the

desired pattern from the substrate when the etchant is applied. “The wet etching process can be presented in three steps: 1) application of the etchant to the substrate; 2) reaction between the etchant and the material being removed; and 3) diffusion of the reaction byproducts from the reacted surface. The process of dry etching does not require any liquid chemicals or etchants. Dry etching can be accomplished by any of the following methods: 1) using chemically reactive gases or plasma; 2) physical removal of the material, usually by momentum transfer; or 3) a combination of both physical removal and chemically reactive gases or plasma [2,3].”

Some etching parameters that need to be taken into account are the etch rate and the etch selectivity. The etch rate refers to the rate of material removal ($\mu\text{m}/\text{min}$). The etch selectivity refers to the ability of the reactive chemical to etch away only the material intended for removal, while leaving all other materials intact [4].

Wet and dry etchings have characteristics suitable for different applications. Wet etching is an isotropic process (uniform direction) while dry etching is anisotropic (directionally dependent). Since wet etching is isotropic, it is quick, easy, and cheap. It provides a unilateral and high etching rate and good selectivity rate for most materials. The disadvantage to wet etching is that it is inadequate for defining features smaller than $1\mu\text{m}$ and has the potential for chemical handling hazards. Dry etching allows for defining features smaller than 100nm , but it is relatively expensive, hard to implement, provides poor selectivity, and has the potential for radiation damage [5].

Etching has been the most commonly used method for fabricating RFID tags. This process can be used for fast prototyping of RFID tags. Off-the-shelf supplies and equipment may be used for inexpensive prototypes. For mass production purposes metal etching is impractical due to wasted materials and chemicals. Since etching is a subtractive process only a portion of raw materials are consumed while the rest is either recycled or thrown away. The loss of wasted materials has an effect on the overall price of production. Furthermore, because aggressive chemicals are used, maintenance fees for their removal must also be taken into consideration. This is why etching is perceived as an environmentally unfriendly method.

Although etching provides high conductivity and reliability it lacks in flexibility. Etching can only be used on substrates that can tolerate the chemical baths such as ferric chloride for copper and sodium hydroxide for aluminum. To fabricate a prototype RFID tag utilizing the wet etching method, the supplies needed include: the substrate, the acid/etchant, the solvent/development chemical, the photoresist varnish, a transparency sheet, a heating chamber, and an ultraviolet (UV) machine. The procedure below describes one method in which wet etching can be performed in laboratory settings. The procedure is conducted on an aluminum substrate.

Procedure:

- First apply the photoresist onto the substrate, as seen in Fig. 1.
- Next, place metallic substrate with the photoresist varnish into a heating chamber at 75°C for 20 minutes. The thermal treatment will typically be completed in 20 minutes if not then repeat heating process.



Fig. 1. Application of the photoresist to the aluminum substrate via spraying.

- Next, place a transparency sheet with the printed antenna design on top of the varnished metallic substrate. Then insert both items into the UV machine. Set the UV machine to approximately 45 seconds (time may vary with different varnish thickness). If completed correctly the design will noticeably appear on the varnished metallic substrate.

Next, the chemical process requires two containers one containing the solvent and the other containing the acid. In this procedure an aluminum substrate was used, therefore, the solvent consisted

of 70ml of NaOH and approximately 1.5 to 2 liters of water. The etchant solution consisted of 80ml of water, 30ml of HCl, and 30ml H₂O₂. Place the varnished metallic substrate within the container of the solvent. The solvent will remove the photoresist varnish, as seen in Fig. 2.



Fig. 2. Placement of varnished aluminum substrate within the solvent.

- Next, place the substrate into the etchant solution. Agitate the substrate within the container. This process will begin dissolve the metallic substrate. When the appearance of oxidation occurs remove the substrate from the container and rinse under cool running water. Repeat these steps until the metallic substrate around the design has been completely removed. The end product will be a transparent plastic with the metallic substrate design, as seen in Fig. 3.



Fig. 3. Placement of varnished aluminum substrate within the solution.

These etchant solutions operate by dissolving any metallic substrate uncovered by a photoresist. This process result in the formation of hydrogen gasses at the surface of the substrate, therefore

removal of these bubbles is necessary because it masks the metal needing to be dissolved. Therefore rinsing the substrate resolves this problem by detaching the bubbles from the substrate [6].

B. Printing Fabrication Process

Printing is an additive process that allows designs to be selectively imprinted on to certain areas. It can be as simple as cutting out a stencil and applying a layer of conductive material to achieve the imprint. The method of printing has been used for many products such as clothing, printed circuit boards, and containers. The flexibility of printing allows it to be applied to almost any surface or material.

Printing can have a great potential for RFID antenna fabrications. With the use of RFID tags in almost every industrial sector, the need for a universal fabrication method is apparent. Printing holds the key to provide high volume and low manufacturing costs. Compared to the traditional method of fabrication (etching) screen printing is more stable, reliable, cost-effective, flexible, and has a low environmental impact compared to etching [7].

The use of printing allows for intricate and minute details to be fabricated while still maintaining conductivity throughout the entire design. Printing is an additive process which only uses the minimal amount of material needed to complete the task. Even the amount of raw materials used for printing can be reduced since the layers of conductive ink can vary in thickness. Due to the consumption of fewer raw materials, its application for mass production of a design provides the best cost per development ratio allowing a company to sell at the lowest price. Printing can be used to fabricate an RFID antenna on almost any substrate or material such as metal, paper, and plastic. With the use of flexible substrates for RFID antennas, added characteristics to the tag include the ability to bend and twist that was impossible with metal substrates. Though some environmental issues do still occur with screen printing due to the use of conductive silver or copper inks it is relatively incomparable to etching which contains far more chemical waste. The disadvantage to screen printing is its resolution which has its maximum at 50 lines per centimeter [8-10].

Compared to pure metals, such as copper or aluminum, conductive inks cause small degradation to the antenna gain, but they affect the input impedance of the tag antenna and produce high resistivity compared to pure metals. However, due to these variations their effect on the read ranges of the tag antennas are relatively small [11]. Conductive inks are composed of a polymer matrix and conductive fillers with a thermo-plastic polymer binder or resin [7]. For the conductive inks to remain imprinted onto a substrate, the conductive inks must be cured. Curing is the process of preserving the ink by heating. When the conductive ink is heated the polymers shrink and bond with nearby polymers which produce a conductive path through out the design. There are two important parameters during the curing of a substrate: the curing temperature and the curing time. These have an effect on the conductivity of the imprint and must always be taken into consideration when fabricating RFID tags [11].

There are many printing techniques that can be used to manufacture RFID tags such as screen printing, flexography, gravure, and ink jet. The speed at which tags can be produced and the cost per tag are as listed from slowest to fastest and highest to lowest in prices, respectively [12]. Different printing technologies require different ink characteristics. Some characteristics of the most typical printing processes are shown in Table 1 [11,13].

Table 1: Characteristics of the most typical printing processes.

Process	Screen Printing	Flexography	Gravure	Ink Jet
Substrate	All	Papers, Boards, Polymers	Coated papers, Boards, Polymers	All
Ink film Thickness (µm)	0.02-100	6-8	8-12	Depends on ink
Ink Viscosity (Pa.s)	0.1-10	0.01-0.1	0.01-5	0.01
Resolution (lines/cm)	50	60	100	60(continuous) 250 (DOD)

Screen printing is a stenciling process where the ink is transferred on to the substrate through a stencil covering a fine fabric mesh, as shown in

Fig. 4. The fabric mesh is stretched onto a frame, allowing pressure to be applied to the stencil by a squeegee [15]. The ink is poured on to the stencil and the squeegee is drawn across the frame, forcing the ink through the stencil (see Fig. 4) [15]. Screen printing allows versatility in its ink thicknesses from 20 nm to 100 µm. Among the limitations of screen printing, its maximum resolution remains usually under 50 lines per centimeter and its speed is slow in comparison to other conventional printing processes [13].

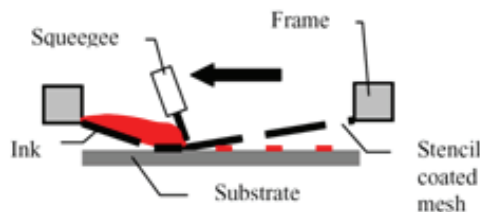


Fig. 4. Diagram of the screen printing process.

Screen printing is the cheapest method to implement for laboratory scale prototyping. To fabricate a prototype RFID tag using the screen printing the supplies needed include: a screen printing machine, conductive ink, a substrate, and a heating chamber. The machine used for the fabrication of the RFID tags in the procedure section was the Simatic Sim 20 semiautomatic screen and stencil printer.

Procedure:

- First attach stencil screen unto the frame of the screen printing machine, as seen in Fig. 5.

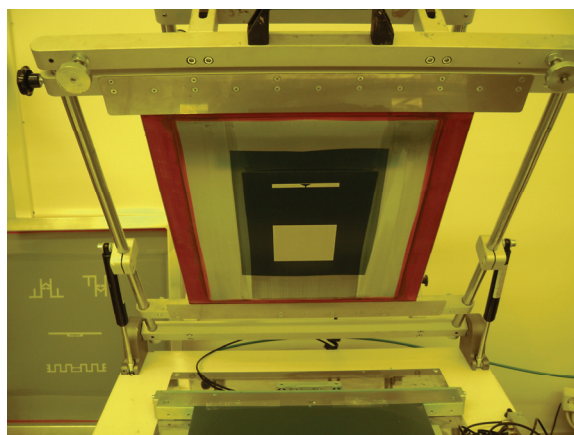


Fig. 5. Placement of the stencil screen onto the screen printing machine.

- Next, initiate air tight suction via floor pedal. Apply conductive silver ink above the screen design, as shown in Fig. 6.

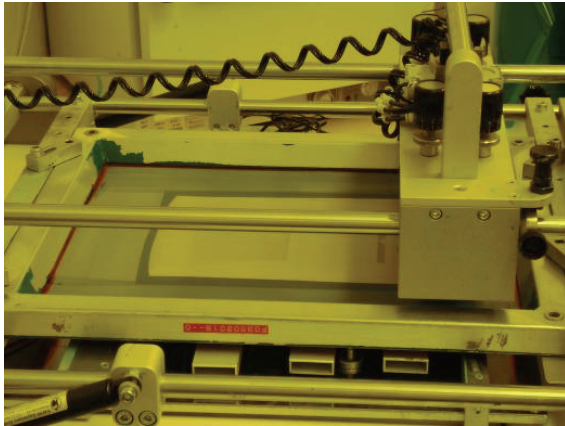


Fig. 6. Placement of the silver conductive ink onto the stencil screen.

Then, lower and initiate the front squeegee and slide it across the frame as shown in Fig. 7. Raise squeegee and allow excess ink to accumulate onto the screen.

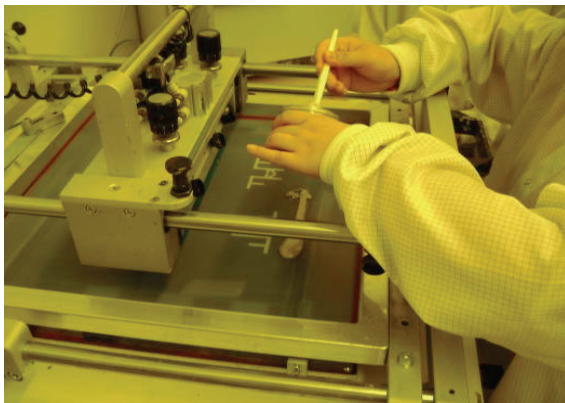


Fig. 7. Transferring the squeegee across the stencil to imprint the design on the substrate.

- Then, lower and initiate the back squeegee and return to starting position. Release the vacuum suction via floor pedal. Raise the frame and remove the substrate from the platform.
- Finally, place the substrate into an oven preheated to 120 degrees Celsius. After approximately 20 minutes, the silver conductive ink will cure. Repeat thermal treatment if necessary.

III. PROTOTYPE RFID TAG FABRICATION EXAMPLE

Two RFID antenna designs corresponding to the operating frequencies of 886 MHz and 915 MHz were developed using high frequency structural simulator (HFSS). The details of the design's characteristics and procedure can be found in [19]. Both designs were fabricated by the process techniques described in this paper. Each design was fabricated on multiple substrates (paper, thin transparent film, polyethylene terephthalate (PET), and fabric).

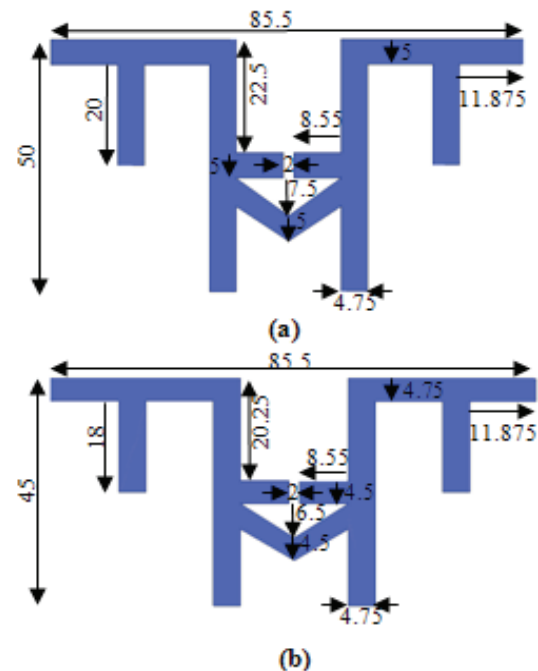


Fig. 8. The design layout of a Logo RFID tag (a) 866MHz and (b) 915MHz, (all dimensions are in mm).

The measurements of operational characteristics of these two tags were conducted using the Voyantic Tagformance reader [16]. The read ranges measurements were based on the electromagnetic threshold measurements technique, in which the frequency was changed from 830 MHz to 990 MHz by increments of 1 MHz. At each frequency the transmitted power was increased by 0.1dB until the tag responded and the minimum transmitted power to activate the tag at that frequency was measured. The device calculated the read range by using free space Friis formula [17] and taking into account the path and

cable losses and the antenna gain. The read range was calculated using the following equation:

$$r_{\max}(f) = \sqrt{\frac{EIRP}{P_{t\min} L G_t}} \quad (1)$$

where $EIRP$ is the effective isotropic radiated power, $P_{t\min}$ is the minimum transmitted power to activate the tag, L is the factor considering the cable and path loss, and G_t is the transmitting antenna gain [18]. The material composition of the fabricated tags are shown in Table 2.

Table 2: The material composition of the RFID tags and their fabrication method.

Tag No.	Substrate	Conductive Material	Fabrication process	Read Range [m]	Frequency of Operation [MHz]
1	PET	Copper	Etching	12.5	866
2	Thin film	Sliver Ink	Screen Printing	9.5	866
3	Thin film	Sliver Ink	Screen Printing	6	915
4	Thin film	Aluminum	Etching	9	866
5	Paper	Sliver Ink	Screen Printing	9	866
6	Fabric	Sliver Ink	Screen Printing	11.2	866
7	Fabric	Sliver Ink	Screen Printing	7	915

Table 2 presents the results of fabricated tags categorized by their substrate, conductive material, and fabrication process. The simulated and measured antenna parameters and design processes can be referred to in [19]. Table 2 portrays the effectiveness of the step-by-step fabrication procedure in developing RFID tags with multiple substrates and conductive materials. From this step-by-step procedure laboratory scale fabrication of RFID tags can be developed with a relatively simple and cost effective method.

IV. CONCLUSION

In this paper two fabricating techniques (etching and screen printing) were described. The advantages and disadvantages of each method were discussed and a step by step procedure was

conveyed. Two prototype RFID tags were designed using numerical simulations and fabricated using the discussed techniques and procedure. Their read ranges were measured to demonstrate the feasibility of the fabrication methods.

ACKNOWLEDGMENT

The Authors would like to thank Alien Technology Company for providing the Chips and Voyantic Company for making the Tagformance device available for conducting read range measurements. This research has been funded by TEKES and the Academy of Finland.

REFERENCES

- [1] K. V. S. Rao, P. V. Nikitin, and S. F. Lam, "Antenna Design for UHF RFID Tags: A Review and a Practical Application", IEEE Transaction on Antennas and Propagation, vol. 53, no. 12, Dec. 2005.
- [2] "Wet Etching," <http://www.siliconfareast.com/wetetch.htm>.
- [3] "Dry Etching," <http://www.siliconfareast.com/dryetch.htm>.
- [4] A. G. Andreou and J. Wang, "Wet Etching," Advanced Topics in Fabrication and Microengineering.
- [5] E. Chen, Wet and Dry Etching, 2004
- [6] "(WO/1990/013443) Etchant Solution for Photoresistant-Patterned Metal Layer," <http://www.wipo.int/pctdb/en/wo.jsp?IA=US1989005264&DISPLAY=DESC>.
- [7] "Screenprinting RF Antennae: The green, stable and low-cost solution," OnBoard Technology, pp. 22, October 2004.
- [8] T. L. Landers, D. B. Brown, E.W. Fant, E. M. Malstrom, and N. M. Schmitt, Electronics Manufacturing Processes, Prentice Hall, 1994.
- [9] J. Costenoble, "Rotary screen printing: the productive solution for HF/UHF RFID labels," SGIA Journal, pp. 7-10, 2005
- [10] S. B. Hoff, Screen Printing: A Contemporary Approach, Delmar Publishers, 2006
- [11] S. Merilampi, L. Ukkonen, L. Sydanheimo, P. Ruuskanen, and M. Kivikoski, "Analysis of Silver Ink Bow-Tie RFID Tag Antennas Printed on Paper Substrates," International

- Journal of Antennas and Propagation, vol. 2007, Article ID 90762, 9 pages, 2007.
- [12] S. Ludmerer, Parelec Inc., "Conductive Inks for RFID Antenna," *RFID Journal Live*, http://www.rfidjournal.net/live05/Packaging/Room_colo_245pm_ludmerer.pdf
- [13] A. Blayo and B. Pineaux, "Printing processes and their potential for RFID printing," *Proceedings of the 2005 Joint Conference on Smart Objects and Ambient Intelligence: Innovative Context-Aware Services: Usages and Technologies*, pp. 27-30, October 2005.
- [14] W. Zoomer, "Printing Technologies Make Their Mark in Radio Frequency Identification," *Screenweb*, 2006.
- [15] R. H. Leach, and R. J. Pierce, ed., *The Printing Ink Manual*, 5th edition, Van Nostrand Reinhold International, 1993.
- [16] Voyantic Tagformance™ Lite, <http://www.voyantic.com>.
- [17] H. T. Friis, "A note on a simple transmission formula," *Proc. IRE*, vol. 34, no. 5, pp. 254-256, May 1946.
- [18] C. Loo, K. Elmahgoub, F. Yang, A. Elsherbeni, D. Kajfez, A. Kishk, T. Elsherbeni, L. Ukkonen, L. Sydänheimo, M. Kivikoski, S. Merilampi, and P. Ruuskanen, "Chip Impedance Matching for UHF RFID Tag Antenna Design", *Progress In Electromagnetics Research (PIER 81)*, pp. 359-370, 2008.
- [19] K. ElMahgoub, T. Elsherbeni, F. Yang, A. Elsherbeni, L. Sydänheimo, and L. Ukkonen, "Logo-Antenna Based RFID Tags for Advertising Application", *25th Annual Review of Progress in Applied Computational Electromagnetics*, pp. 801-805, March 2009.



Tamer Elsherbeni currently working towards his B. Sc. in Electrical Engineering with RF/Wireless emphasis at the University of Mississippi. He was selected to participate in the NSF Research Experience for Undergraduates (REU) program at The College of

Optics and Photonics at University of Central

Florida in the summer of 2009. He also received the Science, Mathematics, and Research for Transformation Program (SMART) scholarship in 2009. His current research interests include RFID systems, measurements and fabrication techniques for electromagnetic application, wireless power and infrared systems.



Khaled ElMahgoub

received the B.Sc. and M.Sc. degrees in electronics and electrical communications engineering from Cairo University, Egypt, in 2001 and 2006, respectively. Currently, he is working towards the Ph.D. degree in

the Department of Electrical Engineering at the University of Mississippi, USA. His current research interests include RFID systems, FDTD, antenna design and numerical techniques for electromagnetic. Mr. ElMahgoub is a member of IEEE, ACES, and Phi Kappa Phi honor society. From 2001 to 2006, he was teacher assistant at Cairo University, and since 2007 he has been a research assistant at the University of Mississippi.



Lauri Sydänheimo

received the M.Sc. and Ph.D. degrees in electrical engineering from Tampere University of Technology (TUT). He is currently a Professor with the Department of Electronics, TUT, and works as the Research Director of

Tampere University of Technology's Rauma Research Unit. He has authored over 120 publications in the field of RFID tag and reader antenna design and RFID system performance improvement. His research interests are focused on wireless data communication and radio frequency identification (RFID).



Leena Ukkonen received the M.Sc. and Ph.D. degrees in electrical engineering from Tampere University of Technology (TUT) in 2003 and 2006, respectively. She is currently working at the TUT Department of Electronics as Senior Research Scientist,

leading the RFID research group. She has authored over 60 publications in the field of RFID antenna design and industrial RFID applications.

Her research interests are focused on passive UHF radio frequency identification (RFID) antenna development for tags and readers.



Atef Elsherbeni is a Professor of Electrical Engineering and Associate Dean for Research and Graduate Programs, the Director of The School of Engineering CAD Lab, and the Associate Director of The Center for Applied Electromagnetic Systems

Research (CAESR) at The University of Mississippi. In 2004 he was appointed as an adjunct Professor, at The Department of Electrical Engineering and Computer Science of the L.C. Smith College of Engineering and Computer Science at Syracuse University. On 2009 he was selected as Finland Distinguished Professor by the Academy of Finland and TEKES. Dr. Elsherbeni has conducted research dealing with scattering and diffraction by dielectric and metal objects, finite difference time domain analysis of passive and active microwave devices including planar transmission lines, field visualization and software development for EM education, interactions of electromagnetic waves with human body, RFID and sensors development for monitoring soil moisture, airports noise levels, air quality including haze and humidity, reflector and printed antennas and antenna arrays for radars, UAV, and personal communication systems, antennas for wideband applications, antenna and material properties measurements, and hardware and software acceleration of computational techniques for electromagnetics. Dr. Elsherbeni is the co-author of the book *“The Finite Difference Time Domain Method for Electromagnetics With*

MATLAB Simulations”, SciTech 2009, the book *“Antenna Design and Visualization Using Matlab”*, SciTech, 2006, the book *“MATLAB Simulations for Radar Systems Design”*, CRC Press, 2003, the book *“Electromagnetic Scattering Using the Iterative Multiregion Technique”*, Morgan & Claypool, 2007, the book *“Electromagnetics and Antenna Optimization using Taguchi's Method”*, Morgan & Claypool, 2007, and the main author of the chapters *“Handheld Antennas”* and *“The Finite Difference Time Domain Technique for Microstrip Antennas”* in Handbook of Antennas in Wireless Communications, CRC Press, 2001. Dr. Elsherbeni is a Fellow member of the Institute of Electrical and Electronics Engineers (IEEE) and a Fellow member of The Applied Computational Electromagnetic Society (ACES). He is the Editor-in-Chief for ACES Journal and an Associate Editor to the Radio Science Journal.



Fan Yang received the B.S. and M.S. degrees from Tsinghua University in 1997 and 1999, and the Ph.D. degree from University of California, Los Angeles (UCLA) in 2002. From 1994 to 1999, he was a Research Assistant in the State Key

Laboratory of Microwave and Digital Communications, Tsinghua University, China. From 1999 to 2002, he was a Graduate Student Researcher in the Antenna Lab, UCLA. From 2002 to 2004,

he was a Post-doc Research Engineer and Instructor in the Electrical Engineering Department, UCLA. In August 2004, he joined the Electrical Engineering Department, The University of Mississippi as an Assistant Professor and was promoted to Associate Professor in 2009.

Dr Yang's research interests include antenna theory, designs, and measurements, electromagnetic band gap (EBG) structures and their applications, computational electromagnetics and optimization techniques, and applied electromagnetic systems such as the radio frequency identification (RFID) system and concentrating solar energy system. He has published over 100 technical journal articles and conference papers, five book chapters, and two

books entitled *Electromagnetic Band Gap Structures in Antenna Engineering* and *Electromagnetics and Antenna Optimization Using Taguchi's Method*.

Dr. Yang is a Senior Member of IEEE and was Secretary of IEEE AP Society, Los Angeles chapter. He is also a Full Member of URSI/USNC. Dr. Yang serves as the Associate Editor-in-Chief of the Applied Computational Electromagnetics Society (ACES) Journal. He is also a frequent reviewer for over twenty scientific journals and book publishers, and has chaired numerous technical sessions in various international symposiums. Dr. Yang was a Faculty Senator at The University of Mississippi, and currently is a Member of the University Assessment Committee.

For his contributions, Dr. Yang has received several prestigious awards and recognitions. In 2004, he received the *Certificate for Exceptional Accomplishment in Research and Professional Development Award* from UCLA. Dr. Yang was the recipient of *Young Scientist Award* in the 2005 URSI General Assembly and in the 2007 International Symposium on Electromagnetic Theory. He was also appointed as The University of Mississippi *Faculty Research Fellow* in year 2005 and 2006. In 2008, Dr. Yang received the *Junior Faculty Research Award* from The University of Mississippi. In 2009, he received the inaugural IEEE Donald G. Dudley Jr. Undergraduate Teaching Award.

2010 INSTITUTIONAL MEMBERS

DTIC-OCP LIBRARY
8725 John J. Kingman Rd, Ste 0944
Fort Belvoir, VA 22060-6218

AUSTRALIAN DEFENCE LIBRARY
Northcott Drive
Canberra, A.C.T. 2600 Australia

BEIJING BOOK CO, INC
701 E Linden Avenue
Linden, NJ 07036-2495

BUCKNELL UNIVERSITY
69 Coleman Hall Road
Lewisburg, PA 17837

ROBERT J. BURKHOLDER
OHIO STATE UNIVERSITY
1320 Kinnear Road
Columbus, OH 43212

DARTMOUTH COLLEGE
6025 Baker/Berry Library
Hanover, NH 03755-3560

DSTO EDINBURGH
AU/33851-AP, PO Box 830470
Birmingham, AL 35283

SIMEON J. EARL – BAE SYSTEMS
W432A, Warton Aerodome
Preston, Lancs., UK PR4 1AX

ELLEDIEMME
Libri Dal Mondo
PO Box 69/Poste S. Silvestro
Rome, Italy 00187

ENGINEERING INFORMATION, INC
PO Box 543
Amsterdam, Netherlands 1000 Am

ETSE TELECOMUNICACION
Biblioteca, Campus Lagoas
Vigo, 36200 Spain

OLA FORSLUND
SAAB MICROWAVE SYSTEMS
Nettovagen 6
Jarfalla, Sweden SE-17588

GEORGIA TECH LIBRARY
225 North Avenue, NW
Atlanta, GA 30332-0001

HRL LABS, RESEARCH LIBRARY
3011 Malibu Canyon
Malibu, CA 90265

IEE INSPEC
Michael Faraday House
6 Hills Way
Stevenage, Herts UK SG1 2AY

IND CANTABRIA
PO Box 830470
Birmingham, AL 35283

INSTITUTE FOR SCIENTIFIC INFO.
Publication Processing Dept.
3501 Market St.
Philadelphia, PA 19104-3302

KUWAIT UNIVERSITY
Postfach/po box 432
Basel, Switzerland 4900

LIBRARY – DRDC OTTAWA
3701 Carling Avenue
Ottawa, Ontario, Canada K1A 0Z4

LIBRARY of CONGRESS
Reg. Of Copyrights
Attn: 407 Deposits
Washington DC, 20559

LINDA HALL LIBRARY
5109 Cherry Street
Kansas City, MO 64110-2498

RAY MCKENZIE – TELESTRA
13/242 Exhibition Street
Melbourne, Vic, Australia 3000

MISSISSIPPI STATE UNIV LIBRARY
PO Box 9570
Mississippi State, MS 39762

MISSOURI S&T
400 W 14th Street
Rolla, MO 64609

MIT LINCOLN LABORATORY
Periodicals Library
244 Wood Street
Lexington, MA 02420

OSAMA MOHAMMED
FLORIDA INTERNATIONAL UNIV
10555 W Flagler Street
Miami, FL 33174

NAVAL POSTGRADUATE SCHOOL
Attn: J. Rozdal/411 Dyer Rd./ Rm 111
Monterey, CA 93943-5101

NDL KAGAKU
C/O KWE-ACCESS
PO Box 300613 (JFK A/P)
Jamaica, NY 11430-0613

OVIEDO LIBRARY
PO BOX 830679
Birmingham, AL 35283

PENN STATE UNIVERSITY
126 Paterno Library
University Park, PA 16802-1808

DAVID J. PINION
1122 E PIKE STREET #1217
SEATTLE, WA 98122

KATHERINE SIAKAVARA -
ARISTOTLE UNIV OF
THESSALONIKI
Gymnasiou 8
Thessaloniki, Greece 55236

SWETS INFORMATION SERVICES
160 Ninth Avenue, Suite A
Runnemede, NJ 08078

TIB & UNIV. BIB. HANNOVER
DE/5100/G1/0001
Welfengarten 1B
Hannover, Germany 30167

UNIV OF CENTRAL FLORIDA
4000 Central Florida Boulevard
Orlando, FL 32816-8005

UNIVERSITY OF COLORADO
1720 Pleasant Street, 184 UCB
Boulder, CO 80309-0184

UNIVERSITY OF KANSAS –
WATSON
1425 Jayhawk Blvd 210S
Lawrence, KS 66045-7594

UNIVERSITY OF MISSISSIPPI
JD Williams Library
University, MS 38677-1848

UNIVERSITY LIBRARY/HKUST
CLEAR WATER BAY ROAD
KOWLOON, HONG KONG

UNIV POLIT CARTAGENA
Serv Btca Univ,
Paseo Alfonso XIII, 48
Cartagena, Spain 30203

THOMAS WEILAND
TU DARMSTADT
Schlossgartenstrasse 8
Darmstadt, Hessen, Germany 64289

STEVEN WEISS
US ARMY RESEARCH LAB
2800 Powder Mill Road
Adelphi, MD 20783

YOSHIHIDE YAMADA
NATIONAL DEFENSE ACADEMY
1-10-20 Hashirimizu
Yokosuka, Kanagawa,
Japan 239-8686

ACES COPYRIGHT FORM

This form is intended for original, previously unpublished manuscripts submitted to ACES periodicals and conference publications. The signed form, appropriately completed, MUST ACCOMPANY any paper in order to be published by ACES. PLEASE READ REVERSE SIDE OF THIS FORM FOR FURTHER DETAILS.

TITLE OF PAPER:

RETURN FORM TO:

Dr. Atef Z. Elsherbeni
University of Mississippi
Dept. of Electrical Engineering
Anderson Hall Box 13
University, MS 38677 USA

AUTHORS(S)

PUBLICATION TITLE/DATE:

PART A - COPYRIGHT TRANSFER FORM

(NOTE: Company or other forms may not be substituted for this form. U.S. Government employees whose work is not subject to copyright may so certify by signing Part B below. Authors whose work is subject to Crown Copyright may sign Part C overleaf).

The undersigned, desiring to publish the above paper in a publication of ACES, hereby transfer their copyrights in the above paper to The Applied Computational Electromagnetics Society (ACES). The undersigned hereby represents and warrants that the paper is original and that he/she is the author of the paper or otherwise has the power and authority to make and execute this assignment.

Returned Rights: In return for these rights, ACES hereby grants to the above authors, and the employers for whom the work was performed, royalty-free permission to:

1. Retain all proprietary rights other than copyright, such as patent rights.
2. Reuse all or portions of the above paper in other works.

3. Reproduce, or have reproduced, the above paper for the author's personal use or for internal company use provided that (a) the source and ACES copyright are indicated, (b) the copies are not used in a way that implies ACES endorsement of a product or service of an employer, and (c) the copies per se are not offered for sale.

4. Make limited distribution of all or portions of the above paper prior to publication.

5. In the case of work performed under U.S. Government contract, ACES grants the U.S. Government royalty-free permission to reproduce all or portions of the above paper, and to authorize others to do so, for U.S. Government purposes only.

ACES Obligations: In exercising its rights under copyright, ACES will make all reasonable efforts to act in the interests of the authors and employers as well as in its own interest. In particular, ACES REQUIRES that:

1. The consent of the first-named author be sought as a condition in granting re-publication permission to others.
2. The consent of the undersigned employer be obtained as a condition in granting permission to others to reuse all or portions of the paper for promotion or marketing purposes.

In the event the above paper is not accepted and published by ACES or is withdrawn by the author(s) before acceptance by ACES, this agreement becomes null and void.

AUTHORIZED SIGNATURE

TITLE (IF NOT AUTHOR)

EMPLOYER FOR WHOM WORK WAS PERFORMED

DATE FORM SIGNED

Part B - U.S. GOVERNMENT EMPLOYEE CERTIFICATION

(NOTE: if your work was performed under Government contract but you are not a Government employee, sign transfer form above and see item 5 under Returned Rights).

This certifies that all authors of the above paper are employees of the U.S. Government and performed this work as part of their employment and that the paper is therefor not subject to U.S. copyright protection.

AUTHORIZED SIGNATURE

TITLE (IF NOT AUTHOR)

NAME OF GOVERNMENT ORGANIZATION

DATE FORM SIGNED

PART C - CROWN COPYRIGHT

(NOTE: ACES recognizes and will honor Crown Copyright as it does U.S. Copyright. It is understood that, in asserting Crown Copyright, ACES in no way diminishes its rights as publisher. Sign only if *ALL* authors are subject to Crown Copyright).

This certifies that all authors of the above Paper are subject to Crown Copyright. (Appropriate documentation and instructions regarding form of Crown Copyright notice may be attached).

AUTHORIZED SIGNATURE

TITLE OF SIGNEE

NAME OF GOVERNMENT BRANCH

DATE FORM SIGNED

Information to Authors

ACES POLICY

ACES distributes its technical publications throughout the world, and it may be necessary to translate and abstract its publications, and articles contained therein, for inclusion in various compendiums and similar publications, etc. When an article is submitted for publication by ACES, acceptance of the article implies that ACES has the rights to do all of the things it normally does with such an article.

In connection with its publishing activities, it is the policy of ACES to own the copyrights in its technical publications, and to the contributions contained therein, in order to protect the interests of ACES, its authors and their employers, and at the same time to facilitate the appropriate re-use of this material by others.

The new United States copyright law requires that the transfer of copyrights in each contribution from the author to ACES be confirmed in writing. It is therefore necessary that you execute either Part A-Copyright Transfer Form or Part B-U.S. Government Employee Certification or Part C-Crown Copyright on this sheet and return it to the Managing Editor (or person who supplied this sheet) as promptly as possible.

CLEARANCE OF PAPERS

ACES must of necessity assume that materials presented at its meetings or submitted to its publications is properly available for general dissemination to the audiences these activities are organized to serve. It is the responsibility of the authors, not ACES, to determine whether disclosure of their material requires the prior consent of other parties and if so, to obtain it. Furthermore, ACES must assume that, if an author uses within his/her article previously published and/or copyrighted material that permission has been obtained for such use and that any required credit lines, copyright notices, etc. are duly noted.

AUTHOR/COMPANY RIGHTS

If you are employed and you prepared your paper as a part of your job, the rights to your paper initially rest with your employer. In that case, when you sign the copyright form, we assume you are authorized to do so by your employer and that your employer has consented to all of the terms and conditions of this form. If not, it should be signed by someone so authorized.

NOTE RE RETURNED RIGHTS: Just as ACES now requires a signed copyright transfer form in order to do "business as usual", it is the intent of this form to return rights to the author and employer so that they too may do "business as usual". If further clarification is required, please contact: The Managing Editor, R. W. Adler, Naval Postgraduate School, Code EC/AB, Monterey, CA, 93943, USA (408)656-2352.

Please note that, although authors are permitted to re-use all or portions of their ACES copyrighted material in other works, this does not include granting third party requests for reprinting, republishing, or other types of re-use.

JOINT AUTHORSHIP

For jointly authored papers, only one signature is required, but we assume all authors have been advised and have consented to the terms of this form.

U.S. GOVERNMENT EMPLOYEES

Authors who are U.S. Government employees are not required to sign the Copyright Transfer Form (Part A), but any co-authors outside the Government are.

Part B of the form is to be used instead of Part A only if all authors are U.S. Government employees and prepared the paper as part of their job.

NOTE RE GOVERNMENT CONTRACT WORK: Authors whose work was performed under a U.S. Government contract but who are not Government employees are required so sign Part A-Copyright Transfer Form. However, item 5 of the form returns reproduction rights to the U. S. Government when required, even though ACES copyright policy is in effect with respect to the reuse of material by the general public.

January 2002

INFORMATION FOR AUTHORS

PUBLICATION CRITERIA

Each paper is required to manifest some relation to applied computational electromagnetics. **Papers may address general issues in applied computational electromagnetics, or they may focus on specific applications, techniques, codes, or computational issues.** While the following list is not exhaustive, each paper will generally relate to at least one of these areas:

1. **Code validation.** This is done using internal checks or experimental, analytical or other computational data. Measured data of potential utility to code validation efforts will also be considered for publication.
2. **Code performance analysis.** This usually involves identification of numerical accuracy or other limitations, solution convergence, numerical and physical modeling error, and parameter tradeoffs. However, it is also permissible to address issues such as ease-of-use, set-up time, run time, special outputs, or other special features.
3. **Computational studies of basic physics.** This involves using a code, algorithm, or computational technique to simulate reality in such a way that better, or new physical insight or understanding, is achieved.
4. **New computational techniques** or new applications for existing computational techniques or codes.
5. **“Tricks of the trade”** in selecting and applying codes and techniques.
6. **New codes, algorithms, code enhancement, and code fixes.** This category is self-explanatory, but includes significant changes to existing codes, such as applicability extensions, algorithm optimization, problem correction, limitation removal, or other performance improvement. **Note: Code (or algorithm) capability descriptions are not acceptable, unless they contain sufficient technical material to justify consideration.**
7. **Code input/output issues.** This normally involves innovations in input (such as input geometry standardization, automatic mesh generation, or computer-aided design) or in output (whether it be tabular, graphical, statistical, Fourier-transformed, or otherwise signal-processed). Material dealing with input/output database management, output interpretation, or other input/output issues will also be considered for publication.
8. **Computer hardware issues.** This is the category for analysis of hardware capabilities and limitations of various types of electromagnetics computational requirements. Vector and parallel computational techniques and implementation are of particular interest.

Applications of interest include, but are not limited to, antennas (and their electromagnetic environments), networks, static fields, radar cross section, inverse scattering, shielding, radiation hazards, biological effects, biomedical applications, electromagnetic pulse (EMP), electromagnetic interference (EMI), electromagnetic compatibility (EMC), power transmission, charge transport, dielectric, magnetic and nonlinear materials, microwave components, MEMS, RFID, and MMIC technologies, remote sensing and geometrical and physical optics, radar and communications systems, sensors, fiber optics, plasmas, particle accelerators, generators and motors, electromagnetic wave propagation, non-destructive evaluation, eddy currents, and inverse scattering.

Techniques of interest include but not limited to frequency-domain and time-domain techniques, integral equation and differential equation techniques, diffraction theories, physical and geometrical optics, method of moments, finite differences and finite element techniques, transmission line method, modal expansions, perturbation methods, and hybrid methods.

Where possible and appropriate, authors are required to provide statements of quantitative accuracy for measured and/or computed data. This issue is discussed in “Accuracy & Publication: Requiring, quantitative accuracy statements to accompany data,” by E. K. Miller, *ACES Newsletter*, Vol. 9, No. 3, pp. 23-29, 1994, ISBN 1056-9170.

SUBMITTAL PROCEDURE

All submissions should be uploaded to ACES server through ACES web site (<http://aces.ee.olemiss.edu>) by using the upload button, journal section. Only pdf files are accepted for submission. The file size should not be larger than 5MB, otherwise permission from the Editor-in-Chief should be obtained first. Automated acknowledgment of the electronic submission, after the upload process is successfully completed, will be sent to the corresponding author only. It is the responsibility of the corresponding author to keep the remaining authors, if applicable, informed. Email submission is not accepted and will not be processed.

PAPER FORMAT (INITIAL SUBMISSION)

The preferred format for initial submission manuscripts is 12 point Times Roman font, single line spacing and single column format, with 1 inch for top, bottom, left, and right margins. Manuscripts should be prepared for standard 8.5x11 inch paper.

EDITORIAL REVIEW

In order to ensure an appropriate level of quality control, papers are peer reviewed. They are reviewed both for

technical correctness and for adherence to the listed guidelines regarding information content and format.

PAPER FORMAT (FINAL SUBMISSION)

Only camera-ready electronic files are accepted for publication. The term “**camera-ready**” means that the material is neat, legible, reproducible, and in accordance with the final version format listed below.

The following requirements are in effect for the final version of an ACES Journal paper:

1. The paper title should not be placed on a separate page. The title, author(s), abstract, and (space permitting) beginning of the paper itself should all be on the first page. The title, author(s), and author affiliations should be centered (center-justified) on the first page. The title should be of font size 16 and bolded, the author names should be of font size 12 and bolded, and the author affiliation should be of font size 12 (regular font, neither italic nor bolded).
2. An abstract is required. The abstract should be a brief summary of the work described in the paper. It should state the computer codes, computational techniques, and applications discussed in the paper (as applicable) and should otherwise be usable by technical abstracting and indexing services. The word “Abstract” has to be placed at the left margin of the paper, and should be bolded and italic. It also should be followed by a hyphen (–) with the main text of the abstract starting on the same line.
3. All section titles have to be centered and all the title letters should be written in caps. The section titles need to be numbered using roman numbering (I. II.)
4. Either British English or American English spellings may be used, provided that each word is spelled consistently throughout the paper.
5. Internal consistency of references format should be maintained. As a guideline for authors, we recommend that references be given using numerical numbering in the body of the paper (with numerical listing of all references at the end of the paper). The first letter of the authors’ first name should be listed followed by a period, which in turn, followed by the authors’ complete last name. Use a coma (,) to separate between the authors’ names. Titles of papers or articles should be in quotation marks (“ ”), followed by the title of journal, which should be in italic font. The journal volume (vol.), issue number (no.), page numbering (pp.), month and year of publication should come after the journal title in the sequence listed here.
6. Internal consistency shall also be maintained for other elements of style, such as equation numbering. As a guideline for authors who have no other preference, we suggest that equation numbers be placed in parentheses at the right column margin.

7. The intent and meaning of all text must be clear. For authors who are not masters of the English language, the ACES Editorial Staff will provide assistance with grammar (subject to clarity of intent and meaning). However, this may delay the scheduled publication date.
8. Unused space should be minimized. Sections and subsections should not normally begin on a new page.

ACES reserves the right to edit any uploaded material, however, this is not generally done. It is the author(s) responsibility to provide acceptable camera-ready pdf files. Incompatible or incomplete pdf files will not be processed for publication, and authors will be requested to re-upload a revised acceptable version.

COPYRIGHTS AND RELEASES

Each primary author must sign a copyright form and obtain a release from his/her organization vesting the copyright with ACES. Copyright forms are available at ACES, web site (<http://aces.ee.olemiss.edu>). To shorten the review process time, the executed copyright form should be forwarded to the Editor-in-Chief immediately after the completion of the upload (electronic submission) process. Both the author and his/her organization are allowed to use the copyrighted material freely for their own private purposes.

Permission is granted to quote short passages and reproduce figures and tables from an ACES Journal issue provided the source is cited. Copies of ACES Journal articles may be made in accordance with usage permitted by Sections 107 or 108 of the U.S. Copyright Law. This consent does not extend to other kinds of copying, such as for general distribution, for advertising or promotional purposes, for creating new collective works, or for resale. The reproduction of multiple copies and the use of articles or extracts for commercial purposes require the consent of the author and specific permission from ACES. Institutional members are allowed to copy any ACES Journal issue for their internal distribution only.

PUBLICATION CHARGES

All authors are allowed for 8 printed pages per paper without charge. Mandatory page charges of \$75 a page apply to all pages in excess of 8 printed pages. Authors are entitled to one, free of charge, copy of the journal issue in which their paper was published. Additional reprints are available for a nominal fee by submitting a request to the managing editor or ACES Secretary.

Authors are subject to fill out a one page over-page charge form and submit it online along with the copyright form before publication of their manuscript.

ACES Journal is abstracted in INSPEC, in Engineering Index, DTIC, Science Citation Index Expanded, the Research Alert, and to Current Contents/Engineering, Computing & Technology.